

Lawrence Berkeley National Laboratory

Recent Work

Title

THERMODYNAMIC ANOMALY IN MAGNESIUM HYDROXIDE DECOMPOSITION

Permalink

<https://escholarship.org/uc/item/330422p9>

Author

Reis, T.A.

Publication Date

1983-08-01



Lawrence Berkeley Laboratory

UNIVERSITY OF CALIFORNIA

Materials & Molecular Research Division

RECEIVED
LAWRENCE
BERKELEY LABORATORY
--B 21 1984
LIBRARY AND
DOCUMENTS SECTION

THERMODYNAMIC ANOMALY IN MAGNESIUM HYDROXIDE
DECOMPOSITION

T.A. Reis
(Ph.D. Thesis)

August 1983

TWO-WEEK LOAN COPY

*This is a Library Circulating Copy
which may be borrowed for two weeks.
For a personal retention copy, call
Tech. Info. Division, Ext. 6782.*



LBL-15725
c.2

DISCLAIMER

This document was prepared as an account of work sponsored by the United States Government. While this document is believed to contain correct information, neither the United States Government nor any agency thereof, nor the Regents of the University of California, nor any of their employees, makes any warranty, express or implied, or assumes any legal responsibility for the accuracy, completeness, or usefulness of any information, apparatus, product, or process disclosed, or represents that its use would not infringe privately owned rights. Reference herein to any specific commercial product, process, or service by its trade name, trademark, manufacturer, or otherwise, does not necessarily constitute or imply its endorsement, recommendation, or favoring by the United States Government or any agency thereof, or the Regents of the University of California. The views and opinions of authors expressed herein do not necessarily state or reflect those of the United States Government or any agency thereof or the Regents of the University of California.

THERMODYNAMIC ANOMALY IN MAGNESIUM HYDROXIDE DECOMPOSITION

Thomas Anthony Reis

(PhD Dissertation)

Materials and Molecular Research Division
Lawrence Berkeley Laboratory
University of California
Berkeley, California 94720

August 1983

Copyright © 1983 Thomas Anthony Reis

The United States Department of Energy has the right to use
this thesis for any purpose whatsoever including the right
to reproduce all or any part thereof.

ABSTRACT

Thermodynamic Anomaly in $\text{Mg}(\text{OH})_2$ Decomposition

Thomas Anthony Reis

(PhD Dissertation)

The purpose of the research reported here is to investigate the origin of the discrepancy in the equilibrium water vapor pressure measurements for the reaction $\text{Mg}(\text{OH})_2(\text{s}) = \text{MgO}(\text{s}) + \text{H}_2\text{O}(\text{g})$ when determined by Knudsen effusion and static manometry at the same temperature. For this reaction undergoing continuous thermal decomposition in Knudsen cells, Kay and Gregory observed that by extrapolating the steady-state apparent equilibrium vapor pressure measurements to zero-orifice, the vapor pressure was $\sim 10^{-4}$ of that previously established by Giauque and Archibald as the true thermodynamic equilibrium vapor pressure using statistical mechanical entropy calculations for the entropy of water vapor. This large difference in vapor pressures suggests the possibility of the formation in a Knudsen cell of a higher energy MgO that is thermodynamically metastable by about 48 kJ / mole.

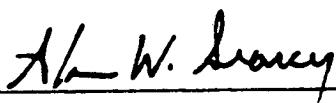
It has been shown here that experimental results are qualitatively independent of the type of $\text{Mg}(\text{OH})_2$ used as a starting material, which confirms the inferences of Kay and Gregory. Thus, most forms of $\text{Mg}(\text{OH})_2$ are considered to be the stable thermodynamic equilibrium form.

In efforts to determine if metastable MgO is being formed, methods such as x-ray diffraction, surface area analysis, thermogravimetry, scanning electron microscopy, and solution calorimetry were used to characterize $\text{Mg}(\text{OH})_2$ samples after partial or complete decomposition,

in terms of structure, particle size, surface area, porosity, morphology, and heat-of-formation.

X-ray diffraction results show that during the course of the reaction only the equilibrium NaCl-type MgO is formed, and no different phases result from samples prepared in Knudsen cells. Surface area data indicate that the MgO molar surface area remains constant throughout the course of the reaction at low decomposition temperatures, and no significant annealing occurs at less than 400°C. Scanning electron microscope photographs show no change in particle size or particle surface morphology. Solution calorimetric measurements indicate no inherent higher energy content in the MgO from the solid produced in Knudsen cells.

The Knudsen cell vapor pressure discrepancy may reflect the formation of a transient metastable MgO or Mg(OH)₂-MgO solid solution during continuous thermal decomposition in Knudsen cells.



Alan W. Searcy, Chairman, Dissertation Committee

This dissertation is dedicated to my wife, Pamela , whose committed effort, encouragement and interest were most important for this doctoral degree to have been possible.

ACKNOWLEDGEMENT

My appreciation to Professor Alan Searcy for his genuine interest in this research and the many discussions associated with it, and for imparting to me many of the invaluable subtleties of scientific investigation. The surroundings in his laboratory made doing physical chemistry there a satisfying scientific experience.

My special thanks to Dr. Dave Meschi for his technical expertise and assistance with the solution calorimeter, and for the many helpful and valuable suggestions and interesting discussions.

My thanks to Prof. Dario Beruto, Universita di Genova, for the many valuable scientific discussions during his summers spent here.

The unique kind of experience and awareness acquired while at Berkeley could not have been possible anywhere else.

This research was funded by the Director, Office of Energy Research, Office of Basic Energy Sciences, Materials Science Division of the U.S. Department of Energy under Contract Number DE - AC03 - 76SF00098.

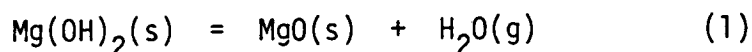
TABLE OF CONTENTS

Dedication.....	i
Acknowledgement.....	ii
Table of Contents.....	iii
INTRODUCTION.....	1
EXPERIMENTAL.....	8
Starting Material.....	8
MgO Sample Preparation.....	9
Sample Characterization.....	11
Thermogravimetry.....	12
Surface Area.....	13
Scanning Electron Microscopy.....	14
X-Ray Diffraction.....	14
Solution Calorimetry.....	16
RESULTS & DISCUSSION.....	22
Scanning Electron Microscopy.....	28
X-Ray Diffraction.....	29
Surface Area.....	32
Solution Calorimetry.....	38
GENERAL DISCUSSION.....	41
SUMMARY & CONCLUSIONS.....	43
References.....	46
Tables.....	57
Appendices.....	61
Figure Captions.....	77
Figures.....	81
End Page.....	115

INTRODUCTION

The endothermic decomposition of solid compounds into solid and gaseous products has been investigated in some manner for about two centuries.^{1,2} Initially, product improvement and production prompted these investigations, but later a quest for scientific understanding of decomposition³ and decomposition reactions⁴⁻⁸ and their products became an important motivation.

The particular endothermic decomposition,



sometimes referred to as the brucite dehydration to periclase, has been studied by researchers of varied disciplines for many years.⁹⁻¹⁸ The thermodynamics of the reaction was studied with exceptional care by Giauque and Archibald^{19,20} in order to demonstrate that statistical mechanical calculations of entropy of a gas (in this case water vapor) agrees with the entropy measured thermochemically. Later, Kay and Gregory^{21,22} showed that apparent equilibrium $\text{H}_2\text{O}(\text{g})$ pressures measured for the reaction by the Knudsen effusion method^{23,24} is known to yield the true equilibrium pressure for many reactions^{22,25} but has since been shown to yield for dolomite, also apparent equilibrium pressures which are many orders of magnitude below the true equilibrium pressures.²⁶

The purpose of the research reported here is to investigate the origin of the discrepancy between the manometric measurements of the $\text{H}_2\text{O}(\text{g})$ equilibrium pressure measured by Giauque and Archibald (G&A) for reaction (1), and the much lower apparent equilibrium pressures which were measured by Kay and Gregory (K&G) in Knudsen effusion cells. Probably the discrepancy originates in some characteristic common to many decomposition reactions.

Many researchers in different groups, and separately, have each done extensive research on the $\text{Mg}(\text{OH})_2$ decomposition reaction and its solid product²⁷⁻⁶⁷ in some way over the last four decades. In particular, x-ray investigations by many researchers⁶⁸⁻⁸⁰ have been done on $\text{Mg}(\text{OH})_2$ and MgO from its decomposition, and as a result, the $\text{Mg}(\text{OH})_2(\text{s}) - \text{MgO}(\text{s})$ system has been carefully characterized crystallographically. Recent investigators⁴⁴ have found only two solid phases, $\text{Mg}(\text{OH})_2(\text{s})$ and $\text{MgO}(\text{s})$, when high purity $\text{Mg}(\text{OH})_2$ is used, whether natural brucite or chemically prepared reagent powder. Intermediate phases such as "metabrucite"¹³ or a spinel-like solid,¹⁸ described by some investigators, were found not to be present by others.⁴⁴ This spinel-like phase which had been identified as metabrucite was later shown to be a result of a high iron impurity content in the brucite.⁴⁴

$\text{Mg}(\text{OH})_2$ crystallizes in layered CdI_2 -type structure as shown in Fig 1. Natural brucite often occurs as very pure, well-crystallized, and easily-cleaved crystals. The structure is composed of hexagonal close packed (HCP) double layers of OH^- anions. The Mg^{2+} cations occupy all the octahedral interstices between each pair of hydroxyl layers. The a and c spacings of the hexagonal unit cell are 3.11 \AA and 4.74 \AA respectively. X-ray studies indicate that there are no significant irregularities in the stacking sequence of the hexagonal layers of the $\text{Mg}(\text{OH})_2$ structure in the brucite crystals.⁸⁰

MgO crystallizes in the NaCl -type structure as shown in Fig 2. The lattice can be viewed as formed of face-centered (FCC) arrays of Mg^{2+} and O^{2-} ions. Each kind of ion is octahedrally coordinated by oppositely charged ions. The lattice edge a of the FCC unit cell, which consists of four "molecules", is 4.20 \AA .

Thermal decomposition of $\text{Mg}(\text{OH})_2$ in an electron microscope^{38,50,52,65-67} has been used to determine the orientation between the parent $\text{Mg}(\text{OH})_2$ crystals and the product MgO crystallites. The TEM studies confirm the conclusion from single crystal x-ray diffraction studies⁷⁰ that dehydration of HCP $\text{Mg}(\text{OH})_2$ produces NaCl-type MgO in an ordered form. The MgO crystallites were found to be in parallel array with their $\langle 111 \rangle$ and $\langle 110 \rangle$ axes parallel to the c and a axes respectively of the parent $\text{Mg}(\text{OH})_2$ crystal. Consequently, the $(111)\text{MgO}$ planes are parallel to the $(101)\text{Mg}(\text{OH})_2$ or $(0001)\text{Mg}(\text{OH})_2$ basal planes of the parent $\text{Mg}(\text{OH})_2$ crystal. Above 500°C additional reflections were purported to be a result of a change in the orientation of some of the MgO crystallites.¹³ No intermediate phases were observed in the XRD or TEM studies.

In order to test the agreement between the calorimetrically measured entropy of $\text{H}_2\text{O}(\text{g})$ and the values calculated from spectroscopic data, G&A carefully determined the thermodynamics of the $\text{Mg}(\text{OH})_2(\text{s})-\text{MgO}(\text{s})-\text{H}_2\text{O}(\text{g})$ system near 200°C , by obtaining equilibrium data for the $\text{Mg}(\text{OH})_2$ decomposition directly from static manometric $\text{H}_2\text{O}(\text{g})$ pressure measurements (Fig 3). Pressures measured as functions of time rose ~ 0.2 torr (~ 27 Pa) / day for two weeks, but the initial measured pressures were only 2 % to 10 % below the final equilibrium pressures, indicating an immediate rise from $\sim 10^{-4}$ of the true equilibrium pressure to within ~ 10 % of it. An intermediate rise in the vapor pressure when the decomposition was stopped and then resumed, was also observed by K&G^{21,22} who found a return to the very low pressure shortly after resumption of the decomposition. Razouk and Mikhail^{31,32} confirm a slow approach to equilibrium by means of sorption experiments using various MgO samples.

The G&A equilibrium vapor pressure data near 200°C, when plotted on a Log P vs 1/T plot as shown in Fig 4, gives from the slope a heat-of-reaction (ΔH_{rxn}) which agrees with the value determined from their calorimetric measurements of the heat-of-solution (ΔH_{soln}) for ~95 % decomposed samples (App I).

This particular decomposition can be carried to, at most ~95 % of completion at decomposition temperatures less than 400°C in vacuum or air. As my thermogravimetry data indicate, a reasonably complete decomposition, ~99.5 % , is obtained only above 650°C. G&A corrected for retained water in their ΔH_{soln} measurements by assuming that the ~5 % retained water was in the form of unreacted $Mg(OH)_2(s)$. From measured $H_2O(g)$ pressures, heat capacities, and ΔH_{soln} , G&A were able to calculate the absolute entropy, $S_{H_2O}^{calc}$, of the water vapor above solid phases, $Mg(OH)_2(s)-MgO(s)$ (App I). They found that the $S_{H_2O}^{calc}$ agreed with the entropy calculated from band spectra, $S_{H_2O}^{band}$, to within a 0.3 J / deg-mole experimental error. Thus, the manometrically measured vapor pressures were the true thermodynamic values for the $Mg(OH)_2$ decomposed and the MgO formed in their reaction

The MgO produced in the experiments of G&A had a high surface area, and relative to the macrocrystalline MgO had a free energy and enthalpy calculated by Giaouque⁸¹ to be ~3.3 kJ / mole and ~3.8 kJ / mole respectively.

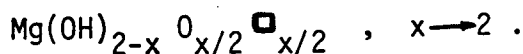
Equilibrium solid phases are not necessarily equilibrium macrocrystalline phases, according to Giaouque,⁸¹ who states that, "the third law gives accurate agreement with the measured equilibrium pressures, when the entropy and heat content are measured on the actual finely divided magnesium oxide in equilibrium. Thus, the colloidal particles approached essentially zero

entropy at very low temperatures and evidently approximated a perfect crystalline structure. It is concluded that neither reproducibility of equilibrium measurements based on approach from each side nor agreement with the third law of thermodynamics, can be accepted as proof that an equilibrium corresponds to the thermodynamic properties of macrocrystalline phases."

K&G investigated the decomposition of brucite platelets in small orifice Knudsen cells (App II), and found, regardless of orifice size, that after a short time the water vapor pressure decreased rapidly to a steady-state vapor pressure, P_s , which remained constant throughout most of the decomposition. If the reaction was stopped and then resumed, the phenomenon was repeated; that is, a higher initial pressure decreased to a lower steady-state pressure. K&G plotted P_s vs A_0 , the Knudsen cell orifice area, as shown in Fig 5a, and extrapolated to $A_0 = 0$. They found that P_s approached a constant value at $A_0 = 0$, which was different for each temperature selected, and plotted these values on a $\text{Log } P$ vs $1/T$ plot (Fig 5b). The slope gives $\Delta H_{\text{rxn}} = 130.5 \text{ kJ / mole (31.2 kcal / mole)}$, which differs from the $\Delta H_{\text{rxn}} = 82.8 \text{ kJ / mole (19.8 kcal / mole)}$ measured by G&A by $47.7 \text{ kJ / mole (11.4 kcal / mole)}$. Both are compared on a $\text{Log } P$ vs $1/T$ plot shown in Fig 4.

Using DTA, it was observed by Rao & Pitzer⁸² and others⁸³, that for MgO obtained from the decomposition of reagent Mg(OH)_2 and MgCO_3 , that small exothermic ($\sim 1.5 \text{ kJ / mole}$) peaks extending over a small temperature interval ($\sim 50^\circ\text{C}$) followed the large endothermic decomposition DTA peaks in each case. Thus, these were attributed to crystal defect and strain removal or a disorder - order transformation from a metastable MgO^* to a more nearly completely stable MgO.

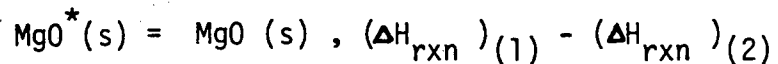
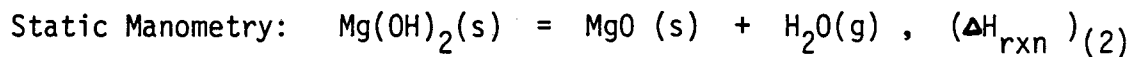
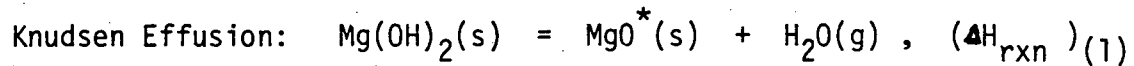
Freund⁵⁵ has done some very interesting research on $Mg(OH)_2$ decomposition using finely divided microgram quantities in a mass spectrometer. His results show several maxima in the rate of water vapor evolution, which he attributes to the formation of an overlayer of partially decomposed magnesium hydroxide,



The square denotes an anion-sized vacancy left by H_2O molecules in the hydroxide lattice. This hypothesized overlayer, while basically a defect layer, is assumed to represent a diffusion barrier for further H_2O molecules. When a critical thickness is reached, it spontaneously re-crystallizes to a cubic MgO , exposing fresh $Mg(OH)_2$ surface. In most other analytical methods, a smooth reaction is observed when milligram quantities are used. In a later publication on the application of x-ray analysis to this reaction, Freund and Sperling⁵⁷ found by examination of the survival of the (001) and (110) reflections of the $Mg(OH)_2$ beyond substantial dehydration to nearly anhydrous MgO as well as the shift of these reflections with increasing temperature with little or no line broadening, some additional evidence to support this defect structure concept.

Although the other x-ray diffraction and electron microscopy experiments, as previously described, show no evidence for a metastable^{7,81-84} decomposition product, the MgO produced in Knudsen cells might be thermodynamically metastable by about 48 kJ / mole. Such a large difference in the heats-of-reaction, if interpreted as a difference in the heats-of-formation of the MgO product, $\Delta H_f^{\circ}{}_{MgO}$, can be measured indirectly by means of the heat-of-solution of the MgO , ΔH_{soln}^{MgO} , in an acid solution (App III).

Thus,



$$\Delta H_{\text{fMgO}}^* = (\Delta H_{\text{rxn}})_{(1)} - (\Delta H_{\text{rxn}})_{(2)} + \Delta H_{\text{fMgO}}$$

In this study, in efforts to determine if a metastable product is formed, Thermogravimetry (TG), B.E.T. Surface Area (S_{BET}), Scanning Electron Microscopy (SEM), X-Ray Diffraction (XRD), and Heat-of-Solution calorimetry (ΔH_{soln}) were used to characterize Mg(OH)_2 samples after partial or complete decomposition, in terms of structure, particle size, surface area, porosity, morphology, and heat-of-formation.

EXPERIMENTAL

Starting Material

High purity $\text{Mg}(\text{OH})_2$ is relatively easy to prepare by various synthetic procedures.^{19,27,37,38,44,46,63,66,73,84,98} It is not hygroscopic, corrosive, or toxic, making it very easy to handle.

The $\text{Mg}(\text{OH})_2$ starting material used in the initial experiments was a commercial, reagent-grade powder manufactured by Ventron-Alfa Products of Danvers, Massachusetts, which will be denoted V- $\text{Mg}(\text{OH})_2$, or simply Ventron or V. The $\text{Mg}(\text{OH})_2$ used later as a starting material, denoted G- $\text{Mg}(\text{OH})_2$, or simply G&A or G, was synthesized in the laboratory according to the method described by Giauque and Archibald(G&A).¹⁹ A synopsis of their method and my yield data for the synthesis is given in App IV. G&A used a platinum-lined vessel, but in the present research a teflon beaker was used. The teflon beaker was tested in the laboratory with the $\text{Mg}(\text{OH})_2$ synthesis materials in it at 220°C, the required synthesis temperature, and found to have satisfactory mechanical stability and chemical inertness. Chemical inertness was indicated by no significant change in the chemical elemental analysis of successive preparations relative to other starting materials(App V). Magnified visual scrutiny of the beaker surface also showed no evidence of reaction.

Chemical analyses of several natural brucites^{38,52} were averaged to provide an estimate of the chemical elemental composition of the natural brucite used by Kay and Gregory(K&G)^{21,22} in their Knudsen cell experiments. They do not report an analysis of their material. This natural brucite starting material will be denoted K- $\text{Mg}(\text{OH})_2$, or simply K&G or K.

One possible, though unlikely, explanation for the discrepancy between the G&A and K&G results is that it arose from differences in the starting

material used for manometric and effusion studies.

Most experiments initially done using the V-Mg(OH)₂ were repeated using the G-Mg(OH)₂ under the same or similar experimental conditions. For experiments that were done in the high vacuum furnace (~10⁻⁵ torr) with a Knudsen cell, only G-Mg(OH)₂ was used as the starting material. The fact that no significant qualitative change in behavior was observed with different starting materials will be discussed later.

MgO Sample Preparation

The experimental conditions used in this research to produce MgO from either starting material resemble Knudsen cell conditions more closely than they do conditions in a static manometric study.

Initially, V-Mg(OH)₂ was decomposed in a low vacuum (~2.0 torr) apparatus using a quartz helix U-tube as in Fig 6. The sample cup of the U-tube had a cross-sectional area of ~2.0 cm², and a corresponding volume of ~3.0 cm³. The extent of decomposition was determined from the sample weight loss, with only water assumed to escape. An outline of the calculation is given in App VI. The validity of the assumption that only water was lost is confirmed to ~0.5 wt % by comparing actual and theoretical weight losses for the reaction (App VII). In order to minimize powder loss by entrainment during the decomposition, which would cause error in the calculations, the exit arm of the U-tube was made into a three coil helix. The U-tube was constructed of quartz, so that samples could be annealed in situ at 1000°C. However, prolonged heating at 1000°C caused SiO₂ embrittlement and ultimately resulted in mechanical failure of the U-tube.

Since the pressure measuring sensor was not located at the powder

bed surface, the pressure there was estimated to within 0.1 torr by inserting a helix coil of the same dimensions as the helical arm of the U-tube between the pressure measuring sensor and the vacuum pump.

After the decomposition, the vacuum in the U-tube was equalized to atmospheric pressure by slowly adding dry nitrogen gas through a micrometer valve into the closed-off U-tube. This procedure prevented part of the powdered sample from being blown-out through the arms of the U-tube when the U-tube assembly was disconnected for transfer to the surface area analyzer. The apparatus as shown in Fig 6, was designed to allow transfer of the sample to the surface area analyzer without exposure to air.

The temperature near the sample cup of the U-tube was measured using a standard Pt/Pt-10% Rh thermocouple connected to a Type S calibrated Doric 412A Trendicator temperature gauge with LED digital display. The sample temperature was estimated to be within 5°C of the displayed temperature.

The tube furnace shown in Fig 6 was a resistance furnace of Kanthal wire wound on a 2.5 cm diameter by 20 cm long alumina tube. The tube was then mounted in a 15 cm diameter cylindrical metal vessel surrounded by glass wool insulation. The maximum furnace temperature of about 1200°C could be held for one hour without causing malfunction or failure of the furnace. It consistently produced a steady temperature of 1000°C \pm 5°C for 15 hours when initially tested for high temperature stability.

For higher vacuum and better furnace control, the modified high vacuum furnace shown in Fig 7 was used for decompositions. This is a tungsten element resistance furnace that uses a large Varian model 0183 silicone oil diffusion pump backed with a Duo-Seal model 1397 mechanical pump to obtain a vacuum of $\sim 10^{-6}$ torr. The electrobalance shown in Fig 7 is a Cahn RG.

In the high vacuum furnace experiments, an alumina Knudsen cell was used in place of the U-tube to contain the sample. The cell had a cross-sectional area of $\sim 3.3 \text{ cm}^2$ compared to $\sim 2.0 \text{ cm}^2$ for the U-tube sample cup. The Knudsen cell becomes simply a crucible when the lid is removed. The alumina cell or crucible is more inert and durable at 1000°C than the quartz U-tube. The dimensions of the various Knudsen cells and crucibles used in this and other related research are given in Tables 1 & 2. These dimensions are similar to those of the U-tube sample cup.

The same type of thermocouple and temperature gauge already described for the U-tube apparatus was used to measure the sample cell temperature in the high vacuum furnace and electrobalance. This temperature was controlled to within 5°C of the set temperature by a Eurotherm proportional control unit with a Pt/Pt-10% Rh thermocouple temperature feedback sensor attached to the furnace heating elements. A maximum set temperature of 1200°C was available with this unit. The furnace temperature was changed by means of a Eurotherm temperature ramping unit capable of controlled heating or cooling rates from $1^\circ\text{C} / \text{minute}$ to $40^\circ\text{C} / \text{minute}$ in $1^\circ\text{C} / \text{minute}$ intervals. A maximum set temperature of 1000°C is available with this temperature ramping unit. The proportional control unit could be used at 1000°C to 1200°C .

Sample Characterization

Thermogravimetry, surface area, x-ray diffractometer, and scanning electron microscope data were obtained for reactants and products of each of the two different starting materials. Calorimetric data was obtained only for the G-Mg(OH)_2 decomposed in the high vacuum furnace.

Since the MgO re-hydrated slightly on exposure to air, weight gain

tests were carried out in the ambient atmosphere using a Mettler single pan microbalance sensitive to ~ 0.01 mg. The different starting materials were at complete or near complete decomposition. A weight gain of 1 mg for a 100 mg decomposed sample exposed 5 minutes to the ambient was typical; this gain was so slow as to be considered negligible.

Thermogravimetry (TG)

Two weight-loss vs time measurements were made using the $V-Mg(OH)_2$ reagent powder in a cubic Pt basket, 1 cm on an edge, suspended by a quartz stirrup from the electrobalance, midway into the high vacuum furnace (Fig 7).

At convenient decomposition temperatures, about $350^\circ C$, only $\sim 95\%$ decomposition is achieved before the decomposition rate decreases to a negligible value. To find a temperature at which essentially complete decomposition occurs, the following procedure was followed: A sample was heated to $\sim 95\%$ decomposition in the high vacuum furnace at $350^\circ C$ using the electrobalance to monitor the weight-loss until no weight-loss was observed on the balance scale. The temperature was then increased at the rate of $1^\circ C / \text{minute}$, which caused the sample to decompose further. Eventually, a temperature was reached at which no further weight-loss was observed. This temperature was then taken as the minimum temperature required for essentially complete decomposition. This temperature was maintained for an additional 30 minutes to observe that complete decomposition had been achieved. The temperature for essentially complete decomposition by this procedure was found to be $650^\circ C$ for $V-Mg(OH)_2$.

Appreciable sintering does not occur at $345^\circ C$ (Fig 25) in the low vacuum U-tube (Fig 6). In the high vacuum furnace, sintering is minimized because of the absence of water vapor.^{40,42} Slow heating minimizes sintering

of MgO,^{33,34} which has been extensively studied.^{29,47,58,64,85,86,102}

Since samples using G-Mg(OH)₂ were prepared in Knudsen cells with small orifices, it was a simple matter to measure the time of reaction and calculate the flux, J_{H₂O}, from the weight lost and orifice dimensions. These samples were prepared in the high vacuum furnace, but without the use of the electrobalance. Using the Hertz-Knudsen-Langmuir(H-K-L) equation⁸⁷ with appropriate values substituted,

$$P_s = 760 \frac{(MT)^{1/2}}{2650} J_{H_2O} = 1.217 J_{H_2O} (T)^{1/2}$$

the maximum steady-state pressure of the water vapor inside the Knudsen cell, P_s, was calculated. M is the molecular weight of the water, 18.015 gms / mole, the vaporizing species. T is the temperature in degrees Kelvin, and J_{H₂O} is the flux in moles / cm²-min. P_s is in torr.

Surface Area(S_{BET})

Surface areas were determined by the B.E.T. method,⁸⁸⁻⁹⁰ either with the sample left in the helix U-tube, which was designed to serve as a sample for the surface area analyzer, or in a standard surface area analyzer sample tube. No difference in the results was observed regardless of whether the sample was rapidly transferred to the standard sample tube and analyzed or whether the sample was decomposed directly in the sample tube. The surface area analyzer was a Quantasorb Surface Analyzer manufactured by Quantachrome Corporation of Greenvale, New York. Reproducibility for high surface area MgO samples produced from Mg(OH)₂ is ~1%. Weighing to determine final sample weight and the extent of decomposition could be done after the surface area measurement since it did not affect the sample weight.

Scanning Electron Microscopy (SEM)

SEM micrographs were taken of the two different starting materials and of the products when decomposition was ~95 % complete. Some samples were prepared for SEM study by lightly dusting them onto a slightly damp carbonized substrate. This substrate was prepared from a fine suspension of powdered carbon in a viscous, quick-drying organic liquid. A more convenient method was to disperse the powdered samples in CCl_4 immediately after their removal from a vacuum or dry nitrogen environment, and then apply a few drops of this well-mixed suspension onto a nearly dried carbonized substrate surface with an eyedropper. After a sample had dried under a drying lamp for 15 minutes, a ~200Å gold film was sputtered onto the sample.

X-Ray Diffraction (XRD)

After surface area measurements were made on a powdered sample a portion of it was rapidly transferred into the 15x12x1.5 mm cavity of a specially designed lucite sample holder for x-ray measurements. The powder surface was smoothed with a glass microscope slide. The sample was irradiated in a Picker model 3488K x-ray diffractometer operating at 40 kV and 14 mA using either $\text{CuK}\alpha$ (1.542Å) or $\text{FeK}\alpha$ (1.937Å) x-rays. The chart speed was fixed at a constant rate of 2° / minute. The 2θ scan was from 20° to 120°, which includes almost the entire range of x-ray reflections for $\text{Mg}(\text{OH})_2$ and MgO listed in the ASTM / JCPDS file (App VIII) and in the literature.⁹¹ A test scan of the empty lucite sample holder showed no reflections.

A resolution of 1000 counts / second (cps) was used for most of the samples examined, but 400 cps was also used for some samples. The entire

range of resolutions from the highest at 200 cps through 400, 1000, 2000, 4000, and 10,000 cps was used in experiments designed to investigate the effect of resolution on the structure of the spectra. 20,000 cps, the lowest resolution, was not used since test spectra showed that the principal peaks were too small for accurate measurement at this resolution.

XRD spectra were taken of $V-Mg(OH)_2$ and $G-Mg(OH)_2$, the two different starting materials. Several samples of $V-Mg(OH)_2$ and different batches of $G-Mg(OH)_2$ showed no spectral inconsistencies. Using the radiations and resolutions already described, spectra were also taken of samples after partial or complete decomposition under a variety of conditions, and after high temperature annealing.

The maximum heights of the $(101)Mg(OH)_2$ and the $(200)MgO$ principal peaks were measured from the baseline near the peak center. At half the maximum peak height the full width was measured to give the full width at half maximum (FWHM). Using a Dietzgen model 1804A compensating optical reading polar planimeter, several area measurements of the same reflections were made for each spectrum taken, and the average area calculated. Integral breadths (IB) were calculated for these same reflections. The IB is defined as the total peak area divided by the maximum peak height.^{92,93} Typical calculations are shown in App IX. The IB can be used as a measure of the degree of crystallinity.⁹⁴ The IB decreases as the peak height increases, and a decreasing IB is a measure of increasing crystallinity.

Substitution of $CuK\alpha$ for $FeK\alpha$ radiation causes about a 10-12 degree shift in the positions of the peaks of the spectra. But within limits of $\sim 2\%$ error, the choice of $CuK\alpha$ or $FeK\alpha$ radiation made no difference in the calculated IB for the same starting material.

The IB for all materials examined was also observed to be independent,

within experimental error, of the resolution of the diffractometer, except for the lowest resolution, 10,000 cps. At this resolution peak heights were too small for accurate measurement.

$IB_{(101)}^V$, $IB_{(200)}^V$, $IB_{(101)}^G$, and $IB_{(200)}^G$, used later as notations when discussing the results, denote the integral breadth for (101)V-Mg(OH)₂, (200)V-MgO, (101)G-Mg(OH)₂, and (200)G-MgO, respectively.

The sample was unprotected from air during the approximately 20-25 minutes which were required to do an x-ray diffractometer scan. A re-scan at the highest resolution while the sample was still in the x-ray diffractometer, indicated no additional reflections after more than 30 minutes exposure to air.

Solution Calorimetry(ΔH_{soln})

The solution calorimeter^{19,95,96} used in all the heat-of-solution measurements(Fig 8) was constructed in this laboratory. The calorimeter consists of an acid-filled standard 2 liter wide-mouth dewar flask, which is the calorimeter reaction vessel (CRV). The CRV is weighted with 10 lbs of small pieces of lead cemented into the base to anchor it in the surrounding water of the controlled temperature bath (CTB).

The temperature of the acid solution in the CRV was measured to within 0.005°C with a thermistor connected to a modified Wheatstone bridge,⁹⁷ referred to here as the thermistor bridge (TB). The thermistor is a Type YSI 44105 rated at 3000 ohms at 25°C, manufactured by the Yellow Springs Instrument Company of Yellow Springs, Ohio. To compensate for any change in resistance of the thermistor lead wires with temperature,⁹⁷ an additional wire leading to the TB was connected as close as possible to the thermistor in the CRV of the calorimeter.

The thermistor itself was mounted in the 5 cm thick heat-insulating styrofoam lid. An O-ring was used to fit the lid snugly into the top. Additional holes in the lid were used to admit a stirrer, and also an ampoule bursting device at the end of which the sample was held in the evacuated pyrex ampoule. The CRV temperature could be raised or lowered by inserting into the CRV through the hole for the ampoule bursting device, either a hotfinger resistance heater or a coldfinger (Fig 8).

Small glass beads were put into the bottom of the CRV to prevent the ampoule bursting device from slipping on the smooth bottom of the dewar flask during the bursting maneuver.

The ampoule bursting device, shown in Fig 8, was constructed from acid-resistant tantalum metal and a hard, fiberized plastic material, Nema G-10.

The 1500 ml of 1.00 ± 0.01 M HCl solution for the CRV was made using concentrated reagent-grade HCl. This solution was calibrated against a standard NaOH solution by titration to the phenolphthalein endpoint.

The CTB was made from a 40 liter urethane insulated, rectangular Thermos[®] ice chest. As a test of its insulation against heat-loss, the temperature in the CRV and CTB was set at $25.000 \pm 0.005^\circ\text{C}$, as measured with an accurate thermometer. Both were covered by lids devoid of openings. After 2 hours at an ambient temperature of 23°C in the laboratory, the temperature was carefully measured at various points horizontally and vertically, avoiding any significant mixing. The CRV temperature had decreased 0.03°C and the CTB temperature 0.1°C . Both temperatures were independent of horizontal or vertical position to within 0.01°C .

In the course of the calorimetric measurements the CTB temperature was

kept within $\sim 0.1^\circ\text{C}$ of the desired temperature by means of a Thermomix controller combined with the CTB cooling coils as shown in Fig 8.

Prior to a heat-of-solution (ΔH_{soln}) measurement, the CRV temperature was maintained constant to $\pm 0.1^\circ\text{C}$ for at least 30 minutes to assure that no error was introduced by extraneous heat effects during the actual ΔH_{soln} measurement. The constancy of the CRV temperature could be observed on a chart recorder. Thus, the apparatus is really a constant heat flux calorimeter rather than an adiabatic one, since there is a very small heat-loss from the CRV which must be compensated for by the CTB.

Typically, a temperature rise in the CRV of 0.07°C would occur during a ΔH_{soln} measurement. This temperature rise from an initial equilibrium horizontal baseline to the final horizontal baseline covers more than 90 % of the chart recorder scale, giving maximum scale measurement accuracy.

The stirrer in the CRV was driven at 200 rpm by a Slo-Syn constant speed motor to maintain a thermally homogeneous acid solution. During the ΔH_{soln} measurement, the acid solution was temporarily inhomogeneous. Equilibrium was assumed to have been re-established when the temperature vs time plot on the chart recorder became horizontal again, a process that typically required ~ 10 minutes.

The complete CRV system operating with the CTB was calibrated against a standard mercury thermometer which is accurate to within 0.01°C . The CRV acid solution temperature (T_{calor}) as a function of the TB setting is shown in Figs 9 & 10. Fig 9 shows the entire temperature range for the full TB scale; Fig 10 shows the temperature range of interest, $24.50^\circ - 25.50^\circ\text{C}$, in an expanded scale.

After surface area measurement in the helix U-tube or standard sample tube, a sample was quickly removed, divided into two parts, and one part

rapidly transferred to an ampoule, shown in Fig 8, which was evacuated and sealed. This process will be referred to as vacuum ampoulization. The other part of the sample was quickly transferred to an x-ray diffractometer sample holder and scanned in the x-ray diffractometer, and then vacuum ampoulized. The two parts showed no difference in their ΔH_{soln} as measured in the solution calorimeter.

A test for sample handling error on the ΔH_{soln} , shown in App X, gave results within 5 % of the theoretical value, and is within the limits of other experimental error.

The pyrex ampoules were made from 15 cm sections of 6 mm OD / 4 mm ID pyrex glass tubing. An 18 mm diameter bulb was blown onto one end, and the bottom flattened to promote easy bursting. The bulb thickness is important, especially on the flattened bottom, which must easily break when forced against the pin of the ampoule bursting device. Too thin a bulb breaks easily during handling and vacuum ampoulization, causing loss of precious sample.

For evacuation, an ampoule was inserted into the Cajon fitting connected to the mechanical pump, shown in Fig 6. After ~ 1 torr pressure was reached, the ampoule was carefully sealed-off about 2 cm above the bulb with a small oxyacetylene torch. Sealing-off close to the bulb prevented significant amounts of the sample powder from being pushed up into the stem during the bursting operation. If sample is in the stem, the solution reaction in the CRV is slowed sufficiently to affect the accuracy of the ΔH_{soln} measurements. It was important to cool the hot lower stem near the bulb rapidly after sealing with the torch to prevent $\text{Mg}(\text{OH})_2$ decomposition or other changes of the sample. Cooling was done with a stream of compressed air, after which the ampoule was cut-away about 6 cm further up the stem and this part also

cooled the same way. Vacuum ampoulization required about 3-5 minutes.

Several blank ΔH_{soln} measurements were made using empty evacuated ampoules to determine if any heat effects are associated with bursting the evacuated ampoules in the acid solution. None were observed.

The heat of dilution resulting from the water formed as a product in the solution reactions is estimated to be within experimental error.

Reaction of the sample with the acid decreases the acid strength, so several acid strength tests were carried out for HCl solutions, both before use and after each one had been used for many solution reactions. A standard NaOH solution titration to the phenolphthalein end-point was used to measure the HCl solution strength. After 28 ΔH_{soln} measurements which included the chemical calibrations, starting with fresh HCl solution, the acid strength decreased from 1.00 M to 0.90 M. For two ΔH_{soln} measurements of partly decomposed samples and five associated chemical calibrations with V-Mg(OH)_2 , the HCl acid solution strength decreased from 1.00 M to 0.98 M.

Any change in the acid strength was corrected for by calibrations run before and after a ΔH_{soln} measurement. This correction was found from a set of two ΔH_{soln} measurements and five calibration measurements to be less than the error in the calibration of a fresh HCl solution.

A typical ΔH_{soln} measurement for a decomposed sample began with dividing the sample into approximately equal parts. The parts were then transferred into pyrex ampoules and vacuum ampoulized. Calibrations were carried out before and after ΔH_{soln} measurements using V-Mg(OH)_2 as the chemical calibration standard(App XI). A quantity of ~ 200 mg of V-Mg(OH)_2 gives almost a full sweep on the chart recorder, comparable to that of a sample run, and provides the same scale measurement accuracy. The calibration

run and the sample run were made as similar as possible to minimize error. The heat-of-solution of the MgO in the partly decomposed sample ($\Delta H_{\text{soln}}^{\text{MgO}}$) was calculated from the measured ΔH_{soln} , as shown in App XI.

The heat-of-solution of $\text{Mg}(\text{OH})_2$ ($\Delta H_{\text{soln}}^{\text{Mg}(\text{OH})_2}$) is accurately known.^{19,37,98,99} Its use is described in App XI. Powdered V- $\text{Mg}(\text{OH})_2$ was used as the calibration standard because it dissolves readily in 1 M HCl to give a rapid response in the CRV. The G- $\text{Mg}(\text{OH})_2$ responded more slowly and gave less reproducible results probably because of its larger particle size and lower porosity, which are evident from the SEM and surface area data to be discussed later.

RESULTS & DISCUSSION

K&G showed that unusually low steady-state pressures were established in Knudsen cells with 0.38 - 1.03 mm orifices regardless of whether large natural brucite flakes (10x10x0.5 mm), brucite platelets (250 - 840 μm), or commercial $\text{Mg}(\text{OH})_2$ reagent powder was used as the starting material (No particle size was reported for their commercial $\text{Mg}(\text{OH})_2$ reagent powder, but it was probably $\sim 30 \mu\text{m}$ in cross-section, like the commercial V- $\text{Mg}(\text{OH})_2$ reagent powder used in this research). K&G extrapolated measured pressures to zero orifice diameter, as shown in Fig 5a, for the brucite platelets only, but for an orifice of 1.03 mm diameter they found a close similarity to steady-state pressures for brucite flakes and commercial $\text{Mg}(\text{OH})_2$ reagent powder. This similarity implies that extrapolation to zero orifice for any of their different starting materials would yield about the same steady-state pressure. This pressure, obtained by means of the Whitman-Motzfeldt equation,^{23,24,100} when translated onto a $\text{Log } P$ vs $1/T$ plot, as shown in Fig 5b, gives from the slope, 130.5 kJ / mole (31.2 kcal / mole) as the apparent heat-of-reaction for the dehydration of $\text{Mg}(\text{OH})_2$ under Knudsen cell conditions, compared to 82.8 kJ / mole (19.8 kcal / mole) calculated from G&A thermochemical data (App I).

Data gotten at 300°C from the G- $\text{Mg}(\text{OH})_2$ synthesized in this laboratory, with Knudsen cells of different cell and orifice sizes are compared in Fig 11 to K&G's data extrapolated to the same temperature since K&G's highest temperature was 235°C. The plot of $1/P_s$ vs A_o , the cross-sectional area of the orifice, should be linear if the rate-limiting step does not change with pressure.¹⁰¹ Agreement between the extrapolated value in the present work, and in K&G's study, ~ 1 torr, is good.

A plot of $1/P_s$ vs A_o has a slope of cA_s , which yields a linear plot

if cA_s is constant. The Clausing factor^{23,24,100} of the Knudsen cell orifice is assumed to be approximately unity. If A_s can be estimated from the cell cross-sectional area or some fraction of the reactant-product surface area, the dissociation or reaction coefficient, c , can then be estimated. A low apparent value of c may result from a slow step in the decomposition reaction.^{7,8}

My data confirm K&G's data for P_{eqm} , which demonstrates that the same low apparent equilibrium pressures in the Knudsen cells with small orifices are generated whether larger $Mg(OH)_2$ flakes or $Mg(OH)_2$ powders of $\sim 30 \mu m$ average cross-section are decomposed; the phenomenon is independent of the particle size, porosity, and morphology.

Table 1 presents some effusion data of K&G, including some experimental details such as reaction temperature, physical character of the reactant, and Knudsen cell details such as cell and orifice size, and channel length. The steady-state vapor pressure, P_s , is given for different orifice sizes. In the lower part of Table 1 K&G's zero-orifice pressure, P_{eqm}^{KE} , is evaluated at 463 K and 485 K, the temperatures at which G&A made their measurements, and extrapolated to 573 K (300°C), the temperature at which the present measurements were made. It is this Knudsen effusion equilibrium vapor pressure, P_{eqm}^{KE} , that differs by four orders of magnitude from the static manometric true equilibrium vapor pressure, P_{eqm}^{SM} . Thus, $P_{eqm}^{KE} \sim 10^{-4} \cdot P_{eqm}^{SM}$.

Table 2 presents corresponding experimental details and data from my effusion experiments.

Using the P_{eqm} from my G- $Mg(OH)_2$ data in Fig 11, ~ 1 torr, obtained from the extrapolation of the Knudsen cell orifice area, A_o , to zero, the slope, $\sim 7.5 \times 10^6 \text{ torr}^{-1} \text{ m}^{-2}$, and the effective surface area of the sample, A_s , represented by the Knudsen cell cross-sectional area, $\sim 3.3 \times 10^{-4} \text{ m}^2$,

the Whitman-Motzfeldt equation in reciprocal form,

$$1/P_s = 1/P_{eqm} + A_o(1/cA_s P_{eqm}) \quad (1)$$

yields an apparent dissociation coefficient, $c \sim 4 \times 10^{-4}$. K&G obtained a value of $\sim 18 \times 10^{-4}$ under similar conditions. They report a cross-sectional area of $\sim 2.1 \times 10^{-4} \text{ m}^2$.

The total surface area for a $\sim 125 \text{ mg}$ sample of K&G brucite platelets (K-Mg(OH)_2), $550 \mu\text{m}$ across (an average of the size range $250 - 840 \mu\text{m}$) is $\sim 7.5 \times 10^{-4} \text{ m}^2$ (App XII). This is not very different from the Knudsen cell cross-sectional area used in the calculation above. If this total surface area is used to calculate c instead of the cell cross-sectional area, the result is $\sim 1.8 \times 10^{-4}$. This result is consistent with the theoretical treatments of Rosenblatt¹⁰⁰ and Searcy,⁶ which predict that for very low values of c the entire surface area of the sample would be effective in vaporization.

It appears that the magnitude of the increase in the surface area in going from reactant to product does not effect the observed Knudsen cell vapor pressures since my data with G-Mg(OH)_2 are similar to K&G's with K-Mg(OH)_2 , as shown in Fig 11. This has also been observed to be the case to some extent when comparing K&G's Knudsen cell vapor pressures for brucite flakes and brucite platelets,²² although these two starting materials are not largely different in specific surface area. G-Mg(OH)_2 and K-Mg(OH)_2 do differ significantly in specific surface area, and are the basis of the observation that vapor pressure is independent of the magnitude increase in the specific surface area. The specific surface areas of the different reactants and products estimated near 200°C along with the magnitude of increase in going from reactant to product is,

$$\begin{array}{lll} \text{G-Mg(OH)}_2: & \sim 1 \text{ m}^2 / \text{gm} & \text{G-MgO: } \sim 175 \text{ m}^2 / \text{gm} \quad 175\text{X} \\ \text{K-Mg(OH)}_2: & \sim 10^{-2} \text{ m}^2 / \text{gm} & \text{K-MgO: } \sim 175 \text{ m}^2 / \text{gm} \quad 17500\text{X} \end{array}$$

The surface area of a G-MgO sample prepared in a Knudsen cell at 300°C is estimated to be $\sim 4200 \text{ m}^2 / \text{mole}$ (Fig 28). Using Fig 31 with this value, the surface area near 200°C can be estimated by parallel extrapolation with the V-MgO data to be $\sim 7500 \text{ m}^2 / \text{mole}$. The K-MgO surface area near 200°C is assumed to be similar to that of G-MgO.

A temperature of 200°C is near the midpoint of the temperatures 190°C (463 K) and 212°C (485 K) used by G&A to obtain their equilibrium data as well as being close to the midpoint of the temperature range 145° - 235°C used by K&G to obtain their Knudsen effusion steady-state vapor pressure data (Fig 5b).

The surface area for the K-Mg(OH)₂ platelets is calculated in App XII to be $\sim 6 \times 10^{-3} \text{ m}^2 / \text{gm}$. K-Mg(OH)₂ is assumed to be similar in size and shape to G-Mg(OH)₂, and is also assumed to behave in a similar manner during decomposition to K-MgO as a result of the data in Fig 11. Thus, a $\sim 125 \text{ mg}$ sample would decompose to $\sim 86 \text{ mg}$ of K-MgO with a total surface of $\sim 15 \text{ m}^2$.

In Figs 12 & 13 are plotted the weight-loss vs time curves, both absolute and relative, for V-Mg(OH)₂ reagent powder decomposed at two temperatures. The electrobalance in the high vacuum furnace was used for these measurements. These initial weight-loss experiments were carried out to see if any uncharacteristic weight-loss phenomenon occurred during a normal decomposition in high vacuum. The temperatures of 280°C and 345°C were chosen because they are near the limits of the decomposition temperature range used throughout this research.

The measured weight-loss curves show "steps", which correspond to rapid bursts of powder sample escaping the platinum basket sample holder. At the lower temperature, 280°C, there is only one large and early "step" that accounts for ~25 % of the total weight lost (Fig 12). At 345°C, the higher temperature, there are two smaller, nearly equal "steps", one early and one near the midpoint of the decomposition, that together constitute ~10 % of the total weight lost (Fig 13).

The "steps" in the weight-loss curves shown in Figs 12 & 13 may result from localized water¹⁰² vapor pressure build-up in the compacted bed of micron-sized, partially sintered particles during decomposition. If large enough, this pressure could cause a sudden vapor burst to relieve the pressure, causing a quantity of small sample fragments and particles to escape from the sample holder. The size of the "steps" as well as their occurrence during the decomposition appears to be random. A small orifice Knudsen cell might significantly reduce or eliminate the observation of this effect, which may still be occurring though undetectable in a weight-loss experiment. The influence of water vapor pressure in powder beds on the decomposition process is discussed by others.^{39,42}

As can be deduced from the equations given in Figs 12 & 13, the corrections for these powder losses shift these corrected relative weight-loss curves, particularly near the end of the decomposition, causing more deviation from the theoretical weight-loss limit. These corrected curves now show the sigmoid shapes which are considered characteristic of isothermal decomposition.^{4,5}

Others^{27,38,51,52,59,62} have done extensive kinetic research on $\text{Mg}(\text{OH})_2$ decomposition, using both brucite of various particle sizes as well as chemically prepared $\text{Mg}(\text{OH})_2$ reagent powder. Induction and acceleratory

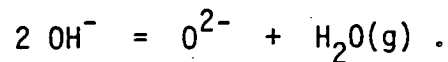
periods were observed in some cases,^{27,51,52} and not in others.³⁸ Where it has been observed,^{51,52} it was stipulated that it was not a result of the time required for sample heating. My weight-loss kinetic data (Figs 12 & 13) do show an initial induction-acceleratory period, but I attribute this apparent induction effect to sample heating time.

Some of my data from Table 2 has been plotted in Fig 27 to illustrate the effect of the extent of decomposition, X_{MgO} , on the steady-state pressure, P_s , for G-Mg(OH)₂ at 300°C. Plotted are the results for a Knudsen cell fitted with a 1.80 mm diameter orifice, and for an open cell 20.5 mm in diameter. The P_s in the closed cell is about 100 times larger than in the open cell. The vapor escapes rapidly from the open cell, and the P_s given is the same as the measured system pressure.

For the cell fitted with the orifice, the dependence of P_s on X_{MgO} at the beginning is probably a result of sample heating time rather than any initial hindered kinetic process. A rapid sample heating would give a more nearly ideal continuous decomposition profile, yielding an almost instantaneous rise of P_s to a constant value as shown in Fig 27 by the dashed line. The gradual decline in the actual P_s near the end of the decomposition may result from a combination of decreasing reactant surface area as the Mg(OH)₂ particle shrinks and is covered with a MgO product layer, and hindrance caused by diffusion of water vapor through this product layer.

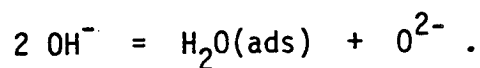
Decomposition of Mg(OH)₂ does not proceed at measurable rates past ~95 %, unless the sample is heated above about 400°C. At 650°C almost 100 % decomposition is achieved. Similar results were observed by others.³⁷ The ~5 % retained water corresponds to 24-30 % of a monolayer of water on the high surface area V-MgO, and 44-76 % of a monolayer on G-MgO (App XVI). Presumably the MgO surface anions are largely OH⁻ ions which must desorb

as water by the reaction,



Even heating at $\sim 900^\circ\text{C}$ is not sufficient to remove all the water present as OH^- ions.¹⁰³ When the MgO is re-heated above $\sim 2000^\circ\text{C}$, some of the OH^- ions are still present apparently associated with Mg defects.¹⁰³

The adsorption energy holding OH^- groups to the MgO surface is much higher than for water molecules, but it has been suggested that the persistence of the OH^- ions may not be a result of high adsorption energy, but the difficulty in bringing widely-spaced OH^- groups together to form water molecules according to the reaction,



Different mechanisms of OH^- combination reactions to form the less strongly adsorbed water molecule are discussed by Freund.⁵³ Others¹⁰⁴⁻¹¹⁰ have also discussed in detail the various theoretical and experimental aspects of adsorption on MgO .

Scanning Electron Microscopy (SEM)

SEM micrographs were taken of each of the two different starting materials before decomposition was started and after it was nearly complete. The two different methods of preparing SEM samples gave similar results when viewed at high magnification (2000X - 5000X), but at low magnification (100X - 500X) the CCl_4 suspension method showed a more uniform general particle distribution over the sample holder surface compared to the powder dusting application method.

Figs 14, 15, & 16 are samples made from $\text{V-Mg}(\text{OH})_2$ decomposed in the low

vacuum U-tube apparatus at 310°C. Fig 14a shows the V-Mg(OH)₂ before any decomposition occurs, and Fig 14b shows the same starting material ~95 % decomposed. There is no significant difference in the appearance. Fig 15 shows at much higher magnification the particle surface morphology of the V-Mg(OH)₂ before decomposition, and in Fig 16, after ~95 % decomposed. There appears to be no significant difference in particle surface morphology at this higher magnification as well.

Figs 17, 18, & 19 are samples made from G-Mg(OH)₂ decomposed in an open alumina cell in the high vacuum furnace at 300°C. Again, Fig 17a shows the undecomposed G-Mg(OH)₂, and Fig 17b the same material ~95 % decomposed. Both are alike in appearance. Figs 18 & 19 show that again the surface morphology does not appear to change significantly from the undecomposed G-Mg(OH)₂ to the ~95 % decomposed G-Mg(OH)₂.

X-Ray Diffraction(XRD)

Using the two different starting materials, XRD spectra were taken before decomposition was begun, about half decomposed, and nearly completely decomposed. Both FeK α and CuK α radiations at their highest resolution were used to scan for anomalous x-ray reflections. Only known reflections for Mg(OH)₂ and MgO were observed (App VIII) regardless of the starting material, apparatus, temperature, or degree of vacuum over the sample. XRD spectra for G-Mg(OH)₂, and partial and nearly completely decomposed G-Mg(OH)₂ are shown in Figs 20 - 22. CuK α radiation was used. The samples for XRD spectra were prepared in a small-orifice alumina Knudsen cell. Corresponding spectra for the V-Mg(OH)₂ samples decomposed in the helix U-tube apparatus at lower vacuum are not shown; these spectra also showed no additional reflections that might indicate intermediate phases or

impurity phases.

Annealing at increasingly higher temperatures up to 1000°C produced no anomalous x-ray reflections. Decreasing FWHM and increasing peak height, or peak sharpening, resulted from this annealing process. These results imply increasing crystallinity, which is also indicated by the decreasing $IB_{(200)}^V$, as shown in Fig 23.

The d-spacings calculated from the spectra for V-Mg(OH)₂, V-MgO, G-Mg(OH)₂, and G-MgO, regardless of radiation or resolution used, agreed with the ASTM / JCPDS values given along with them in App VIII. The d-spacings remained constant as a function of the extent of decomposition, time at low temperature annealing, and time and temperature at high temperature annealing. Sample preparation in a Knudsen cell made no difference.

Both V-Mg(OH)₂ and V-MgO have broader peaks than G-Mg(OH)₂ and G-MgO. The broader peaks may be a result of small particle size⁷⁵ or induced strain⁷⁹ incurred during the reaction. App XIII compares my MgO particle size data with those of Eubank,⁵⁸ who used different techniques of measurement as well as different times and temperatures of preparation. The V-Mg(OH)₂ and V-MgO particles observed by SEM range from ~5 μm to ~25 μm cross-section; the G-Mg(OH)₂ and G-MgO particles from ~2 μm to ~20 μm, with much larger hexagonal plate-like particles (Fig 17) having a diameter of ~350 μm. The dimensions calculated from XRD data, assuming negligible strain, are approximately ~40 Å to ~100 Å. The comparisons imply that the particles observed in SEM photographs are polycrystalline. Particle size calculation from surface area measurements (App XIV) yield approximately the same dimensions (App XIII).

For both starting materials, the (200)MgO principal peak is visible

when only ~8 % of the water has been removed (Fig 24), and the peak area measured as a function of composition extrapolates to zero at $X_{\text{MgO}} = 0$. This observation implies that the $\text{Mg}(\text{OH})_2$ phase does not lose a significant fraction of its water content before the MgO phase nucleates. The (101) $\text{Mg}(\text{OH})_2$ principal peak of either starting material disappears prior to complete decomposition as shown in Fig 24. The early disappearance of the (101) $\text{Mg}(\text{OH})_2$ peak might result because the $\text{Mg}(\text{OH})_2$ particles are covered with a layer of MgO thick enough to reduce the x-rays penetration. Another possibility will be suggested after surface area measurements have been reviewed.

The (200)MgO peaks increase in height as the decomposition proceeds, but the FWHM remains essentially constant. This is indicated in Fig 24 by the values in parentheses, and in App IX.

Fig 25 shows modest decreases in integral breadth and surface area with time of heating at 345°C, with the FWHM remaining relatively constant. But both integral breadths and surface areas markedly decrease with annealing temperature at which MgO samples were held for from 1 to 15 hour periods (Fig 23). When MgO has been annealed at 1000°C for 13 hours (Fig 25), there is a decrease in S_{BET} from 14,000 to 2700 m^2 / mole ; a further annealing period of 15 hours at 1000°C causes no further change in the surface area(Fig 25).

The (101) $\text{Mg}(\text{OH})_2$ and (200)MgO peak areas and heights at a given point in the decomposition are smaller for V- $\text{Mg}(\text{OH})_2$ and V-MgO than for G- $\text{Mg}(\text{OH})_2$ and G-MgO (Fig 24), whereas the FWHM's shown in Fig 24, and the integral breadths shown in Fig 26, are smaller for G- $\text{Mg}(\text{OH})_2$ and G-MgO than for V- $\text{Mg}(\text{OH})_2$ and V-MgO. These observations are evidence that G- $\text{Mg}(\text{OH})_2$ and G-MgO are formed of larger crystals than are V- $\text{Mg}(\text{OH})_2$ and V-MgO. This agrees with SEM data (Figs 14-19) and the surface area data (Fig 28).

For $\text{Mg}(\text{OH})_2$ the $\text{IB}_{(101)}$ does not change appreciably during the decomposition, as shown in Fig 26. For the high vacuum decomposition, the $\text{V-Mg}(\text{OH})_2$ curve is approximately the same distance above the $\text{G-Mg}(\text{OH})_2$ curve as the V-MgO is above the G-MgO (Fig 26), probably because of smaller crystals and lower order in the $\text{V-Mg}(\text{OH})_2$ and V-MgO than in the $\text{G-Mg}(\text{OH})_2$ and G-MgO .

The $\text{IB}_{(200)}^{\text{V}}$ and $\text{IB}_{(200)}^{\text{G}}$ for MgO are not as constant as $\text{IB}_{(101)}^{\text{V}}$ and $\text{IB}_{(101)}^{\text{G}}$ for $\text{Mg}(\text{OH})_2$ for most of the decomposition, as shown in Fig 26. They both decrease just prior to complete decomposition, perhaps because in that same composition range, where $\text{Mg}(\text{OH})_2$ peaks are not observed, removal of water from the MgO phase or its surface increases the crystallinity.

The $\text{IB}_{(200)}$ for the V-MgO prepared in a relatively low vacuum in the helix U-tube is greater than that for the G-MgO prepared in a Knudsen cell or in an open cell in a high vacuum environment, probably because the integral breadths are influenced by the relative dimensions of the $\text{Mg}(\text{OH})_2$ crystallites from which the MgO is formed. The integral breadth for G-MgO formed in the Knudsen cell is somewhat less than that for the G-MgO formed in an open crucible. This difference probably results because the substantially higher steady-state water vapor pressure, $\sim 50 \times 10^{-3}$ torr (~ 6.7 Pa), in the closed cell catalyzes the MgO crystallization reaction³⁹⁻⁴¹ over that in the open crucible, in which the H_2O pressure is $\sim 30 \times 10^{-5}$ torr (~ 0.04 Pa), which is 2 orders of magnitude closer to the system pressure of $\sim 2 \times 10^{-5}$ torr (~ 0.003 Pa). This is shown in Fig 27.

Surface Area (S_{BET})

A linear increase in the molar surface area as a function of the extent of the decomposition reaction is shown by the plot in Fig 28. Although the

slopes differed, both $V\text{-Mg(OH)}_2$ and $G\text{-Mg(OH)}_2$ showed linear behavior. This linearity indicates that the surface area per mole of MgO is constant and independent of the extent of the decomposition for a particular Mg(OH)_2 starting material; sintering was negligible under the conditions of time and temperature of the decomposition (Fig 25).

There is a clear temperature dependence for the $V\text{-Mg(OH)}_2 / V\text{-MgO}$ system that indicates larger surface areas for lower reaction temperatures. An opposite temperature dependence is observed for the $G\text{-Mg(OH)}_2 / G\text{-MgO}$ system (Fig 28), which may be a result of the two very different experimental conditions used for the $G\text{-Mg(OH)}_2$ decomposition there, whereas the $V\text{-Mg(OH)}_2$ has been decomposed under identical conditions at the different temperatures. The higher temperature $G\text{-Mg(OH)}_2$ decomposition shown in Fig 28 was carried out in a U-tube, but the lower temperature $G\text{-Mg(OH)}_2$ decompositions were carried out in a closed Knudsen cell and the same Knudsen cell with the lid removed. It would be expected that the open crucible and U-tube would be essentially experimentally identical since their diameters were approximately the same. The U-tube was made of quartz and the open crucible of alumina, which may have insignificantly affect the initial sample heating or measured sample temperature.

The only other significant experimental difference for the $G\text{-Mg(OH)}_2$ decomposition in Fig 28 was the ambient pressure over the sample. For the U-tube it was ~ 2.0 torr (~ 267 Pa) compared to $\sim 2 \times 10^{-5}$ torr (~ 0.003 Pa), the system pressure, for the open crucible. Fig 27 compares the steady-state pressures during continuous decomposition in the open cell ($\sim 30 \times 10^{-5}$ torr) and closed Knudsen cell ($\sim 50 \times 10^{-3}$ torr) at the same system pressure ($\sim 2 \times 10^{-5}$ torr), indicating that the open cell steady-state pressure increases an order of magnitude above system pressure, and that during

continuous decomposition it is this steady-state pressure that is the effective ambient pressure over the sample, not the system pressure. Thus, allowing for the tenfold pressure increase during continuous decomposition, the 2.0 torr system pressure would create a higher water vapor pressure above the $G\text{-Mg}(\text{OH})_2 / G\text{-MgO}$ sample than would the $\sim 2 \times 10^{-5}$ torr system pressure. Thus, water vapor catalysis of the $G\text{-MgO}$ crystallization reaction^{39,40,42} could be responsible for a more rapidly formed, less porous, and larger particle $G\text{-MgO}$ product to yield lower surface areas at lower temperatures rather than at higher temperatures as with $V\text{-Mg}(\text{OH})_2$ decomposition in the U-tube as shown in Fig 28.

Although the surface area is substantially different for each different starting material and its product, when they are each decomposed at $260^\circ\text{-}350^\circ\text{C}$ to between 82-98 mole % , their respective surface areas do not indicate a large or proportional change, as shown in Table 3. A correlation of the percent retained water with the surface area of MgO along with the disappearance of the $(101)\text{Mg}(\text{OH})_2$ XRD peak before all the water has been driven off could suggest a "surface phase" of adsorbed water molecules. But there is no correlation below 350°C as shown by my data in Table 3. Above 380°C it has been shown³⁷ that there is a correlation between retained water and surface area with preparation temperature (Table 4).

FWHM's for the $\text{Mg}(\text{OH})_2$ and for the MgO (Fig 24 & App IX) remain relatively unchanged as a function of the extent of decomposition for both reactant and product. Annealing the MgO at 345°C for two weeks does not significantly decrease the FWHM or $\text{IB}_{(200)}^V$ (Fig 25), although the surface area is decreased by $\sim 50\%$ of the difference between the initial and annealed values under the same conditions. Thus, the decrease in

surface area appears to be caused by pore closure rather than increased particle size.

The large FWHM for the MgO may result from small particle size, $\sim 100 \text{ \AA}$, and not particle strain because particle size calculations based on surface area, shown in App XIV, give approximately the same values for particle sizes as do calculations based on my x-ray diffraction data, shown in App XIII. Furthermore, if the larger FWHM had been a result of significant strain, there would probably have been a large decrease in the FWHM as a result of relieving the strain during the long anneal at 345°C , but this would not affect the surface areas significantly.

For decomposition temperatures of 300°C and 310°C the surface area vs time curves in Fig 29 are similar for the two different starting materials. The weight-loss kinetic curve for V-Mg(OH)₂ at 345°C (Fig 13) is also similar to its counterpart in Fig 29. The surface area kinetic curves and relative weight-loss kinetic curves are directly compared for identical experimental conditions in Fig 30. The similarity of shapes between the two kinds of curves suggests a relationship between the rate of development of surface area and the rate of weight-loss. Fig 29 indicates that V-Mg(OH)₂ decomposes faster, creating a larger surface area V-MgO product than does G-Mg(OH)₂ to G-MgO.

Gordon⁵² did extensive weight-loss studies on brucite as a function of time at various temperatures, and the shapes of his curves were similar to those I obtained at similar temperatures.

The development of surface area during decomposition from a theoretical standpoint is discussed by Nicholson.¹¹¹

The difference in the surface areas of the two starting materials, shown in Fig 28, reflects the difference in their particle size, which

is evident from the SEM micrographs shown in Figs 14a & 17a. The even larger difference in the surface area for the completely decomposed materials, $X_{\text{MgO}} = 1.00$, probably reflects a difference in the sizes of the crystallites that make up the particles (Figs 14b & 17b).

Calorimetrically, the different starting materials give different heats-of-solution (App XI). They are ~ 111.98 kJ / mole for G-Mg(OH)₂ and ~ 113.13 kJ / mole for V-Mg(OH)₂. The larger surface area of the latter (Fig 28 & App XV) is probably the principal contributor to this difference, although this difference is within experimental error.

A value for the specific surface energy for Mg(OH)₂ of ~ 330 mJ / m² has been given in the literature.^{112,113} Others^{112,114} discuss some methods for estimating the surface tension or specific surface energy of these or similar materials.

Despite the surface area difference of the two starting materials, my thermogravimetry data (Figs 11 & Table 2) indicate similar steady-state pressures. X-ray and SEM data, already discussed, show that G-Mg(OH)₂ has a larger particle size than V-Mg(OH)₂. The SEM micrographs also show different particle size distributions and particle surface morphology between G-M-(OH)₂ and V-Mg(OH)₂. These data imply that the V-Mg(OH)₂ is more porous than G-Mg(OH)₂, which agrees with what the surface area data suggest (Fig 28).

Since the V-Mg(OH)₂ decomposition produces a steeper slope in Fig 28 than the G-Mg(OH)₂ decomposition, the surface area per mole of V-MgO, although a constant value as the decomposition proceeds, is greater than that of G-MgO, which also has a constant, but different, value under similar decomposition conditions. Compare the data in Fig 28 at 345°C and 350°C respectively.

The $\text{Mg}(\text{OH})_2$ vacuum decomposition is so slow near 200°C , the G&A decomposition temperature region, that preparation of the amounts of product required for accurate surface area measurements would require extremely long times. Extrapolating the surface areas for both V-MgO and G-MgO at higher decomposition temperatures to the lower temperature G&A region gives an estimate of their surface areas in this region (Fig 31). The G&A extrapolation in Fig 31 is made from one measurement at 350°C by assuming parallel slopes. This assumption is based on the similarity of the surface area vs temperature curves for the two different materials shown in Fig 23, and the surface area vs time curves in Fig 29. With the estimated surface area, it was possible to approximate the total surface energy, E_{surf} , in the G&A temperature region using values for the MgO specific surface energy that are close to the theoretical and experimentally measured values as given by Boffi and Ricci¹¹⁵ (App XV). The equation for calculating the E_{surf} is also given in App XV.

The molar surface area at 200°C is estimated from Fig 31 to be $\sim 10,500 \text{ m}^2 / \text{mole}$ of G-MgO when extrapolated from the datum at 350°C . If the maximum specific surface energy is taken as near the theoretical value of $\sim 1500 \text{ mJ} / \text{m}^2$, an E_{surf} of $\sim 15.8 \text{ kJ} / \text{mole}$ for G-MgO is calculated.

Using the smallest value for the G-MgO molar surface area from Fig 28, $\sim 3000 \text{ m}^2 / \text{mole}$ of G-MgO, for material decomposed at 300°C , a molar surface area is estimated from Fig 31 to be $\sim 6000 \text{ m}^2 / \text{mole}$ of G-MgO at 200°C . This gives a maximum E_{surf} of $\sim 9.0 \text{ kJ} / \text{mole}$ of G-MgO for the same specific surface energy as above. Thus, the range of E_{surf} at 200°C is $9.0 - 15.8 \text{ kJ} / \text{mole}$ for G-MgO. For V-MgO a value of $\sim 28.0 \text{ kJ} / \text{mole}$ is calculated from an extrapolated molar surface area of $\sim 18,700 \text{ m}^2 / \text{mole}$

of V-MgO.

The E_{surf} for annealed MgO is ~ 2.5 kJ / mole for G-MgO and ~ 4.0 kJ / mole for V-MgO. Hence, the change in the total surface energy, ΔE_{surf} , on decomposition at 200°C is $\sim 6.5 - 13.3$ kJ / mole for G-MgO and ~ 24.0 kJ / mole for V-MgO.

The specific surface energy would have to be at least ~ 3000 mJ / m² to yield the ~ 48 kJ / mole required to explain a factor of $\sim 10^4$ difference in the vapor pressures at 200°C in terms of the solid MgO total surface energy, $E_{\text{surf}}^{\text{MgO}}$. This high value could be expected only if a much higher energy plane than (100)MgO or a combination of such planes were exposed during the MgO formation from the decomposition, but this is unlikely to occur since the (100)MgO plane is electrically neutral and a stable equilibrium plane.

Solution Calorimetry ($\Delta H_{\text{soln}}^{\text{MgO}}$)

MgO heat-of-solution ($\Delta H_{\text{soln}}^{\text{MgO}}$) data collected by various researchers over many years^{37,73,98,116} are compared in Fig 32, which plots the $\Delta H_{\text{soln}}^{\text{MgO}}$ at 25.0°C against the temperature at which the MgO was prepared. A few samples were prepared in vacuum, denoted by v in Fig 32, but most were prepared in air. None were prepared in Knudsen cells. The $\Delta H_{\text{soln}}^{\text{MgO}}$ approaches a constant value near higher temperatures of decomposition or annealing as shown in Fig 32. This result is consistent with my data plotted in Fig 23, which show that as MgO anneals, the surface area and integral breadth also decrease to a constant value. Fig 32 shows ~ 15 kJ / mole of MgO difference in $\Delta H_{\text{soln}}^{\text{MgO}}$ between the highest, 1400°C , and the lowest, 200°C , temperature. This probably represents only a surface area effect, since the value closely corresponds to that for

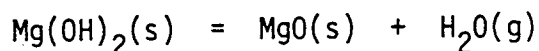
ΔE_{surf} at 200°C that was calculated previously from extrapolated surface areas. This can be shown by calculating an average specific surface energy, γ , for the MgO used in these kinds of ΔH_{soln} experiments using differences in $\Delta H_{\text{soln}}^{\text{MgO}}$ with temperature from Fig 32, and the estimated corresponding surface area differences from Fig 23 for G-MgO. The average specific surface energy calculation is shown in the lower portion of App XV. A value of $\sim 1750 \text{ mJ} / \text{m}^2$ is obtained, which is close to the $\sim 1500 \text{ mJ} / \text{m}^2$ used as the maximum value for (100)MgO used to calculate the E_{surf} values also shown in App XV. Various investigators have theoretically calculated^{115,117-119} or experimentally measured^{84,114} the specific surface energy of MgO.

The plot of $\Delta H_{\text{soln}}^{\text{MgO}}$ as a function of the extent of decomposition, X_{MgO} , shown in Fig 33, indicates that within the $\sim 15 \text{ kJ} / \text{mole}$ scatter in the data there is no dependence of the heat-of-solution of the solid reaction product on the extent of reaction, and the samples prepared in open crucibles did not have significantly higher heats-of-solution than those prepared in Knudsen cells. Thus, the degree of vacuum or $P_{\text{H}_2\text{O}}$ over the sample has no significant effect on the measured $\Delta H_{\text{soln}}^{\text{MgO}}$. The dashed line in Fig 33 is the heat-of-solution for an annealed sample of MgO that is taken as the macrocrystalline equilibrium MgO at true equilibrium. This true equilibrium is taken to correspond closely to that of Giauque and Archibald. Thus, this heat-of-solution is taken as the reference state to which MgO prepared in Knudsen cells as well as in open crucibles is compared. The NBS value indicated in Fig 33 was calculated from NBS thermochemical data¹²⁰ for a sample of low surface area MgO(c) (App III). Clearly, under Knudsen cell conditions the solid product of $\text{Mg}(\text{OH})_2$ decomposition does not show the excess heat-of-solution

of ~ 48 kJ / mole of MgO which is required to explain the large difference in the observed and calculated vapor pressures. The explanation lies elsewhere.

GENERAL DISCUSSION

The measurements reported here eliminate a number of possible explanations of the discrepancy between the apparent heat-of-reaction for,



calculated from Knudsen cell data, and that calculated from static manometry and calorimetry data. Calorimetry data had been obtained from the static manometry samples. The possibility that the discrepancy arose because the Mg(OH)_2 used in the Kay and Gregory study or the MgO produced by its decomposition in Knudsen cells was in some manner profoundly different in properties from the Mg(OH)_2 or MgO for which the static manometry and calorimetry measurements had been made was eliminated by carrying out measurements as a function of the extent of reaction on the same Mg(OH)_2 starting material for which the latter measurements were made.

My effusion results agreed both in terms of the steady-state pressure, P_s , and the condensation coefficient, c , with those reported before. Kay and Gregory give a very low value of c irrespective of the effective surface area, A_s , determined by varying Knudsen cell geometry, and is consistent with what I obtain if the total surface area of the sample of brucite platelets for an average sample size is used instead of the cell cross-sectional area in the condensation coefficient calculation previously discussed. A low value of the condensation coefficient is an experimental manifestation of a kinetic barrier in the decomposition process

The very low P_s that I obtained decomposing G-Mg(OH)_2 at 300°C under Knudsen cell conditions very similar to those used by Kay and Gregory when

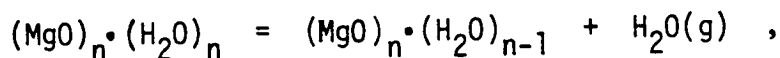
their data at 235°C (their maximum decomposition temperature) was linearly extrapolated to 300°C in Fig 4, confirms their observations of very low pressures and establishes that the phenomenon is independent of the starting material used. This is shown in Fig 11.

SUMMARY & CONCLUSIONS

Kay²² demonstrated that the zero-orifice extrapolation for the $\text{Mg}(\text{OH})_2$ decomposition does not yield H_2O pressures consistent with known thermodynamic data for the reaction, $\text{Mg}(\text{OH})_2(\text{s}) = \text{MgO}(\text{s}) + \text{H}_2\text{O}(\text{g})$. The agreement of my Knudsen cell data with those of Kay means that the zero-orifice extrapolation used for brucite platelets can be extended to a reagent powder. More importantly, the agreement demonstrates that the low steady-state pressures observed when decomposing $\text{Mg}(\text{OH})_2$ in small orifice Knudsen cells is a general phenomenon for $\text{Mg}(\text{OH})_2$ decomposition under those conditions, and is thus independent of the way in which the starting material was formed or prepared. The decomposition kinetics, therefore, do not depend on reactant or product particle size, particle size distribution, porosity, gross particle morphology, or particle surface morphology.

The low H_2O equilibrium pressures in effusion cells would be consistent with a decomposition reaction that yields a metastable form of MgO or a metastable $\text{MgO} - \text{H}_2\text{O}$ solid solution as indicated by MgO^* in Fig 34.

If, in Fig 4, the data of Giauque and Archibald and Kay and Gregory are extrapolated to zero ordinate ($1/T = 0$), the intercepts for the two plots are very close, indicating that the standard entropy change in the Knudsen cell measurements of Kay and Gregory is nearly the same as found for the equilibrium system of Giauque and Archibald. This is consistent with the thesis that the apparent equilibrium in effusion cell experiments can be of the type,¹⁰¹



because the entropies of reaction depend primarily on the number and kinds

of gas molecules produced or consumed in a reaction.

The only product phase identifiable by x-ray diffraction is normal MgO, and my calorimetric data give no indication of the existence of the ~48 kJ / mole of energy that could account for the presence of a metastable phase^{7,26,81-84} in any significant amounts. Perhaps the solid product of the reaction which produces the measured H₂O pressures in effusion cells could be a transient metastable MgO or Mg(OH)₂ - MgO solid solution¹⁰¹ (Fig 34) in significant quantity. Perhaps it forms in small volume elements during the decomposition and returns to the nearly completely stable MgO by a rapid exothermic process when internal strains trigger a martensitic-type transformation.⁴⁹ The blow-out of sample which was sometimes observed (Figs 12 & 13) after a steady-state decomposition had been established may indicate that an unstable phase is formed during decomposition. Such an unstable phase might usually transform into small volume elements, expelling retained water without sufficient force to cause sample blow-out, but could sometimes have the local transformation generate sufficient heat to initiate nearly simultaneous transformation through enough of the sample to expel enough retained water to cause blow-out.

A metastable phase that decomposes and creates thermal strains during temperature cycling would perhaps explain the increase in P_s, when even for a short time, the sample heating was temporarily discontinued, as was observed by Kay and Gregory. The initial P_s on resumption of heating was much higher than P_s at the time the sample heating was interrupted. This effect could be reproduced many times

An alternate explanation might be the transient formation or exposure of higher energy surfaces such as the (111)MgO, during the continuous

decomposition in the Knudsen cell. These surfaces rapidly vanish when the MgO statically equilibrates for even a very short time during the sample transfer. This could involve rapid sub-monolayer water molecule adsorption on the exposed high energy surfaces when the continuous decomposition reaction ceases, lowering their energy to very near that of the true equilibrium state. A change in some of the properties of the MgO surfaces exposed during the decomposition such as specific surface energy or surface defects may also contribute to the explanation.

REFERENCES

1. O. Bowles, "The Lime Industry," U.S. Bur. Mines Info. Circ. 7651 (1952).
2. J. Johnston, "Über die Dissociationsdrucke einiger Metallhydroxyde und Carbonate," Z. Phys. Chem. 62 330 (1908).
3. K.L. Mampel, "Die Zeitzumsatzformeln für ein Pulver aus kugelförmigen Teilchen," Z. Phys. Chem. A187 235 (1940).
4. W.E. Garner, "Kinetics of Endothermic Solid Reactions," Chap. 8, in Chemistry of the Solid State, W.E. Garner (ed.), Academic Press 1955.
5. D.A. Young, Decomposition of Solids, Chap. 3, "Endothermic Decompositions," Pergammon Press 1966.
6. A.W. Searcy, "Kinetics of Evaporation & Condensation Reactions," Chap. 6, in Chemical & Mechanical Properties of Inorganic Materials, A.W. Searcy, D.V. Ragone, & U. Colombo (eds.), Wiley-Interscience 1970.
7. A.W. Searcy & D. Beruto, "Kinetics of Endothermic Decomposition Reactions. I. Steady-State Chemical Steps," J. Phys. Chem. 80 425 (1976).
8. A.W. Searcy & D. Beruto, "Kinetics of Endothermic Decomposition Reactions. II. Effects of the Solid & Gaseous Products," J. Phys. Chem. 82 163 (1978).
9. F. Rinne, "Über den Dimorphismus der Magnesia," Z. Dtsch. Geol. Ges. 43 231 (1891).
10. C.D. West, "Structure of the Dehydrated Pseudomorph of Brucite after Chrysotile," Am. Mineral. 17 316 (1932).
11. C.D. West, "Orientation of Crystallites in the Ignition Products of $Mg(OH)_2$ & $Ca(OH)_2$," Am. Mineral. 19 281 (1934).
12. J. Garrido, "Sur la brucite fibreuse," Z. Krist. 95 189 (1936).
13. J. Garrido, "The Development of Twinning in the Dehydration of Brucite," Am. Mineral. 36 773 (1951).

14. G.J.F. MacDonald, "The Gibbs Free Energy of Water at Elevated Temperatures & Pressures with Applications to the Brucite-Periclase Equilibrium," *J. Geol.* 63 244 (1955).
15. G.C. Kennedy, "The Brucite-Periclase Equilibrium," *Am. J. Sci.* 254 567 (1956).
16. D.M. Roy & R. Roy, "A Re-Determination of Equilibria in the System MgO-H₂O & Comments on Earlier Work," *Am. J. Sci.* 255 574 (1957).
17. W.S. Fyfe, "A Further Attempt to Determine the Vapor Pressure of Brucite," *Am. J. Sci.* 256 729 (1958).
18. M.C. Ball & H.F.W. Taylor, "The Dehydration of Brucite," *Miner. Mag.* 32 754 (1961).
19. W.F. Giauque & R.C. Archibald, "The Entropy of Water from the Third Law of Thermodynamics: The Dissociation Pressure & Calorimetric Heat of Reaction $Mg(OH)_2 = MgO + H_2O$. The Heat Capacities of $Mg(OH)_2$ & MgO from 20 to 300°K," *J. Am. Chem. Soc.* 59 561 (1937).
20. The Scientific Papers of William F. Giauque from 1923-1949, Dover 1969.
21. E. Kay & N.W. Gregory, "Applicability of the Knudsen Effusion Method to the Study of Decomposition Reactions. The Decomposition of $Mg(OH)_2$," *J. Phys. Chem.* 62 1079 (1958).
22. E. Kay, "The Applicability of the Knudsen Effusion Method to the Study of Decomposition Reactions. The $Mg(OH)_2$ -MgO-H₂O & NaOH-Na₂O-H₂O Systems," PhD Dissertation, Chemistry, University of Washington, Seattle, March 1958.
23. K.D. Carlson, "The Knudsen Effusion Method," Chap. 6, in The Characterization of High Temperature Vapors, R.C. Paule & J.L. Margrave (eds.), Wiley 1967.
24. E.D. Cater, "The Knudsen Effusion Method at 69: Current State of the Art," NBS Special Publication 561, pp 3-38, October 1978.

25. N.W. Gregory & R.H. Mohr, "The Equilibrium $2\text{LiOH}(s) = \text{Li}_2\text{O}(s) + \text{H}_2\text{O}(g)$," J. Am. Chem. Soc. 77 2142 (1955).
26. E.K. Powell & A.W. Searcy, "The Kinetics & Thermodynamics of the Decomposition of Dolomite to a Metastable Solid Product," J. Am. Ceram. Soc. 61 216 (1978).
27. S.J. Gregg & R.I. Razouk, "The Kinetics of Thermal Decomposition of $\text{Mg}(\text{OH})_2$," J. Chem. Soc. S36 (1949).
28. S.J. Gregg, "The Production of Active Solids by Thermal Decomposition. Part I. Introduction," J. Chem. Soc. 3940 (1953).
29. S.J. Gregg, R.K. Packer, & K.H. Wheatley, "The Production of Active Solids by Thermal Decomposition, Part V. The Sintering of Active MgO ," J. Chem. Soc. p.46 (1955).
30. S.J. Gregg & R.K. Packer, "The Production of Active Solids by Thermal Decomposition. Part VI. The Calcination of $\text{Mg}(\text{OH})_2$," J. Chem. Soc. p.51 (1955).
31. R.I. Razouk & R.Sh. Mikhail, "The Sorption of H_2O Vapor on MgO ," J. Phys. Chem. 59 636 (1955).
32. R.I. Razouk & R.Sh. Mikhail, "The Hydration of MgO from the Vapor Phase," J. Phys. Chem. 62 920 (1958).
33. R.I. Razouk & R.Sh. Mikhail, "Surface Properties of MgO ," J. Phys. Chem. 61 887 (1957).
34. R.I. Razouk & R.Sh. Mikhail, "Surface Properties of MgO . II," J. Phys. Chem. 63 1050 (1959).
35. D.R. Glasson, Reactivity of Lime & Related Oxides. IX. Production of Activated Lime & Magnesia," J. Appl. Chem. 13 111 (1963).
36. D.R. Glasson, "Reactivity of Lime & Related Oxides. IX. Hydration of MgO ," J. Appl. Chem. 13 119 (1963).

37. D.T. Livey, B.M. Wanklyn, M. Hewitt, & P. Murray, "The Properties of MgO Powders Prepared by Decomposition of $Mg(OH)_2$," Trans. Brit. Ceram. Soc. 56 217 (1957).
38. P.J. Anderson & R.F. Horlock, "Thermal Decomposition of $Mg(OH)_2$," Trans. Faraday Soc. 58 1993 (1962).
39. R.F. Horlock, P.L. Morgan, & P.J. Anderson, "Effects of Water Vapor on the Decomposition of $Mg(OH)_2$," Trans. Faraday Soc. 59 721 (1963).
40. P.J. Anderson & P.L. Morgan, "Effects of Water Vapor on the Sintering of MgO," Trans. Faraday Soc. 60 930 (1964).
41. P.J. Anderson, R.F. Horlock, & J.F. Oliver, "Interaction of Water with the MgO Surface," Trans. Faraday Soc. 61 2754 (1965).
42. P.J. Anderson, R.F. Horlock, & R.G. Avery, "Some Effects of Water Vapor During the Preparation & Calcination of Oxide Powders," Proc. Brit. Ceram. Soc. 3 33 (1965).
43. R.K. Webster, T.L. Jones, & P.J. Anderson, "Proton Magnetic Resonance Studies of Adsorbed Water on MgO," Proc. Brit. Ceram. Soc. 5 153 (1965).
44. N.H. Brett & P.J. Anderson, "Mechanism of Decomposition of Brucite," Trans. Faraday Soc. 63 2044 (1967).
45. P.J. Anderson & R.F. Horlock, "Heats of Adsorption on Microporous MgO Powders," Trans. Faraday Soc. 65 251 (1969).
46. J.F. Guilliatt & N.H. Brett, "Crystallite Size & Shape Relationships in the Product-Precursor Pair $MgO-Mg(OH)_2$," Philos. Mag. 23 647 (1971).
47. W.H. Rhodes & B.J. Wuensch, "Relation Between Precursor & Microstructure in MgO," J. Am. Ceram. Soc. 56 495 (1973).
48. J-C. Niepce, G. Watelle, & N.H. Brett, "Product Crystallite Size Reaction Relationship in $M(OH)_2-MO$ Decomposition," J. Chem. Soc. Faraday Trans. I 74 1530 (1978).

49. J-C. Niepce & G. Watelle, "Shear Transformation in Solid 1 \rightarrow Solid 2 + Gas Endothermic Decompositions," J. de Phys. 38 365 (1977).
50. R.S. Gordon & W.D. Kingery, "Thermal Decomposition of Brucite. I. Electron & Optical Microscope Studies," J. Am. Ceram. Soc. 49 654 (1966).
51. R.S. Gordon & W.D. Kingery, "Thermal Decomposition of Brucite. II. Kinetics of Decomposition in Vacuum," J. Am. Ceram. Soc. 50 8 (1967).
52. R.S. Gordon, "Thermal Decomposition of Brucite," PhD Dissertation, Metallurgy, Massachusetts Institute of Technology, September 1964.
53. F. Freund, "Retention of Hydroxyl Groups on MgO," J. Am. Ceram. Soc. 50 493 (1967).
54. H. Naegerl & F. Freund, "Zeretzungsmechanismus von $Mg(OH)_2$ und $Mg(OD)_2$," J. Thermal Anal. 2 387 (1970).
55. F. Freund, R. Martens, & N.Sh. Ol-Eslami, "Recrystallization Effect During the Dehydration of $Mg(OH)_2$," J. Thermal Anal. 8 525 (1975).
56. F. Freund, "Zusammenhang Zwischen Mikrospannungen und Korngrosse bei der Thermischen Zersetzung von $Mg(OH)_2$," Ber. Dtsch. Ker. Ges. 52 53 (1975).
57. F. Freund & V. Sperling, "MgO Defect Structure of Hexagonal Symmetry," Mater. Res. Bull. 11 621 (1976).
58. W.R. Eubank, "Calcination Studies of MgO," J. Am. Ceram. Soc. 34 225 (1951).
59. R.C. Turner, I. Hoffman, & D. Chen, "Thermogravimetry of the Dehydration of $Mg(OH)_2$," Can. J. Chem. 41 243 (1963).
60. D.T.Y. Chen & P.H. Fong, "Thermal Analysis of $Mg(OH)_2$," J. Thermal Anal. 12 5 (1977).

61. B.S. Girgis, "Activation Energy Evaluation of $Mg(OH)_2$ Dehydration from Conventional & Isothermal DTA Traces," Trans. Brit. Ceram. Soc. 71 177 (1972).
62. J.H. Sharp, "On the Activation Energy for the Dehydroxylation of $Mg(OH)_2$," Trans. Brit. Ceram. Soc. 72 21 (1973).
63. V.A. Phillips, H. Opperhauser, & J.L. Kolbe, "Relations Among Particle Size, Shape, & Surface Area of $Mg(OH)_2$ & Its Calcination Product," J. Am. Ceram. Soc. 61 75 (1978).
64. P.J. Anderson & D.T. Livey, "Physical Methods for Investigating the Properties of Oxide Powders in Relation to Sintering," Powder Metall. 7 189 (1961).
65. J.F. Goodman, "Decomposition of $Mg(OH)_2$ in an Electron Microscope," Proc. R. Soc. London A247 346 (1958).
66. G. Eswara Prasad & V.K. Moorthy, "Hot State Electron Microscope & Electron Diffraction Studies on the Decomposition of $Mg(OH)_2$," Trans. Ind. Ceram. Soc. 62 254 (1979).
67. W. Eitel & H. Kedesdy, "Die Metaphase des Brucits," Abh. Preuss. Akad. Wiss. 5 13 (1943).
68. G. Aminoff, "Über die Struktur Magnesium Hydroxydes," Z. Krist. 56 506 (1921).
69. G.F. Hüttig & W. Frankenstein, "Zur Kenntnis des Systems - Magnesium Oxyd / Wasser," Z. Anorg. Chem. 185 403 (1929).
70. W. Büssem & F. Köberich, "Die Entwässerung des Brucits," Z. Phys. Chem. B17 310 (1932).
71. H.S. Megaw, "Thermal Expansions of Certain Crystals with Layered Lattices," Proc. R. Soc. London A142 198 (1933).

72. J. Garrido, "Sur la deshydrations de al brucites," C. R. Acad. Sci. 203 94 (1936).
73. R. Fricke & J. Lüke, "Wärmeinhalt und Gitterzustand Aktiver Magnesiumoxyde," Z. Elektrochem. 41 174 (1935).
74. L.S. Birks & H. Friedman, "Particle Size Determination from X-ray Line Broadening," J. Appl. Phys. 17 687 (1946).
75. D.K. Thomas & T.W. Baker, "An X-ray Study of the Factors Causing Variation in the Heats-of-Solution of MgO," Proc. Phys. Soc. 74 673 (1959).
76. I.F. Guilliat & N.H. Brett, "X-ray Line Broadening as a Measure of Crystallite Size in Oxide Powders," Philos. Mag. 21 671 (1970).
77. D. Lewis & M.W. Lindley, "An X-ray Line Broadening Study of the Introduction & Removal of Strain in Some Refractory Oxides," J. Am. Ceram. Soc. 47 652 (1964).
78. A. Cimino, P. Porta, & M. Valigi, "Dependence of the Lattice Parameter of MgO on Crystallite Size," J. Am. Ceram. Soc. 49 152 (1966).
79. Z. Librant & R. Pampuch, "X-ray Strain Analysis of MgO Crystallites Derived from Thermal Decomposition of Various Magnesium Compounds," J. Am. Ceram. Soc. 51 109 (1968).
80. G.W. Brindley & G.J. Ogilvie, "The Texture of Single Crystals of Brucite," Acta Crystallogr. 5 412 (1952).
81. W.F. Giaugue, "An Example of the Difficulty in Obtaining Equilibrium Corresponding to a Macrocrystalline Non-Volatile Phase. The Reaction $Mg(OH)_2(s) = MgO(s) + H_2O(g)$," J. Am. Chem. Soc. 71 3192 (1949).
82. C.N.R. Rao & K.S. Pitzer, "Thermal Effects in Magnesium & Calcium Oxides," J. Phys. Chem. 64 282 (1960).

83. C.N.R. Rao, S.R. Yoganarasimhan, & M.P. Lewis, "Exothermic Reactions Due to Annealing Defects in Oxide Lattices: Study of the Decomposition of Carbonates," *Can. J. Chem.* 38 2359 (1960).
84. M. Natarajan, T.S. Sarma, J.C. Ahluwalia, & C.N.R. Rao, "Thermal & Particle Size Effects in MgO," *Trans. Faraday Soc.* 65 3088 (1969).
85. J. White, "Refractories Research. II. Calcination & Sintering of Magnesia," *J. Austr. Ceram. Soc.* 9 60 (1973).
86. R. Pampuch, Z. Librant, & J. Piekarczyk, "Texture & Sinterability of MgO Powders," *Keramurgia Int.* 1 14 (1975).
87. A.W. Searcy, "The Reactions of High Temperature Materials," Chap. 4 in Chemical & Mechanical Properties of Inorganic Materials, A.W. Searcy, D.V. Ragone, & U. Colombo (eds.), Wiley-Interscience 1970.
88. S.J. Gregg & K.S.W. Sing, Adsorption, Surface Area, & Porosity, 2nd Ed., Academic Press 1982.
89. S. Brunauer, J. Skalny, & E.E. Bodor, "Adsorption on Non-Porous Solids," *J. Colloid & Interface Sci.* 30 546 (1969).
90. E.S. Palik, "Specific Surface Area Measurements on Ceramic Powders," *Powder Tech.* 18 45 (1977).
91. Standard X-ray Diffraction Powder Patterns. NBS Circ. 539, MgO, Vol.1, H.E. Swanson & E. Tatge, June 1953, p.37; and, Mg(OH)₂, Vol.2, H.E. Swanson, N.T. Gilfrich, & M.I. Cook, September 1956, p.30.
92. L.V. Azaroff, Elements of X-ray Crystallography, McGraw-Hill 1968, p.552.
93. B.E. Warren, X-ray Diffraction, Addison-Wesley 1974, p.225.
94. D. Beruto & A.W. Searcy, "Characterization of the Porous CaO Particles Formed by Decomposition of CaCO₃ & Ca(OH)₂ in Vacuum," LBL-9713, August 1979.

95. J.C. Southard, "The Heat-of-Hydration of Calcium Sulfates,"
Ind. & Eng. Chem. 32 442 (1940).
96. J.P. Coughlin, "Solution Calorimetry & Silicate Thermochemistry," Chap. 14
in Experimental Thermochemistry, Vol.2, H.A. Skinner (ed.),
Wiley-Interscience 1962.
97. G.P. Harnwell, Principles of Electricity & Electromagnetism, 2nd Ed.,
McGraw-Hill 1949, p.138.
98. K.S. Taylor & L.S. Wells, "Studies of Heat-of-Solution of Calcium &
Magnesium Oxides & Hydroxides," J. Res. NBS 21 133 (1938).
99. D.R. Torgeson & T.G. Sahama, "A Hydrofluoric Acid Calorimeter & the
Determination of the Heats-of-Formation of $MgSiO_4$, $MgSiO_3$, & $CaSiO_3$,"
J. Am. Chem. Soc. 70 2156 (1948).
100. G.M. Rosenblatt, "Interpretation of Knudsen Vapor Pressure Measurements on
Porous Solids," J. Electrochem. Soc. 110 563 (1963).
101. A.W. Searcy, Private Communication, 1982.
102. T. Saito & Y. Kotera, "Some Observations on the Calcination Process of
Precipitated $Mg(OH)_2$," Bull. Chem. Soc. Japan 36 474 (1963).
103. T.H. Nielsen & M.H. Leibold, "Surface Hydroxyl in MgO ,"
J. Am. Ceram. Soc. 49 626 (1966).
104. A.C. Zettlemoyer & W.C. Walker, "Active Magnesia. Surface Areas & Pore
Structures from Nitrogen Adsorption," Ind. & Eng. Chem. 39 69 (1947).
105. W.C. Walker & A.C. Zettlemoyer, "Active Magnesia. V. Adsorption in
Preferred Positions," J. Phys. Chem. 57 182 (1953).
106. P.R. Anderson, "A Model for Localized Physical Adsorption on Ionic Solids,"
Surf. Sci. 27 60 (1971).
107. B.W. Davis, "Adsorption of Ar, N_2 , & $n-C_4H_{10}$ on MgO Smoke, CaF_2 , &
Graphitized Carbon," J. Colloid & Interface Sci. 31 353 (1969).

108. D.C. Hinman & G.D. Halsey, "Adsorption of Ar on a Non-uniform MgO Surface," J. Chem. Phys. 64 3353 (1976).
109. J.G. Dash, R. Ecke, J. Stollenberg, O.E. Vilches, & O.J. Whittemore, Jr., "Uniform MgO Adsorbents," J. Phys. Chem. 82 1450 (1978).
110. R.L. Nelson & A.J. Tench, "Chemisorption on Some Alkaline Earth Oxides. Part 2. Intrinsic Bulk Defects & Adsorption of Oxygen on MgO, CaO, & SrO," Trans. Faraday Soc. 63 3039 (1967).
111. D. Nicholson, "Variation of Surface Area During the Thermal Decomposition of Solids," Trans. Faraday Soc. 61 990 (1965).
112. S. Brunauer, D.L. Kantro, & C.H. Weise, "The Surface Energies of CaO & Ca(OH)₂," Can. J. Chem. 34 729 (1956).
113. R. Fricke, R. Schnabel, & K. Beck, "Oberfläche und Wärmehalt beim Kristallisierten Magnesium Hydroxyd. II. Mitteilung über Struktur, Wärmehalt, und sonstige Eigenschaften aktiver Stoffe," Z. Elektrochem. 42 881 (1936).
114. G. Jura & C.W. Garland, "Experimental Determination of the Surface Tension of MgO," J. Am. Chem. Soc. 74 6033 (1952).
115. S. Boffi & M. Ricci, "On the Cleavage Energy of MgO," Mater. Chem. 1 289 (1976).
116. C.H. Shomate & E.H. Huffman, "Heats-of-Formation of MgO, MgCl₂, MgCl₂·H₂O, MgCl₂·4H₂O, & MgCl₂·6H₂O," J. Am. Chem. Soc. 65 1625 (1943).
117. J.E. Lennard-Jones & P.A. Taylor, "Some Theoretical Calculations of the Physical Properties of Certain Crystals," Proc. R. Soc. London A109 476 (1925).
118. G.C. Benson & R. McIntosh, "Some Calculations of the Surface Energy of MgO," Can. J. Chem. 33 1677 (1955).

119. G.C. Benson & K.S. Yun, "Surface Energy & Surface Tension of Crystalline Solids," Chap. 8 in The Solid-Gas Interface, Vol.1, E.A. Flood (ed.), Marcel Dekker 1967.
120. Selected Values of Chemical Thermodynamic Properties, NBS Technical Note 270-3, D.D. Wagman, W.H. Evans, V.B. Parker, I. Halow, S.M. Bailey, & R.H. Schumm, January 1968, pp.24-27; and, NBS Technical Note 270-6, V.B. Parker, D.D. Wagman, & W.H. Evans, November 1972, pp.9-12.

Table 1. Calculated Steady-State Pressure of $Mg(OH)_2$ -MgO Under Varying Conditions. K&G Data.

Starting Material	Apparatus	T	X_{MgO}	$P_s \times 10^3$
Baker [®] $Mg(OH)_2$ Reagent Powder	Closed Monei Knudsen Cell ($d_{cell} = 16.5mm$)			
(Orifice channel length = 0.1 mm)				
	$d_{orifice} = 1.03mm$	500°K/227°C	0.05-0.55	1.9 Torr/253 Pa
Brucite Platelets	= 0.38	→	→	2.5 /333
-20 + 60 mesh (840 - 250 μm)	= 1.03			7.8 /1040
Large Brucite Flakes	= 0.38	→	→	8.4 /1120
(10x10x0.5 mm)	= 1.03			2.6 /347
	K&G zero orifice area extrapolation ($A_o = 0$) at the temperatures of G&A experiments	463/190 485/212	- -	1.9 /253 8.9 /1187
$\left(\begin{array}{l} KE \\ P \\ eqm \end{array} \right)$				
	K&G data for $A_o = 0$ extrapolated to a temperature of my experiments	573/300	-	1290. /172000

Table 2. Calculated Steady-State Pressure of $Mg(OH)_2$ -MgO Under Varying Conditions. My Data.

Starting Material	Apparatus	T	X_{MgO}	$P_s \times 10^3$
V-Mg(OH) ₂ Reagent Powder	Open Pt basket (1 cm ²) with electrobalance	553°K/280°C	0-0.95	0.84 Torr/112 Pa
		618 /345	0-0.95	3.40 /453
G-Mg(OH) ₂	Open Alumina Knudsen Cell	573 /300	0.203	0.38 /51
			0.484	0.32 /43
	Closed Alumina Knudsen Cells	573 /300	0.733	0.44 /59
			0.804	0.29 /39
			0.603	202 /26933
			0.145	26 /3467
			0.197	40 /5333
			0.441	51 /6800
	Closed Graphite Knudsen Cell	673/400	0.539	67 /8933
			0.606	54 /7200
d _{orifice} = 0.38mm	673/400	0.678	70 /9333	
		0.746	46 /6133	
d _{orifice} = 1.80mm	673/400	0.759	61 /8133	
		0.874	28 /3733	
Closed Graphite Knudsen Cell	d _{orifice} = 1.00 mm	0.798	35 /4667	
		0.863	29 /3867	

Note: The orifice channel length = 1.0 mm, and the Knudsen cell diameter = 20.5 mm for the alumina Knudsen cells, and = 11.1 mm for the graphite Knudsen cell.

Table 3. Surface Area vs Percent Retained Water for Temperatures Less Than 370°C. My Data

T(°C)	time(hrs)	Retained H ₂ O (mole %)	Surface Area (m ² /mole MgO)
V-Mg(OH) ₂ / U-tube & low vacuum			
260	150	7.2	14735
265	110	17.6	16815
280	66	11.5	13440
280	168	14.8	11150
300	5	4.0	8790
310	3	15.0	15020
310	14	14.0	20943
340	0.33	14.0	17583
340	24	13.2	16715
350	0.75	9.9	14680
350	0.25	8.0	16613
350	0.75	5.8	13637
350	0.50	2.0	16078
G-Mg(OH) ₂ / U-tube & low vacuum			
350	0.25	9.0	6064
340	5	4.0	5587
350	1	3.0	8955
350	0.25	5.0	6390
G-Mg(OH) ₂ / Knudsen cells & high vacuum			
300	3	19.6	2160 (open cell)
300	3	12.6	3851 (closed cell)

Table 4. Surface Area vs Percent Retained Water for Temperatures Less Than 370°C. Livey et al.³⁷ Data.

T(°C)	time(hrs)	Retained H ₂ O (mole %)	Surface Area (m ² /mole MgO)
Air-prepared samples			
380	2	3.72	11100
500	1	2.0	7250
700	1	0.75	1490
1000	1.75	0.15	360
1380	1.75	0.12	180
Vacuum-prepared samples			
380	3	4.0	-
540	1.17	1.4	6250
770	1	0.32	2100
1000	1.75	0.20	1340
1340	1.75	0.86	810

APP I

Outline of Giauque and Archibald Calculation of Entropy for H₂O(g)

- Giauque and Archibald measured:

-Heat Capacity (C_p) for G-Mg(OH)₂ & G-MgO from 20 K to 300 - 320 K

-Heat-of-Reaction (ΔH_{rxn}) for G-Mg(OH)₂ decomposition to G-MgO indirectly by means of the Heat-of-Solution (ΔH_{soln}) of G-Mg(OH)₂ and G-MgO at 298 K.

- Giauque and Archibald obtained the following results:

-Entropy of G-Mg(OH)₂ & G-MgO (S_{Mg(OH)₂} and S_{MgO}) using $S = \int_0^T C_p d(\ln T)$

-Entropy of H₂O(g) (S_{H₂O}^{calc}) using all of the above information in the equation,

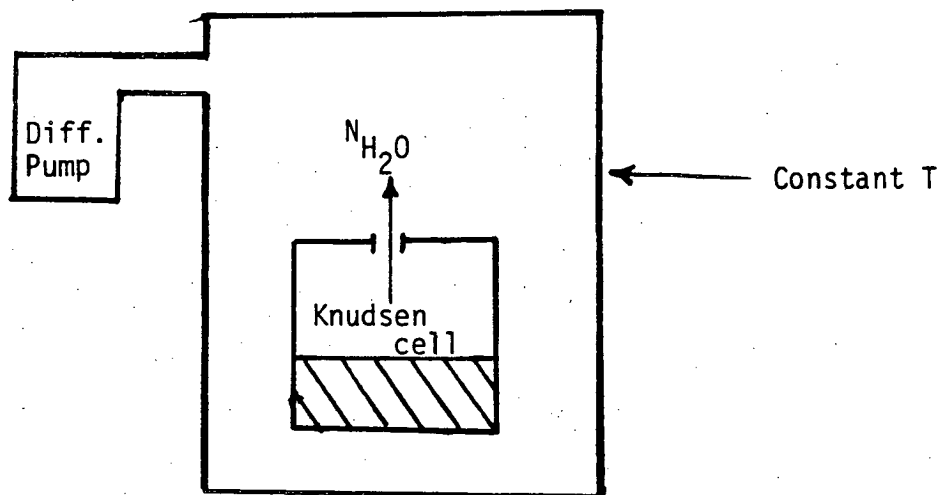
$$S_{H_2O}^{calc} = S_{Mg(OH)_2} - S_{MgO} + \frac{\Delta H_{rxn}}{T} + RT \ln P_{eqm}$$

- Giauque and Archibald obtained the following results:

T	ΔH _{rxn}	P _{eqm}	S _{H₂O} ^{calc}	S _{H₂O} ^{band}
(K)	(kJ / mole)	(Pa)	(J / deg-mole)	(J / deg-mole)
463	82.8	2654	203.55	203.84
485	82.4	7252	205.48	205.43

APP II

The Dynamic Knudsen Effusion Method



From measurement of the sample weight-loss during thermal vacuum decomposition, the quantity of water N_{H_2O} (moles), that escapes through an orifice of area A_o (cm^2) in a time of t (min), the flux, J_{H_2O} (moles / cm^2 -min) of the escaping water can be calculated using,

$$J_{H_2O} = \frac{N_{H_2O}}{A_o t}$$

From J_{H_2O} (moles / cm^2 -min), the molecular weight of the vaporizing species, M (gms / mole), and the temperature, T (K), the maximum steady-state equilibrium pressure, P_s (torr), in the Knudsen cell can be calculated using the HKL equation with the appropriate constants substituted. Thus,

$$P_s = 760 \frac{(MT)^{1/2}}{2650} J_{H_2O} = 1.217 J_{H_2O} (T)^{1/2}$$

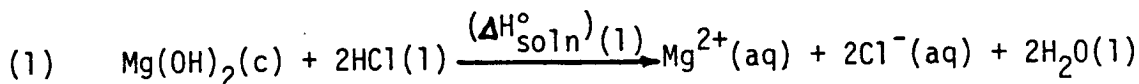
The P_s as a function of T can be plotted on a Log P vs $1/T$ plot to yield ΔH and ΔS° from the slope and intercept respectively, using,

$$\text{Log } P = - \frac{\Delta H}{2.3 R} \frac{1}{T} + \frac{\Delta S}{2.3 R}$$

APP III

Calculations of Heat-of-Solution ($\Delta H_{\text{soln}}^{\circ}$) from Heat-of-Formation (ΔH_f°) Data¹²⁰

$\Delta H_{\text{soln}}^{\circ}$ = Heat-of-Solution in 1.0 M HCl at 25.0°C; (aq) at standard state,
m = 1

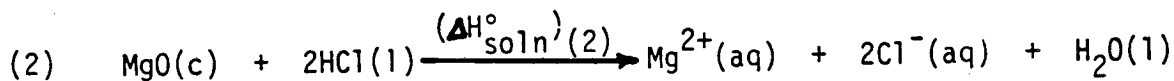


$$\begin{array}{cccccc} \Delta H_{f_1}^{\circ} & & \Delta H_{f_2}^{\circ} & & \Delta H_{f_3}^{\circ} & \Delta H_{f_4}^{\circ} & \Delta H_{f_5}^{\circ} \\ \frac{\text{kJ}}{\text{mole}}: & (-924.7) & + & (-165.4) & & (-466.9) & + & (-167.4) & + & (-285.8) \end{array}$$

$$\begin{aligned} (\Delta H_{\text{soln}}^{\circ})(1) &= [(\Delta H_{f_3}^{\circ} + 2\Delta H_{f_4}^{\circ} + 2\Delta H_{f_5}^{\circ}) - (\Delta H_{f_1}^{\circ} + 2\Delta H_{f_2}^{\circ})] \\ &= -117.8 \text{ kJ / mole} \end{aligned}$$

Note: Compare with the values at the bottom of APP XI.

$$\begin{array}{l} (\Delta H_{\text{soln}}^{\circ}) \quad \text{V-Mg(OH)}_2 = -113.1 \text{ kJ / mole} \\ \quad \quad \quad \quad \text{G-Mg(OH)}_2 = -112.0 \end{array}$$



$$\begin{aligned} \Delta H_{f_6}^{\circ} &= (-601.7) \text{ kJ / mole} \quad (\text{macrocrystalline MgO}) \\ &= (-597.9) \quad (\text{microcrystalline, finely divided, or high surface area MgO}) \\ &= (-554.0) \quad (\text{IF MgO metastable by } 47.7 \text{ kJ / mole}) ?? \end{aligned}$$

$$\begin{aligned} (\Delta H_{\text{soln}}^{\circ})(2) &= [(\Delta H_{f_3}^{\circ} + 2\Delta H_{f_4}^{\circ} + \Delta H_{f_5}^{\circ}) - (\Delta H_{f_6}^{\circ} + 2\Delta H_{f_2}^{\circ})] \\ &= -155.0 \text{ kJ / mole} \quad (\text{macrocrystalline}) \\ &= -158.8 \quad (\text{microcrystalline, finely divided, or high surface area MgO}) \\ &= -202.7 \quad (\text{IF MgO metastable by } 47.7 \text{ kJ / mole}) \end{aligned}$$

Giauque & Archibald Mg(OH)₂ Synthesis Procedure

Use the following quantities of reagent-grade materials in a 600 ml Chemware[®] teflon beaker with its lid. (This particular brand of teflon will not soften significantly below 240°C from repeated tests in our laboratory. It was rated by the manufacturer not to collapse below 280°C.)

343.75 gms	reagent-grade KOH
12.12 gms	reagent-grade MgCl ₂ ·6H ₂ O
60.75 mls	distilled H ₂ O

Weigh out the KOH pellets using a small 150 ml polyethylene beaker. This usually requires about four separate weighings of ~85 grams each. In the same beaker, but rinsed clean of KOH, weigh out the MgCl₂·6H₂O, then add 50 mls of the distilled water to it & dissolve the solid. Pour this solution carefully into the 600 ml teflon beaker containing the KOH. Rinse the 150 ml beaker with the additional ~11 mls of distilled water & pour this into the KOH beaker. Swirl the KOH beaker gently to mix, cover it with the teflon lid, & put it into a laboratory oven at ~220°C for ~1 hour until a transparent liquid results. Turn off the oven & allow to cool to ~25°C over ~10 hours. Dissolve the solid mass out of the beaker with distilled water & filter through a 2-inch fritted disc glass funnel with aspirator-assisted 1 liter vacuum filter flask. Wash thoroughly free of KOH & oven dry for several hours at 125°C. The solubility of the Mg(OH)₂ is low (9 mg/L @ 18°C) relative to the KOH; thus, it will appear as tiny flakes floating on the dissolving solution. 3.48 gms is the maximum theoretical amount from this size charge of reactants. The actual amount obtained is ~3.4 gms, giving ~98% yield in repeated syntheses.

APP V

Spectroscopic Analytical Results for Mg(OH)₂

	<u>G-Mg(OH)₂[*]</u>	<u>V-Mg(OH)₂[*]</u>	<u>G&A¹⁹</u>	<u>K&G^{21,22} (See Note below)</u>
Si	40 ppm	2500 ppm		1000 ppm
Al	30-100	100		1000
B		2000		1
Fe	150	200		1000
Ca	250-600	1500		1000
Ba	10	10		
Na		700		
K			1500 ppm	10
Cu	20	200		10
Ni	200-300			
Mn		20		1000
Ag	5			10
Pb				1
Cl				
CO ₃			0	
SO ₄				
PO ₄			50	

Note: K&G used natural brucite (Texas Brucite) for almost all experiments (except a short series using Baker[®] reagent-grade Mg(OH)₂ powder). K&G gave no elemental analysis of their brucite or Mg(OH)₂ powder. The K&G values shown above have been averaged from values for brucite (Canadian & Rhodesian Brucite) from other sources.^{38,52}

* Analyses done by American Spectrographic Laboratories, San Francisco, CA.

APP VI

Calculation of the Mole Fraction and the Weight Fraction



w_0 = starting weight of Mg(OH)_2
 w_1 = weight of mixture at some point in the decomposition
 (the mixture consists only of Mg(OH)_2 and MgO).

$M_{\text{Mg(OH)}_2}$ = molecular weight of Mg(OH)_2 = 58.326 grams/mole
 M_{MgO} = molecular weight of MgO = 40.312 grams/mole
 $M_{\text{H}_2\text{O}}$ = molecular weight of H_2O = 18.015 grams/mole

$X_{\text{Mg(OH)}_2}$ & X_{MgO} = mole fractions of Mg(OH)_2 & MgO , respectively
 $w_{\text{Mg(OH)}_2}$ & w_{MgO} = weight fractions of Mg(OH)_2 & MgO , respectively

$$\frac{w_0 - w_1}{M_{\text{H}_2\text{O}}} = \text{moles of H}_2\text{O lost} = \text{moles of MgO formed}$$

$$X_{\text{MgO}} = \frac{(w_0 - w_1)}{w_1} \cdot \frac{M_{\text{Mg(OH)}_2}}{M_{\text{H}_2\text{O}}}, \quad X_{\text{Mg(OH)}_2} = 1 - X_{\text{MgO}}$$

$$w_{\text{MgO}} = \frac{(w_0 - w_1)}{w_1} \cdot \frac{M_{\text{MgO}}}{M_{\text{H}_2\text{O}}}, \quad w_{\text{Mg(OH)}_2} = 1 - w_{\text{MgO}}$$

The Mole Fraction and the Weight Fraction are related by,

$$w_{\text{MgO}} = \frac{X_{\text{MgO}} \cdot M_{\text{MgO}}}{X_{\text{MgO}} \cdot M_{\text{MgO}} + X_{\text{Mg(OH)}_2} \cdot M_{\text{Mg(OH)}_2}}$$

APP VII

Mass Balance Test of X_{MgO} Calculated from Weight Loss

Open Knudsen cell has a cross-sectional area of $\sim 3.5 \text{ cm}^2$ (without the lid containing the small orifice).

Samples dried in drying oven at 125°C for 1 hour, then cooled in dessicator.

Run #1: $365.6 \text{ mg G-Mg(OH)}_2 = 6.268 \text{ mmoles G-Mg(OH)}_2$
 \downarrow
 $\times (0.6911) = [M_{MgO} / M_{Mg(OH)_2}] = \text{gravimetric factor}$
 $252.7 \text{ mg G-MgO (Theoretical)} = 6.268 \text{ mmoles G-MgO}$

Evacuate the system containing the carefully weighed G-Mg(OH)_2 to ~ 2 torr, and then carefully return the system to atmospheric pressure.

$365.9 \text{ mg G-Mg(OH)}_2 = 6.273 \text{ mmoles G-Mg(OH)}_2$ NO SAMPLE LOSS from evacuation of system

Evacuate the system containing the same sample carefully replaced, to $\sim 2 \times 10^{-5}$ torr, raise the furnace temperature to 350°C over a 10 minute interval, and hold at that temperature for 1 hour to decompose the G-Mg(OH)_2 to $\sim 95\%$ G-MgO . Now increase the temperature from 350°C to 950°C over a 30-minute interval & hold at that temperature for 3 hours. The pressure at 950°C after 3 hours is 2×10^{-6} torr. 100% decomposed.

$251.2 \text{ mg (Experimental Yield)}$. Thus, $\frac{251.2 \text{ mg}}{252.7 \text{ mg}} \times 100 = \underline{99.41\% \text{ Yield}}$

Run #2: $409.2 \text{ mg G-Mg(OH)}_2 = 7.016 \text{ mmoles G-Mg(OH)}_2$
 $282.5 \text{ mg G-MgO (Theoretical)} = 7.016 \text{ mmoles}$

No Evacuation Test. Same decomposition procedure as above (350°C for 1 hour). Temperature increased to 420°C & held for 1 hour (2×10^{-5} torr). Temperature increased again to 950°C & held for 1 hour (2×10^{-6} torr).

$282.5 \text{ mg (Experimental Yield)}$. Thus, $\frac{282.5 \text{ mg}}{282.8 \text{ mg}} \times 100 = \underline{99.89\% \text{ Yield}}$

APP VIII

X-ray Reflections for Mg(OH)₂ & MgO from ASTM/JCPDS Files* & My Data

	2θ CuK _α **	2θ FeK _α **	I/I ₀	(hkl)	d-ASTM/JCPDS	d-My Data
<u>Mg(OH)₂</u>	18.6°	23.3°	80	001	4.770 Å	4.813 Å
<u>File</u>	33.0	41.6	6	100	2.725	2.730
7-239	38.0	48.2	100	101	2.365	2.370
	50.9	65.4	55	102	1.794	1.796
	58.7	76.0	35	110	1.573	1.575
	62.1	80.8	18	111	1.494	1.493
	68.3	89.7	16	103	1.373	1.372
	68.9	90.6	2	200	1.363	1.364
	72.1	95.4	12	201	1.310	1.310
	80.6	108.7	2	004	1.192	1.193
	81.3	109.9	10	202	1.183	1.185
	87.2	120.1	2	113	1.118	1.118
<u>MgO</u>	37.0	47.0	10	111	2.431	2.436
<u>File</u>	43.0	54.8	100	200	2.106	2.111
4-0832	62.4	81.2	52	220	1.489	1.491
	74.8	99.4	4	311	1.270	1.270
	78.7	105.6	12	222	1.216	1.216
	94.1	133.7	5	400	1.053	1.055

* See also Ref. 91.

** X-ray wavelengths of CuK_α & FeK_α are 1.542Å & 1.937Å, respectively.

APP IX

Integral Breadth Calculation & FWHM Measurement

The Integral Breadth (IB) is defined as the total peak area divided by the maximum peak height^{92,93} as measured from the peak baseline near the center of the peak. Thus,

$$IB = \frac{\text{Peak Area}}{\text{Peak Height}}$$

The FWHM was measured at the point of half the maximum height with a metric rule to the nearest 0.5 mm.

The peak area was measured with a planimeter to the nearest 1 mm².

The chart paper conversion constant is 727.8 mm / radian.

Principal peak reflections in 2θ degrees:

	(101)Mg(OH) ₂	(200)MgO
FeK (1.937Å)	48.2°	54.8°
CuK (1.542Å)	38.0	43.0

Over the range of decomposition ~0-95% the FWHM remained relatively constant for both starting materials & their respective products.

FWHM _{(101)G-Mg(OH)₂}	= 4 - 6 mm	= (5.50 - 8.24) × 10 ⁻³ radians
(101)V-Mg(OH) ₂	= 7 - 8	= (9.62 - 10.99)
(200)G-MgO	= 16 - 23	= (21.98 - 31.60)
(200)V-MgO	= 29 - 36	= (39.85 - 49.46)

Sample calculation:

$$IB_{(101)} = \frac{659 \text{ mm}^2}{121 \text{ mm}} \times \frac{\text{radian}}{727.8 \text{ mm}} = 7.5 \times 10^{-3} \text{ radians}$$

APP X

Admixture Test for Sampling Handling Error

V-Mg(OH)₂ and Annealed G-MgO were mixed in different proportions and vacuum ampoulized. The $\Delta H_{\text{soln}}^{25^\circ\text{C}}$ of these mixed samples were measured.

$$\Delta H_{\text{soln}}^{25^\circ\text{C}} \text{ of V-Mg(OH)}_2 = -1939.7 \text{ J / gm} = -463.6 \text{ cal / gm (App XI)}$$

$$\Delta H_{\text{soln}}^{25^\circ\text{C}} \text{ of Annealed G-MgO} = -3793.2 \text{ J / gm} = -906.6 \text{ cal / gm} = -152.9 \text{ kJ / mole}$$

The value for the $\Delta H_{\text{soln}}^{25^\circ\text{C}}$ for the Annealed G-MgO was obtained from two measurements of Annealed G-MgO from each of three different batches of Annealed G-MgO prepared in the same manner, for a total of six measurements of the $\Delta H_{\text{soln}}^{25^\circ\text{C}}$ of Annealed G-MgO. Thus,

$$(\bar{a}_6)_G = -152.9 \pm 0.7 \text{ kJ / mole}, (\sigma_6 = 0.46 \%).$$

This value, $(\bar{a}_6)_G$, was dependent on five separate calorimeter calibrations using V-Mg(OH)₂ as the calibration standard. (See App XI). Thus,

$$(\bar{a}_5)_V = -471.9 \pm 5.8 \text{ chart divisions / gm of V-Mg(OH)}_2, (\sigma_5 = 1.23 \%),$$

and, the Calorimeter Calibration Factor (CCF) becomes,

$$\text{CCF} = \frac{-1939.7 \text{ J / gm of standard}}{471.9 \text{ chart divisions / gm of standard}} = -4.110 \text{ J / chart division}$$

<u>Run #1:</u>	42.00 mg of Annealed G-MgO	-159.31 J	
	86.10 mg of V-Mg(OH) ₂	-167.01 J	
		-326.32 J,	expected total

Thus, $\frac{311.54 \text{ J}}{326.32 \text{ J}} \times 100 = \underline{\underline{95.47 \%}}$ for the mixture.
 -311.54 J, actually obtained for the mixture.

<u>Run #2:</u>	48.30 mg of Annealed G-MgO	-183.21 J	
	103.40 mg of V-Mg(OH) ₂	-200.56 J	
		-383.77 J,	expected

Thus, $\frac{378.12 \text{ J}}{383.77 \text{ J}} \times 100 = \underline{\underline{98.53 \%}}$ -378.12 J, actual

APP XI

$\Delta H_{\text{soln}}^{\text{MgO}}$ from $\Delta H_{\text{soln}}^{\text{mix}}$ of Partially Decomposed Sample at 25°C

Since the partially decomposed sample was a mixture of Mg(OH)_2 reactant and MgO product, the measured ΔH_{soln} of the mixture, $\Delta H_{\text{soln}}^{\text{mix}}$, contained components from both reactant and product. The ΔH_{soln} of only the MgO , $\Delta H_{\text{soln}}^{\text{MgO}}$, had to be calculated from $\Delta H_{\text{soln}}^{\text{mix}}$ since complete decomposition to MgO could not be achieved at the low temperatures of decomposition used to prepare most samples.

$$\begin{aligned} \Delta H_{\text{soln}}^{\text{mix}} &= \Delta H_{\text{soln}}^{\text{Mg(OH)}_2} \cdot X_{\text{Mg(OH)}_2} + \Delta H_{\text{soln}}^{\text{MgO}} \cdot X_{\text{MgO}} \\ &= \Delta H_{\text{soln}}^{\text{Mg(OH)}_2} \cdot (1 - X_{\text{MgO}}) + \Delta H_{\text{soln}}^{\text{MgO}} \cdot X_{\text{MgO}} \end{aligned}$$

Hence,

$$\Delta H_{\text{soln}}^{\text{MgO}} = \frac{\Delta H_{\text{soln}}^{\text{mix}} - [\Delta H_{\text{soln}}^{\text{Mg(OH)}_2} (1 - X_{\text{MgO}})]}{X_{\text{MgO}}}, \text{ Note: See Figs 32 \& 33}$$

If the sample is from decomposing G- Mg(OH)_2 , then,

$$\begin{aligned} \Delta H_{\text{soln}}^{\text{Mg(OH)}_2} &= \Delta H_{\text{soln}}^{\text{G-Mg(OH)}_2} = -26763 \text{ cal / mole} = -111976 \text{ J / mole} \quad (\text{After G\&A})^{19} \\ &= -458.9 \text{ cal / gm} = -1920.0 \text{ J / gm} \end{aligned}$$

The V- Mg(OH)_2 (Ventron Mg(OH)_2 reagent grade powder) was used for the calibration of the calorimeter since it gave a rapid response and reproducibility. A value for $\Delta H_{\text{soln}}^{\text{V-Mg(OH)}_2}$ was assigned to it that was an average value based on measurements made by various researchers^{19,37,98,99} and measurements made with this calorimeter here in this laboratory using electrical calibration. The values agreed with my data within experimental error of ~2%. A instrument sensitivity of ~5 J was obtained with this calorimeter.

$$\begin{aligned} \Delta H_{\text{soln}}^{\text{V-Mg(OH)}_2} &= -27040 \text{ cal / mole} = -113135 \text{ J / mole} \\ &= -463.6 \text{ cal / gm} = -1939.7 \text{ J / gm} \end{aligned}$$

APP XII

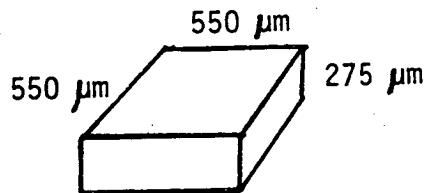
Surface Area Calculation for a Typical Sample of Brucite Platelets

A typical sample size of ~ 125 mg of K&G brucite platelets, K-Mg(OH)_2 , in the size range $250 - 840 \mu\text{m}$ ($550 \mu\text{m}$ average) was used in the calculation. Half of the average size ($275 \mu\text{m}$) was used as the platelet thickness. The density of brucite as listed in most handbooks of chemical and physical properties is $\sim 2.40 \text{ gms} / \text{cm}^3$. From the density of the brucite in the sample, the volume of the sample can be estimated.

Thus,

$$\frac{125 \text{ mg} / \text{sample}}{2400 \text{ mg} / \text{cm}^3} = 0.052 \text{ cm}^3 = 5.2 \times 10^{-8} \text{ m}^3 \text{ of brucite} / \text{sample}.$$

From a typical, average-size brucite platelet of K-Mg(OH)_2 ,



the surface area per platelet and the volume per platelet can be calculated.

Thus,

$$\begin{aligned} 2 \times (550 \mu\text{m})^2 + 4 \times (550 \mu\text{m} \times 275 \mu\text{m}) &= 1.21 \times 10^6 \mu\text{m}^2 / \text{platelet} \\ &= 1.21 \times 10^{-6} \text{ m}^2 / \text{platelet} \end{aligned}$$

and,

$$\begin{aligned} (550 \mu\text{m})^2 \times (275 \mu\text{m}) &= 8.32 \times 10^7 \mu\text{m}^3 / \text{platelet} \\ &= 8.32 \times 10^{-11} \text{ m}^3 / \text{platelet} \end{aligned}$$

Thus,

$$\frac{5.2 \times 10^{-8} \text{ m}^3 / \text{sample}}{8.32 \times 10^{-11} \text{ m}^3 / \text{platelet}} = 625 \text{ platelets} / \text{sample}, \text{ and}$$

$$\begin{aligned} (625 \text{ platelets} / \text{sample}) \times (1.21 \times 10^{-6} \text{ m}^2 / \text{platelet}) &= 7.56 \times 10^{-4} \text{ m}^2 / \text{sample} \\ &= 6.0 \times 10^{-3} \text{ m}^2 / \text{gm K-Mg(OH)}_2 \end{aligned}$$

APP XIII

MgO Particle Size Comparison of My Data with Others⁵⁸

<u>T</u>	<u>time</u>	<u>XRD</u>	<u>Surface Area</u>	<u>SEM</u>
<u>MY DATA</u>				
<u>V-MgO</u>				
265°C	45 hrs	100 Å	41 Å	5-25 μm
310	30	100	44	5-25
<u>G-MgO</u>				
300	3	40	113	2-20(≈350)*
350	3	40	161	2-20(≈350)*

* large ≈350 μm hexagonal particles are also observed (Fig.17).
 (10,000 Å = 1 μm)

<u>EUBANK DATA⁵⁸</u>			<u>TEM</u>
300°C	48 hrs	55 Å	0.01 μm
400	↓	85	0.01
500		139	0.01
600		365	0.035
700		>300	0.05-0.1
1000		12	0.50-1.0
1300	5	↓	5-20
1500	1		20-30
1750	0.3		30-50
2000	0.3		50-100

Note: See also Refs. 74-79.

APP XIV

Particle Size Calculation from Surface Area Data.

Assume uniform, non-porous cubes or spheres of edge or diameter d .

Cubes: $S = 6d^2$ & $V = d^3$ $S =$ surface area & $V =$ volume

Spheres: $S = 4\left(\frac{d}{2}\right)^2\pi$ & $V = \frac{4}{3}\left(\frac{d}{2}\right)^3\pi = \frac{d^3}{6}\pi$

The molar surface area, \bar{S} , in m^2 / mole is given by,

$$\bar{S} = \frac{SxM}{Vxp}, \quad (1).$$

$M =$ molecular weight (gms / mole)

$S =$ surface area / particle (m^2 / particle)

$V =$ volume / particle (cm^3 / particle)

$p =$ density of particle material (gms / cm^3)

$\frac{S}{V} = \frac{6}{d}$, whether have uniform cubes or spheres, & from (1),

$$d = 6xM(1 / \bar{S}xp), \quad (2).$$

$$p_{\text{XRD}} = \text{X-Ray Diffraction density} = \frac{\text{molecular wt.} \times (\text{formula wts.} / \text{unit cell})}{\text{Avogadro's Number} \times \text{volume of unit cell}}$$

The unit cell volume can be obtained from the unit cell dimensions, which can be measured with x-ray or electron diffraction. Using the value of $2x d_{(200)}$ from my XRD data given in APP VIII, gives for the FCC MgO unit cell spacing $d_{(100)}$ a value of $2x(2.111 \text{ \AA}) = 4.222 \text{ \AA}$. This agrees with Goodman's value of 4.20 \AA obtained by electron diffraction.⁶⁵ Thus, the unit cell volume becomes,

$$V = (4.222 \times 10^{-8} \text{ cm})^3 = 7.53 \times 10^{-23} \text{ cm}^3$$

Now,

$$p_{\text{XRD}} = 3.56 \pm 0.02 \text{ gms} / \text{cm}^3 \text{ for FCC MgO, and (2) becomes for MgO,}$$

$$d = 67.94(1 / \bar{S}), \quad (3).$$

Total Surface Energy as a Function of Several Variables

x_{MgO}	γ_{MgO} (mJ/ m ²)	Surface Area (m ² / total moles)		E_{surf} (kJ/ mole MgO)	
		V-Mg(OH) ₂ (265°C)	G-Mg(OH) ₂ (350°C)	V-Mg(OH) ₂	G-Mg(OH) ₂
0.00	1500	2050*	50*	0.70**	0.02**
0.25		5500	1500	8.25	2.25
0.50		9300	3000	13.95	4.50
0.75		12900	4500	19.35	6.70
1.00		16600	6000	24.90	9.00
Annealed MgO		2700	1650	4.05	2.50

Some Specific Surface Energies for MgO

- $\gamma_{(100)}$, theoretical = 1310¹¹⁵, 1362¹¹⁷, 1448¹¹⁵ mJ/m²
- $\gamma_{(100)}$, experimental = 1040¹¹⁴, 1150¹¹⁵, 1200¹¹⁵
- $\gamma_{(110)}$, theoretical = 2591¹¹⁵
- $\gamma_{(011)}$, theoretical = 3940¹¹⁷

* Surface Area of Mg(OH)₂ . ** $\gamma_{Mg(OH)_2} \sim 330$ mJ / m² used in calculation.¹¹²

$E_{surf} = (10^{-6}) (\gamma_{MgO}) \times (\text{Surface Area})$, with units as in above Table

$$\left[\frac{(\Delta H_{soln})_{350^\circ C} - (\Delta H_{soln})_{1000^\circ C}}{(\text{Surface Area})_{350^\circ C} - (\text{Surface Area})_{1000^\circ C}} \right] = \frac{(160.0 - 152.4) \text{ kJ / mole G-MgO}}{(6000 - 1650) \text{ m}^2 / \text{mole G-MgO}}$$

$$= 1747 \text{ mJ / m}^2 \text{ of G-MgO .}$$

FIGURE CAPTIONS

- Fig 1 - HCP $\text{Mg}(\text{OH})_2$ unit cell & dimensions.
- Fig 2 - FCC MgO unit cell & dimensions.
- Fig 3 - Giaque & Archibald Static Manometry Apparatus & plot of some of their data.
- Fig 4 - Comparison of Knudsen Effusion (Kay & Gregory) and Equilibrium Static Manometry (Giaque & Archibald) data on Log P vs $1/T$ plot.
- Fig 5 - (a) Plot of Whitman-Motzfeltd equation, P_s vs A_o , extrapolated to zero orifice area, $A_o = 0$ (after Kay & Gregory).
(b) Log P vs $1/T$ plots for decreasing orifice sizes (after Kay & Gregory).
- Fig 6 - Low-vacuum decomposition apparatus.
- Fig 7 - High-vacuum decomposition apparatus & electrobalance.
- Fig 8 - Solution calorimeter with associated electronics & ampoule bursting device.
- Fig 9 - Full-scale calibration curve for the Thermistor Bridge setting (TB) vs Calorimeter Reaction Vessel (CRV) Temperature (T_{calor}).
- Fig 10- Working scale from the calibration curve in Fig. 9.
- Fig 11- Plot of reciprocal of Whitman-Motzfeltd equation, $1/P_s$ vs A_o , of my data using G- $\text{Mg}(\text{OH})_2$ [=G&A] in Knudsen cell of decreasing orifice. (See Eq. (1), p.24). Also relevant K&G data plotted.
- Fig 12- Relative weight-loss & Actual weight-loss vs time plots using V- $\text{Mg}(\text{OH})_2$ [=Ventron] in open Pt basket at 280°C using electrobalance.
- Fig 13- The same as Fig. 12, except at 345°C .

- Fig 14- SEM micrographs at 500X
(a) undecomposed V-Mg(OH)₂.
(b) ~95% decomposed V-Mg(OH)₂.
- Fig 15- Fig. 14(a) at 5000X.
- Fig 16- Fig. 14(b) at 5000X.
- Fig 17- SEM micrographs at 100X
(a) undecomposed G-Mg(OH)₂.
(b) ~95% decomposed G-Mg(OH)₂.
- Fig 18- Fig. 17(a) at 5000X.
- Fig 19- Fig. 17(b) at 5000X.
- Fig 20- XRD spectra of undecomposed G-Mg(OH)₂.
- Fig 21- Same as Fig. 20, except ~44% decomposed G-Mg(OH)₂.
- Fig 22- Same as Fig. 20, except ~87% decomposed G-Mg(OH)₂.
- Fig 23- S_{BET} & (200)MgO Integral Breadth with FWHM vs Temperature.
These are sintering/annealing curves for both V-MgO [=V, Ventron]
& G-MgO [G, G&A].
- Fig 24- (101)Mg(OH)₂ & (200)MgO peak area with FWHM vs X_{MgO} for both
V-Mg(OH)₂ [=V, Ventron] & G-Mg(OH)₂ [=G, G&A] starting materials.
Closed circles = Knudsen cell conditions & open circles
= non-Knudsen cell conditions.
- Fig 25- S_{BET} & (200)MgO Integral Breadth with FWHM vs Time at 345°C.
Closed circles & open circles are for the low temperature heat
treatment of ~95% decomposed V-Mg(OH)₂. Open squares & open
triangles are for S_{BET} & (200)MgO Integral Breadth,
respectively, of MgO annealed at 1000°C.

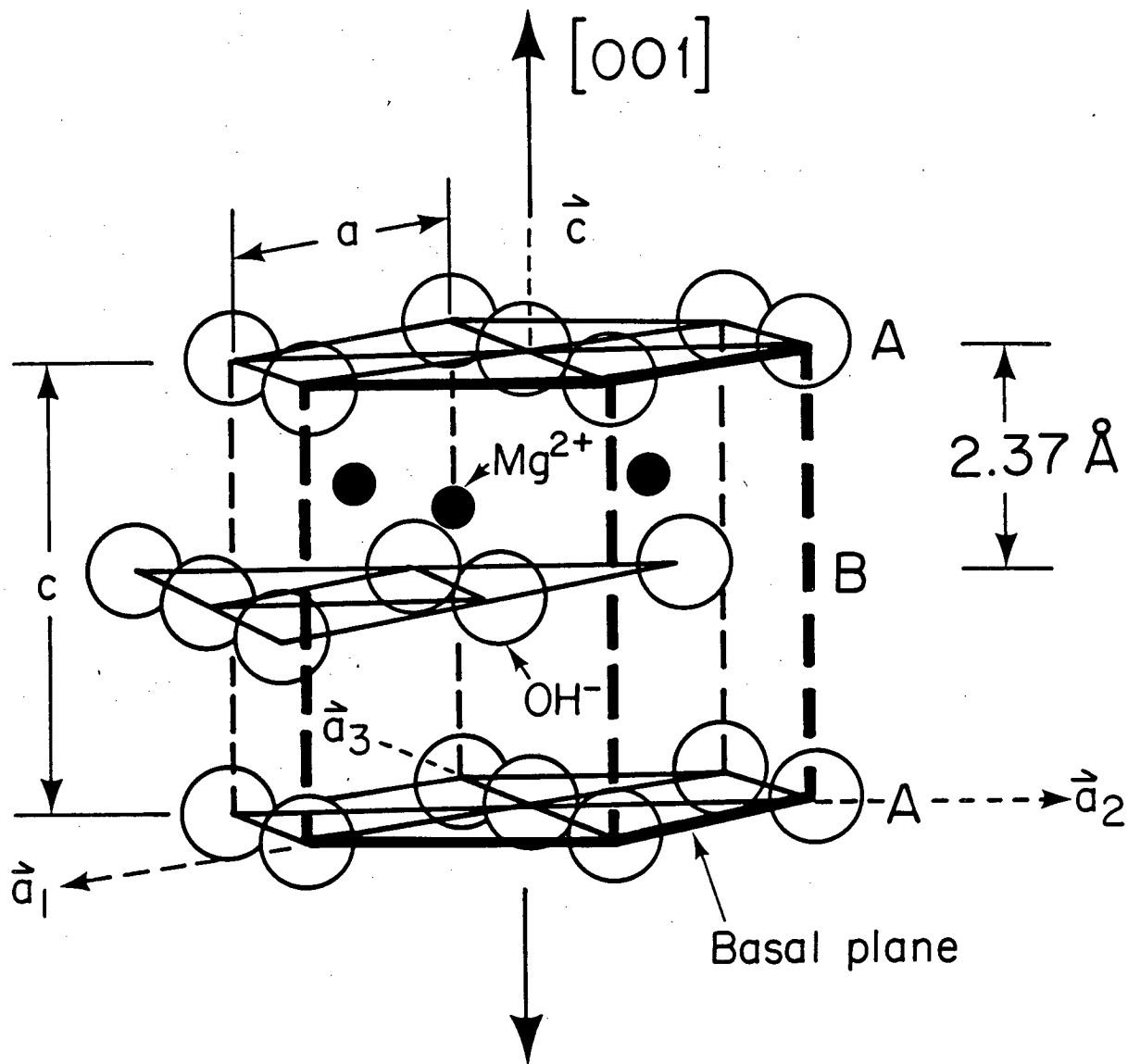
- Fig 26- $(101)\text{Mg}(\text{OH})_2$ & $(200)\text{MgO}$ Integral Breadths vs X_{MgO} for both $\text{V-Mg}(\text{OH})_2$ [=V, Ventron] & $\text{G-Mg}(\text{OH})_2$ [=G, G&A] starting materials under Knudsen cell & non-Knudsen cell conditions at similar temperatures.
- Fig 27- P_s vs X_{MgO} for $\text{G-Mg}(\text{OH})_2$ [=G&A] decomposition under Knudsen cell (closed circles) & non-Knudsen cell (open circles) conditions at the same temperature.
- Fig 28- S_{BET} vs X_{MgO} for both $\text{V-Mg}(\text{OH})_2$ [=Ventron] & $\text{G-Mg}(\text{OH})_2$ [=G&A] under Knudsen cell (closed circles) & non-Knudsen cell (all other symbols) conditions at the same & different temperatures.
- Fig 29- S_{BET} vs Time for both $\text{G-Mg}(\text{OH})_2$ [=G&A] & $\text{V-Mg}(\text{OH})_2$ [=Ventron] under Knudsen cell (closed triangle) & non-Knudsen cell (all other symbols) conditions.
- Fig 30- S_{BET} & Relative weight-loss vs Time curves for $\text{G-Mg}(\text{OH})_2$ [=G&A] under Knudsen cell (closed circles & closed triangles) & non-Knudsen cell (open circles & open triangles) conditions at 300°C .
- Fig 31- S_{BET} vs $T_{\text{decomposition}}$ for $\text{V-Mg}(\text{OH})_2$ (open circles) & $\text{G-Mg}(\text{OH})_2$ (closed circle) under non-Knudsen cell conditions.
- Fig 32- $\Delta H_{\text{soln}}^{\text{MgO}}$ vs Temperature for $\text{Mg}(\text{OH})_2$ prepared & decomposed under various conditions by various researchers over the years. The v denotes that the MgO samples were prepared under vacuum conditions.³⁷

Fig 33- $\Delta H_{\text{soln}}^{\text{MgO}}$ vs X_{MgO} for G-Mg(OH)₂[=G&A] under Knudsen cell (closed circles) & non-Knudsen cell (open circles) conditions at 300°C.

The annealed sample indicated in the figure was prepared at 1000°C for 10 hours under vacuum.

Fig 34- Hypothetical Gibbs Free Energy vs Composition diagram for the system MgO - Mg(OH)₂ - H₂O.

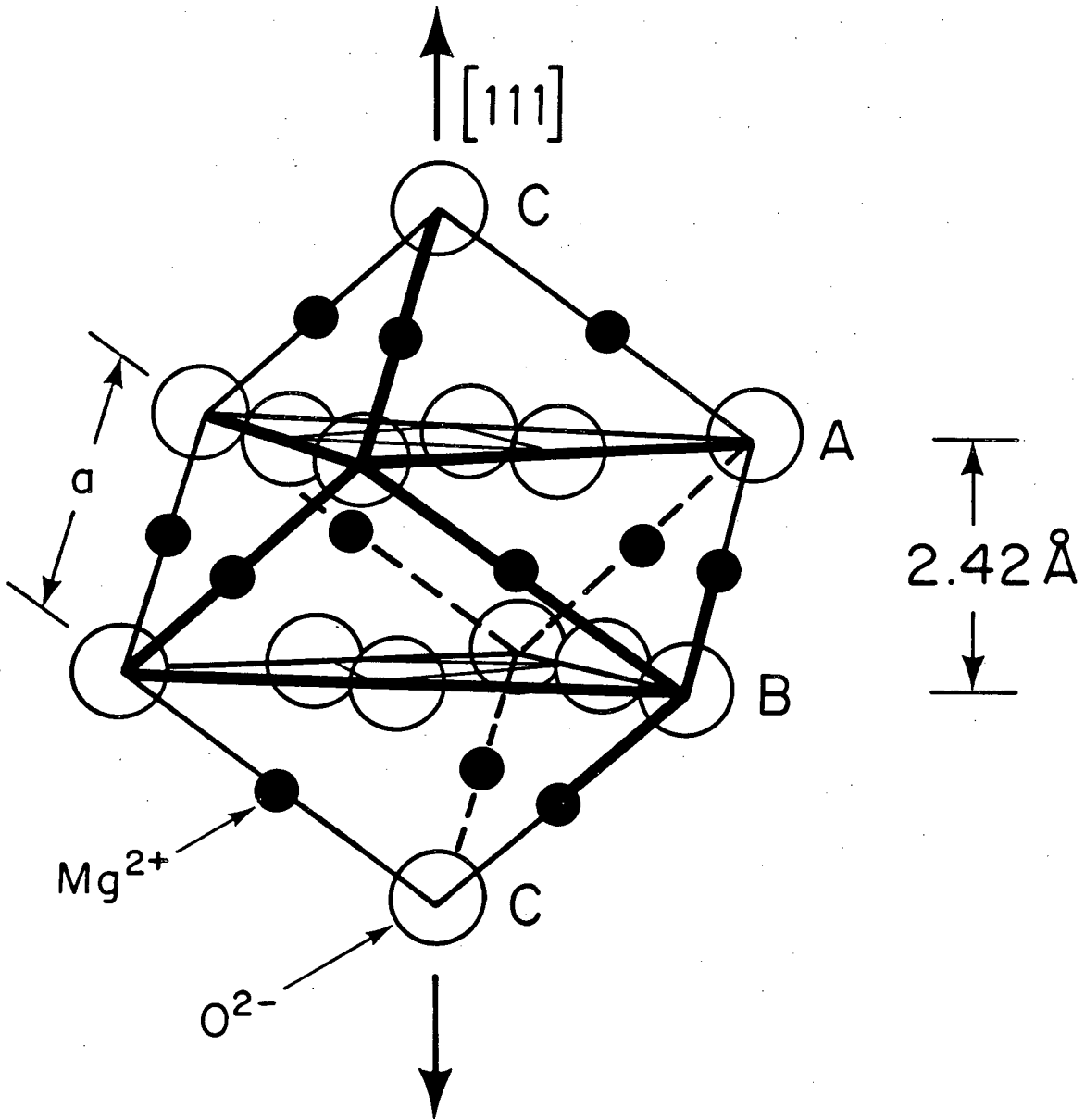
HCP Mg(OH)₂



XBL 823-289

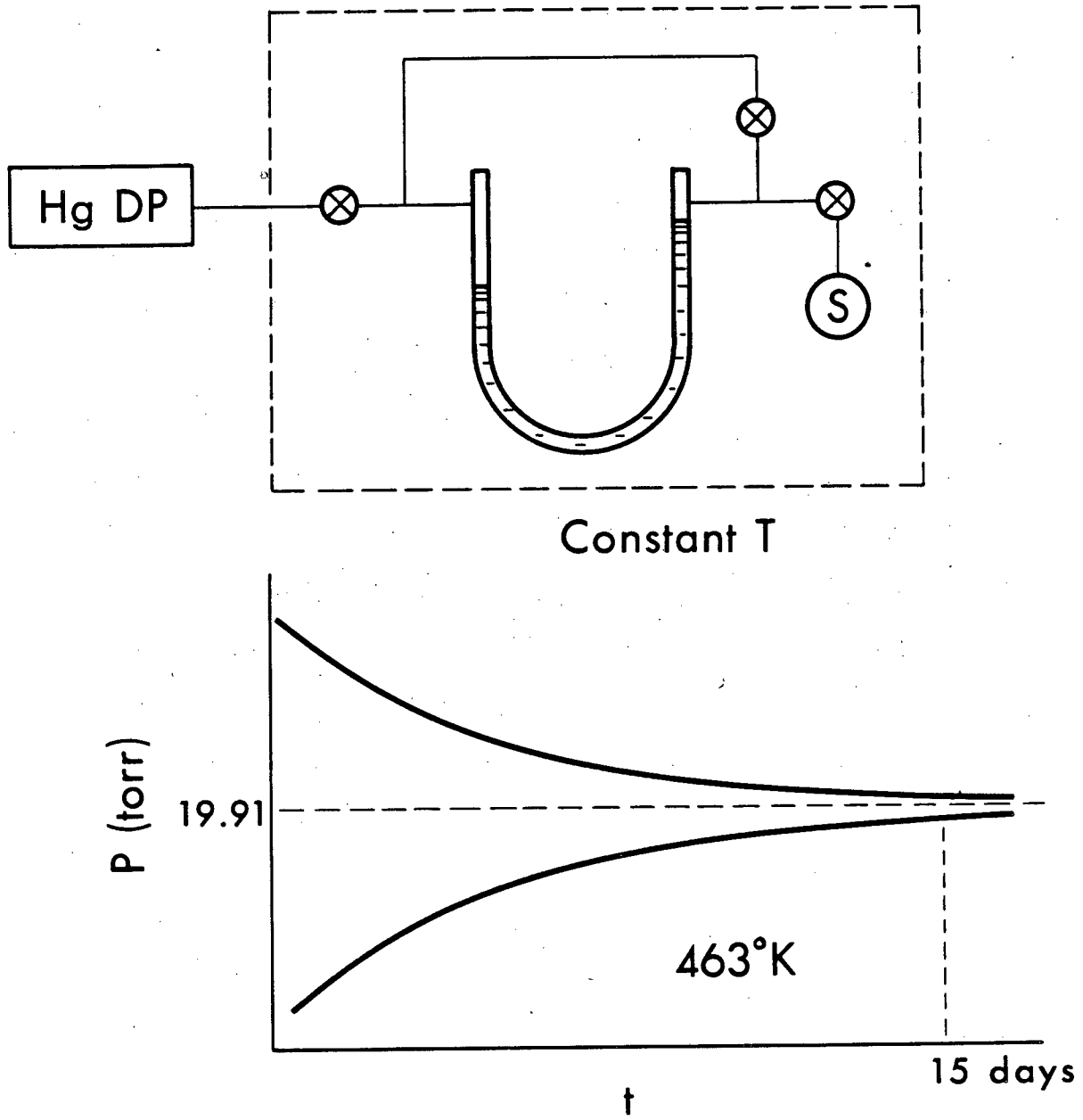
FIG 1

FCC MgO



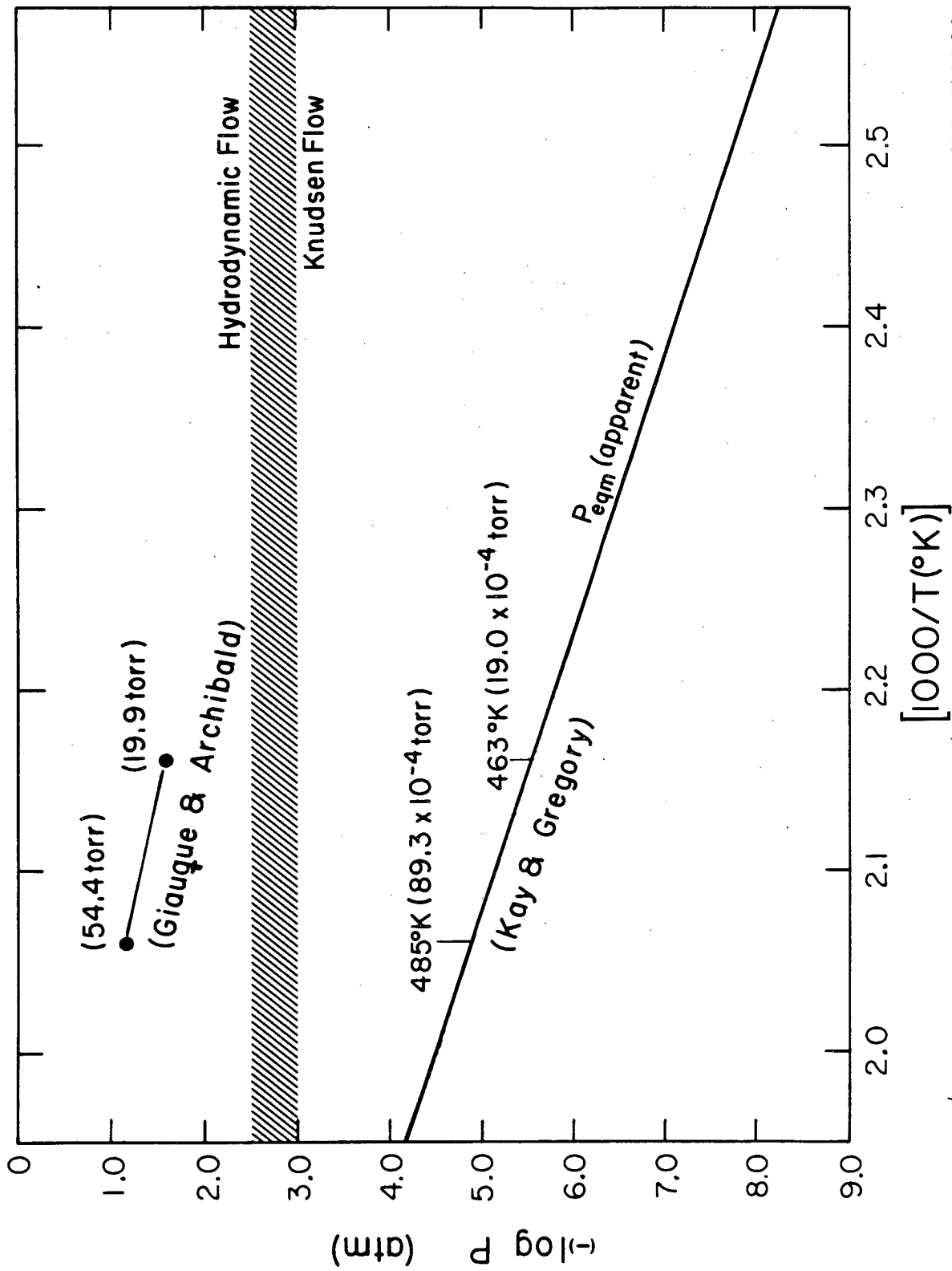
XBL 823-288

FIG 2



XBL 8110-1433

FIG 3



XBL 7810 - 11608A

FIG 4

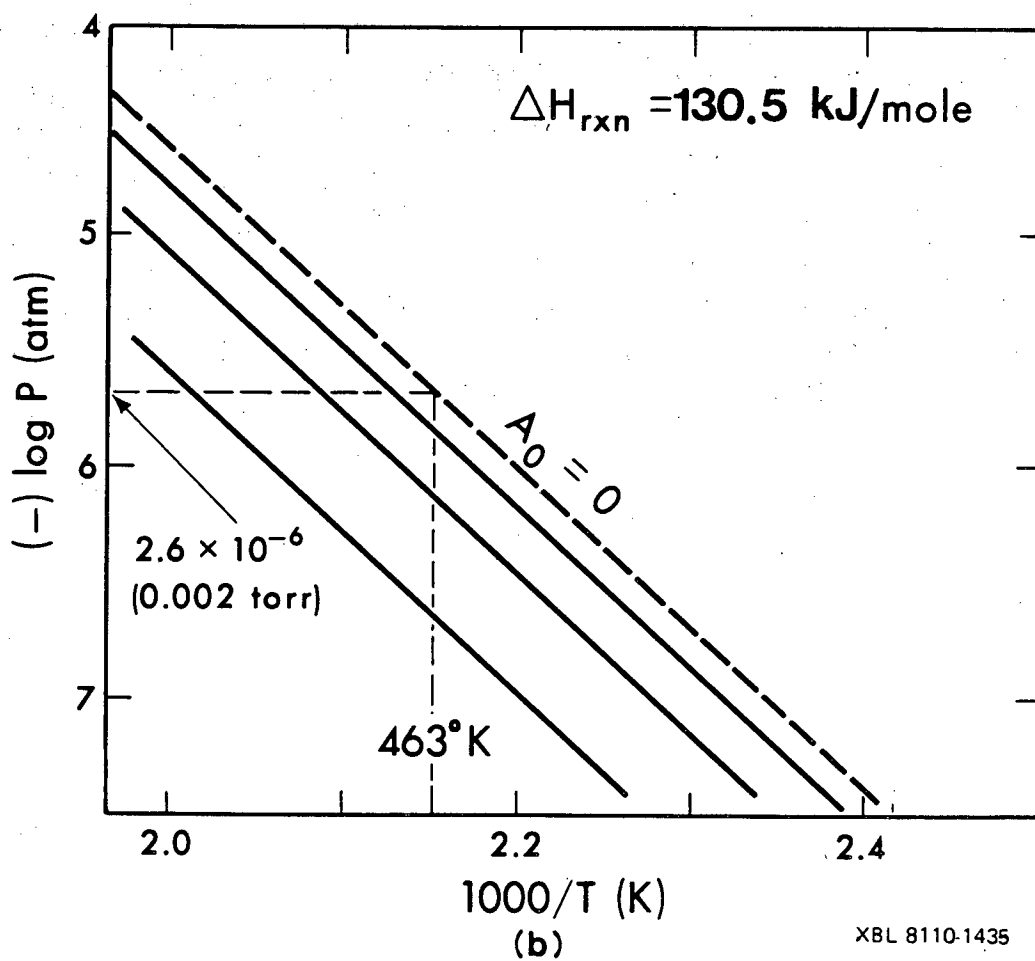
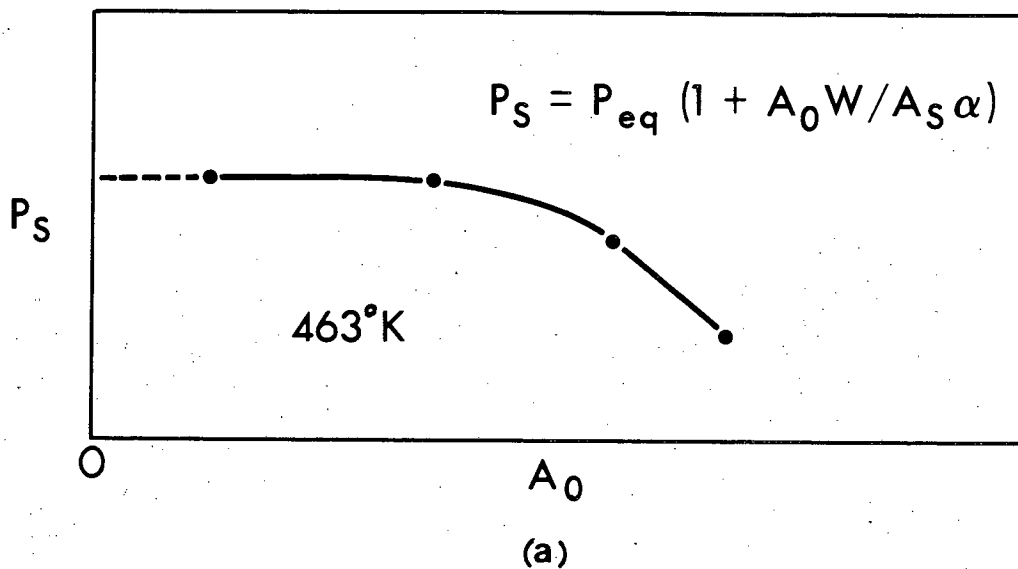
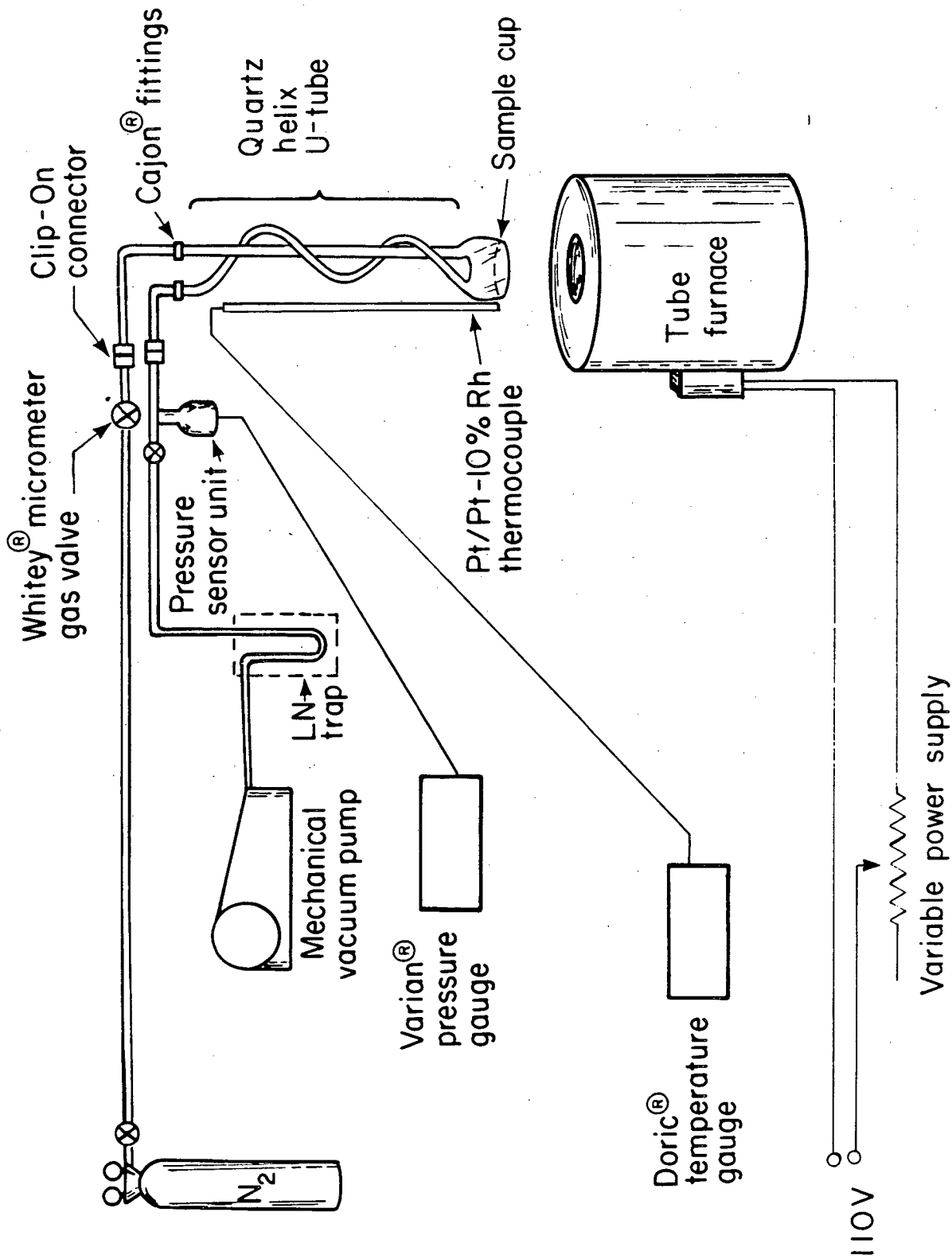
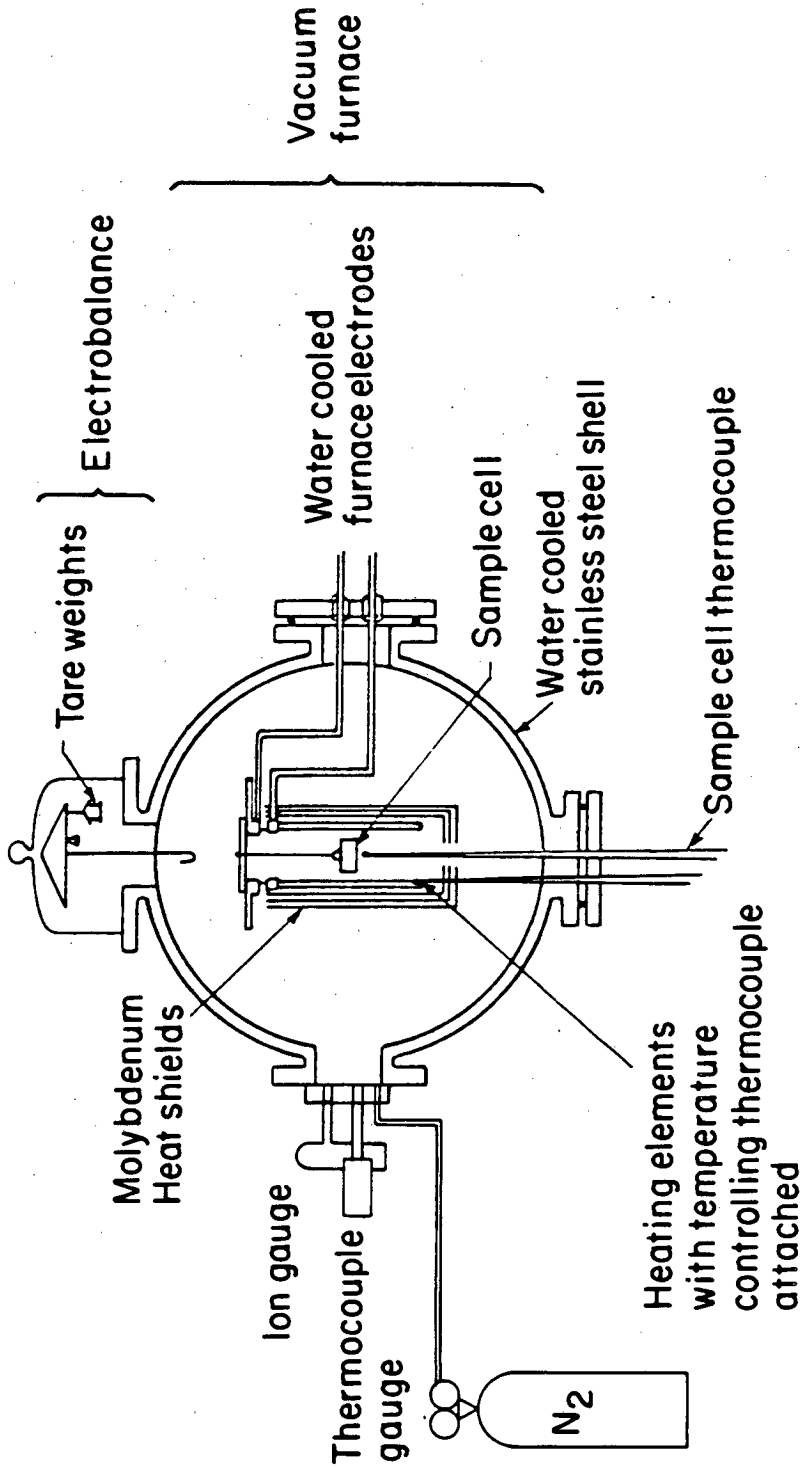


FIG 5



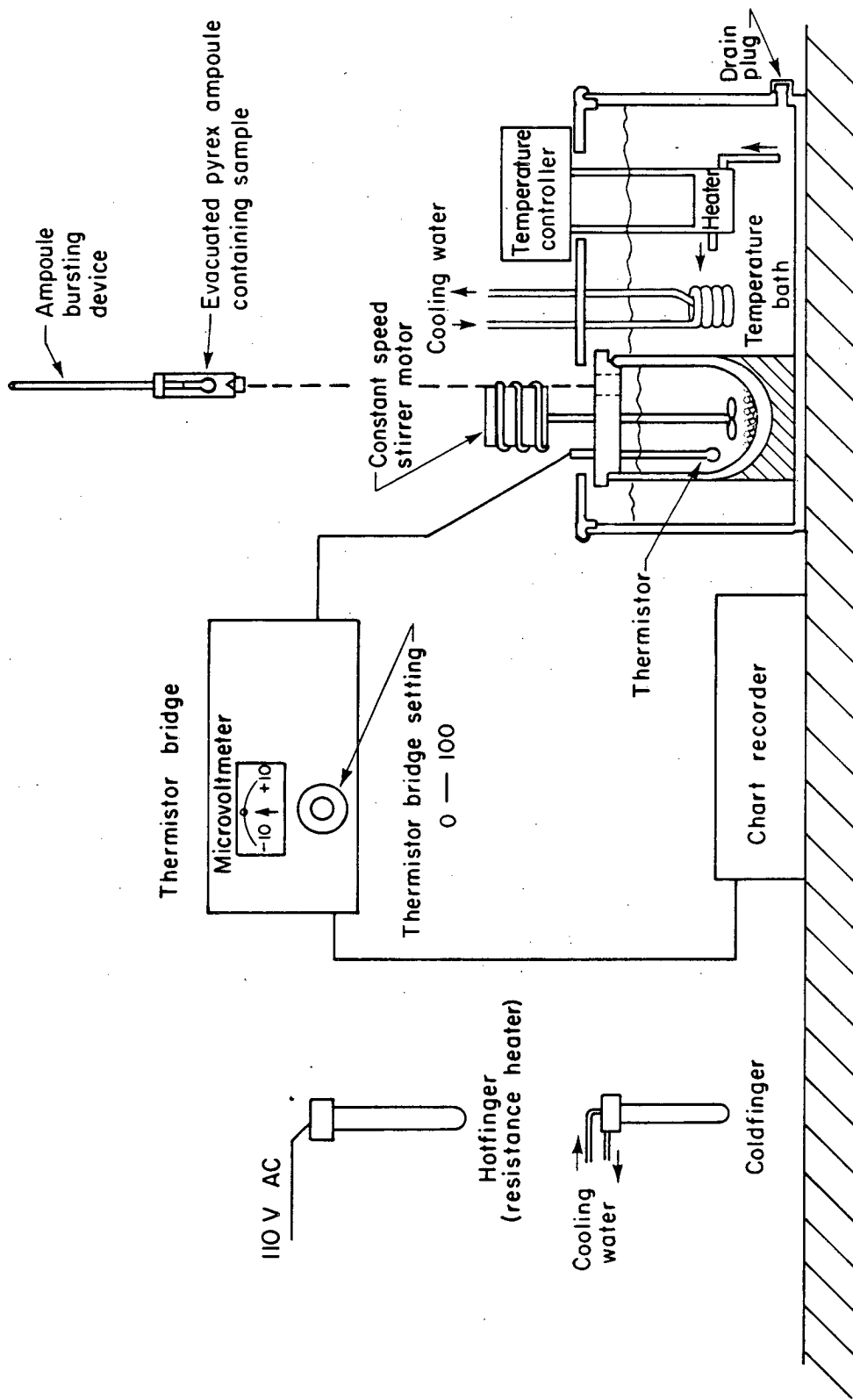
XBL 7810-11605

FIG 6



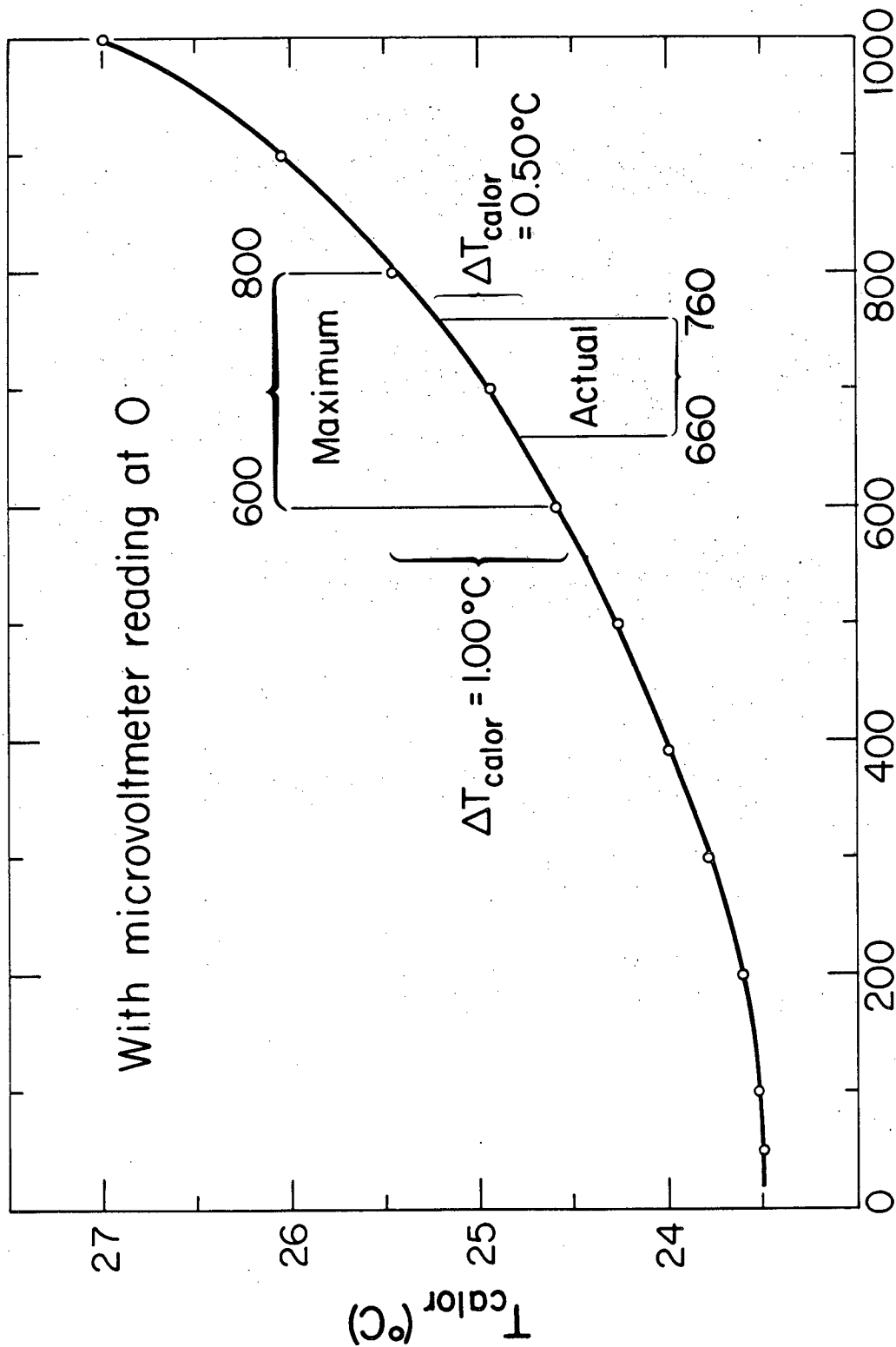
XBL 784 -4857A

FIG 7



XBL 822-152

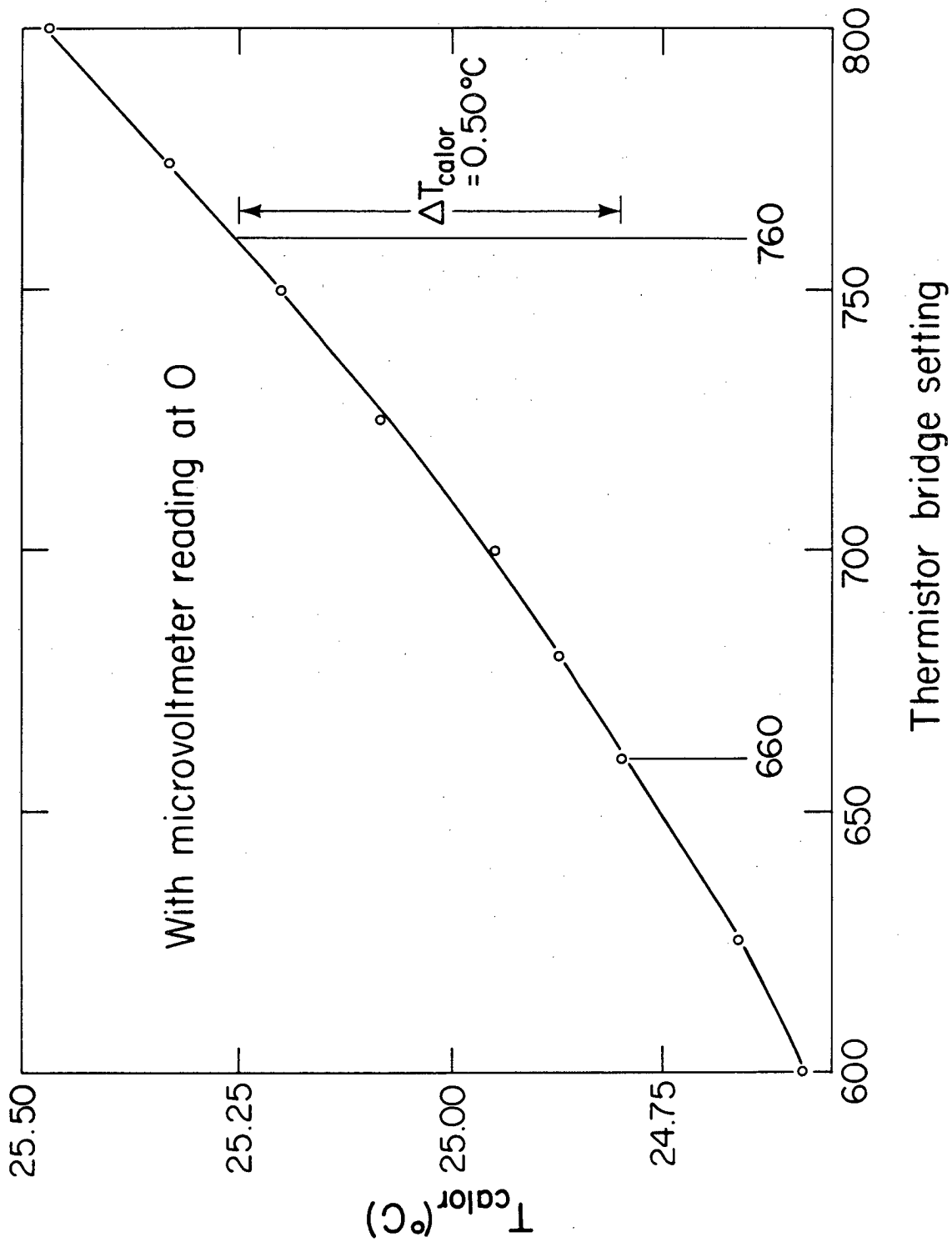
FIG 8



Thermistor bridge setting

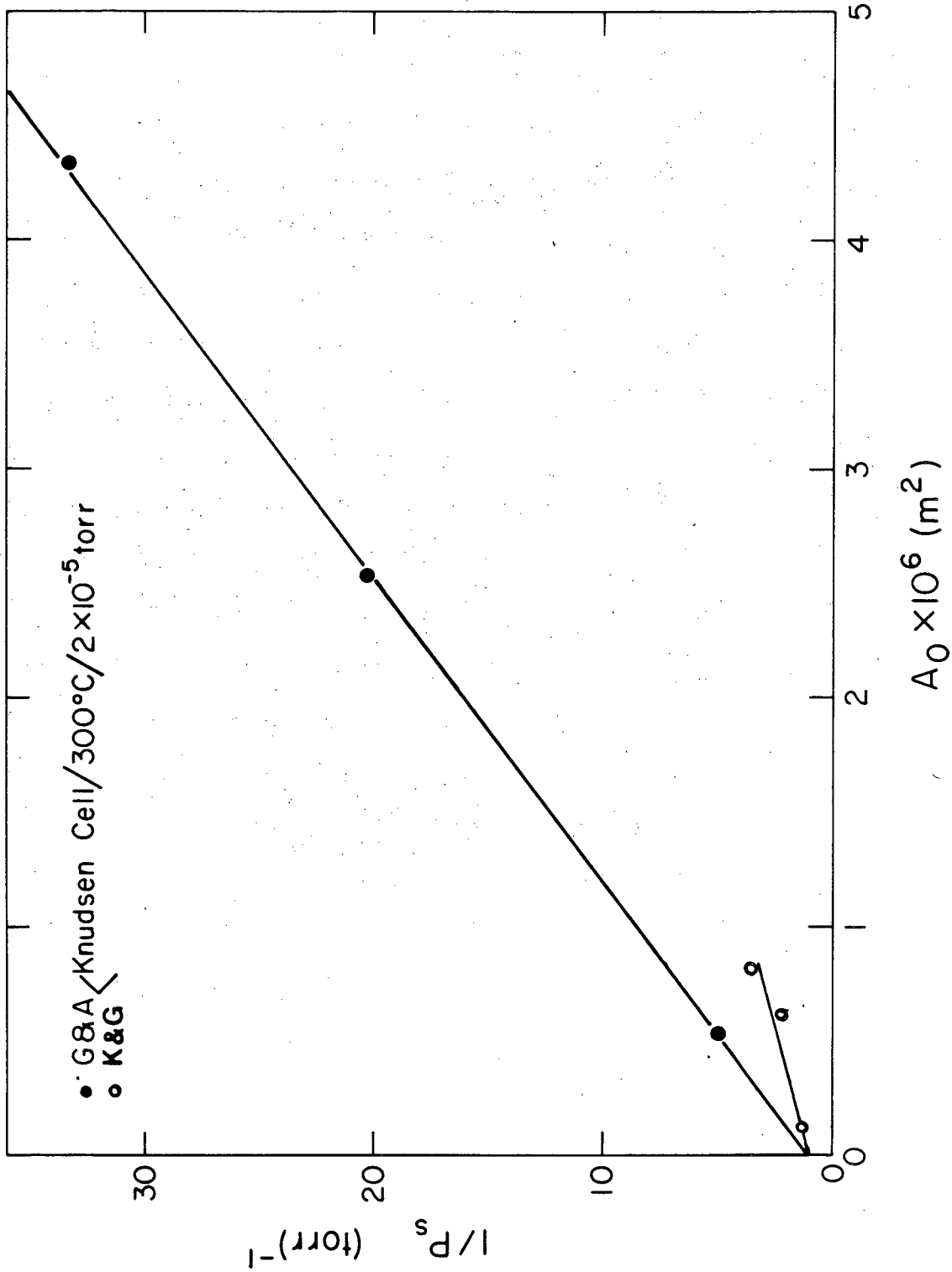
XBL 822-151

FIG 9



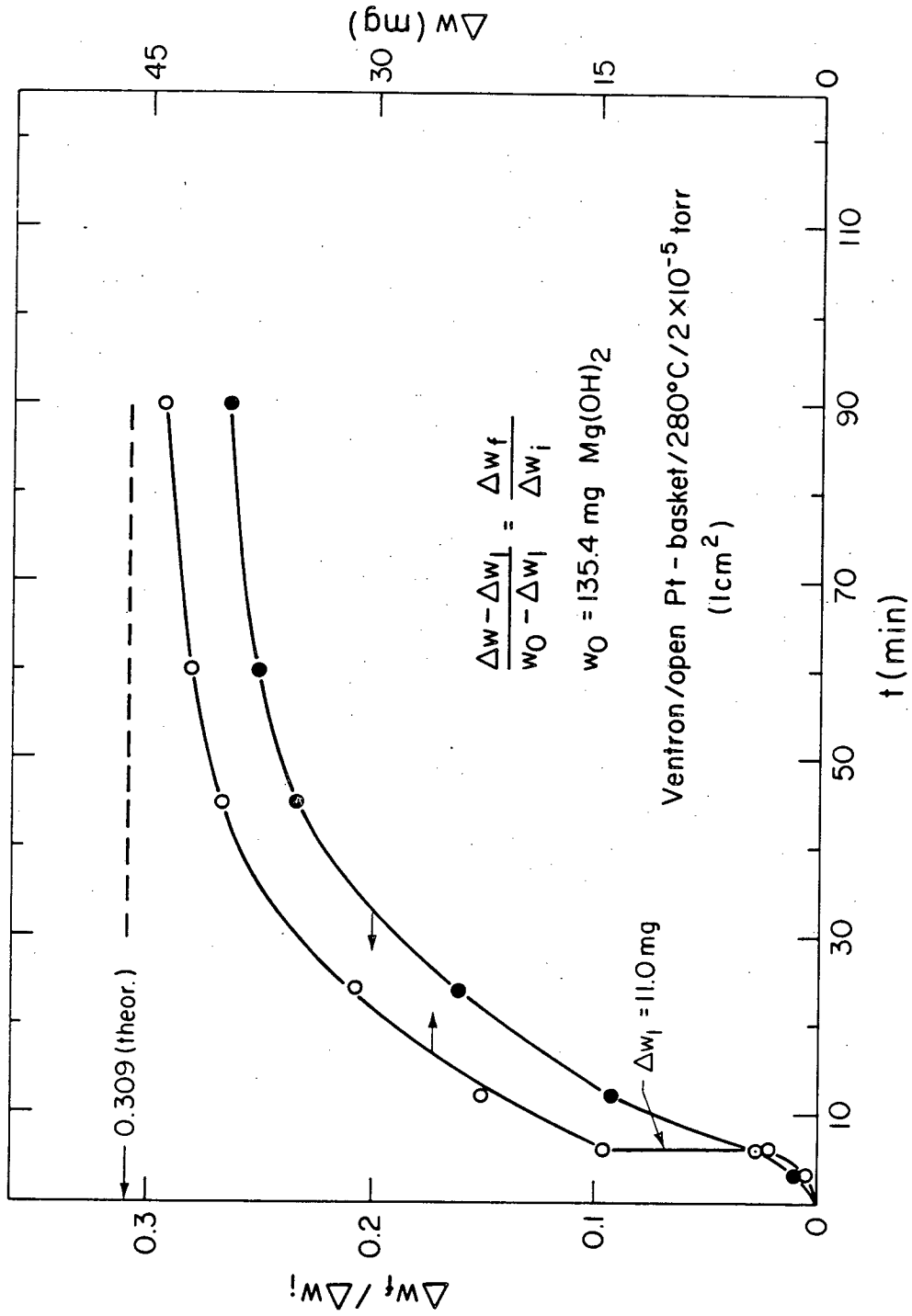
XBL 822-150

FIG 10



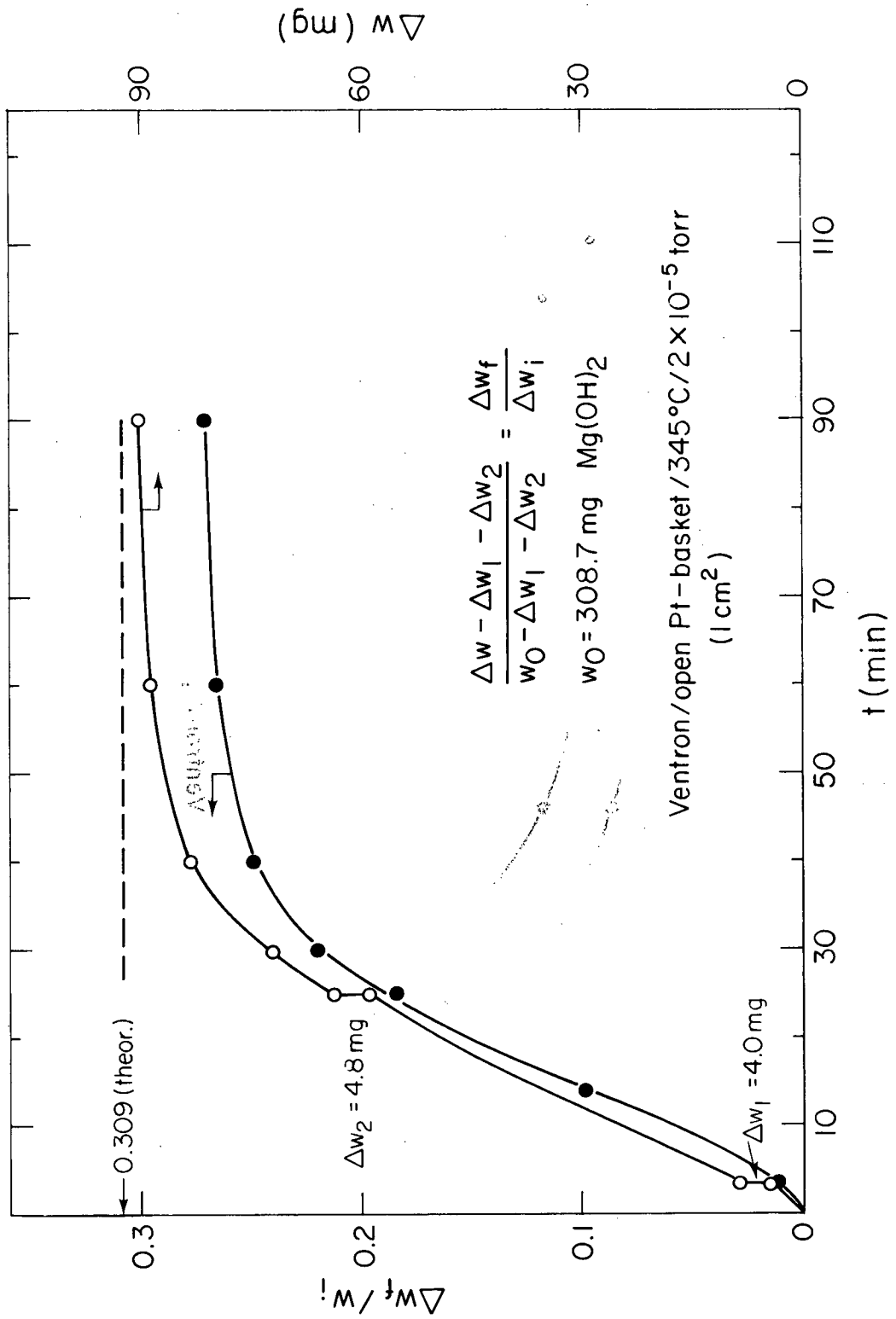
XBL 825-566

FIG 11



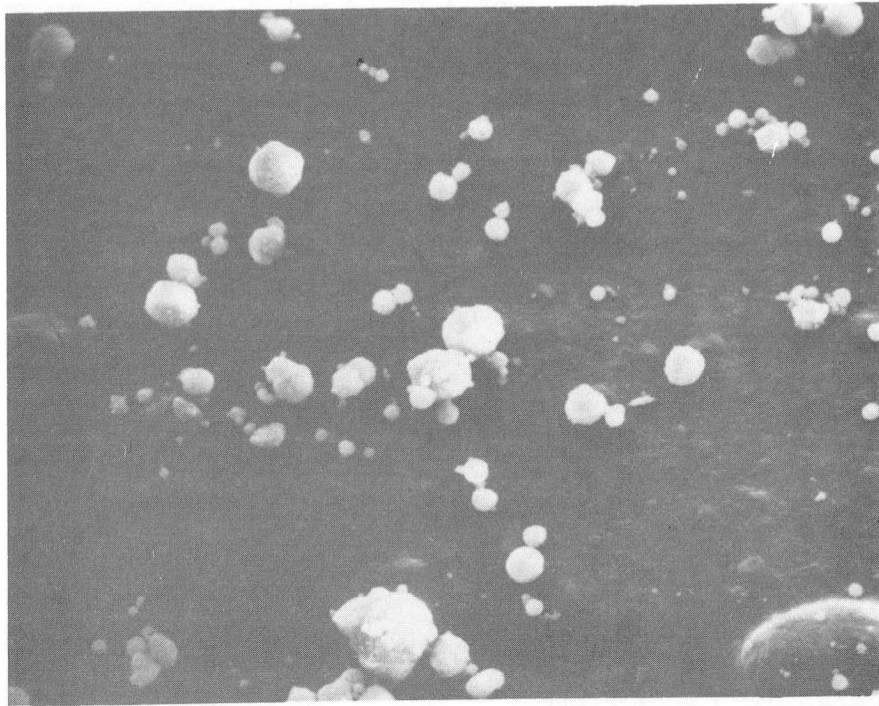
XBL 825-564

FIG 12

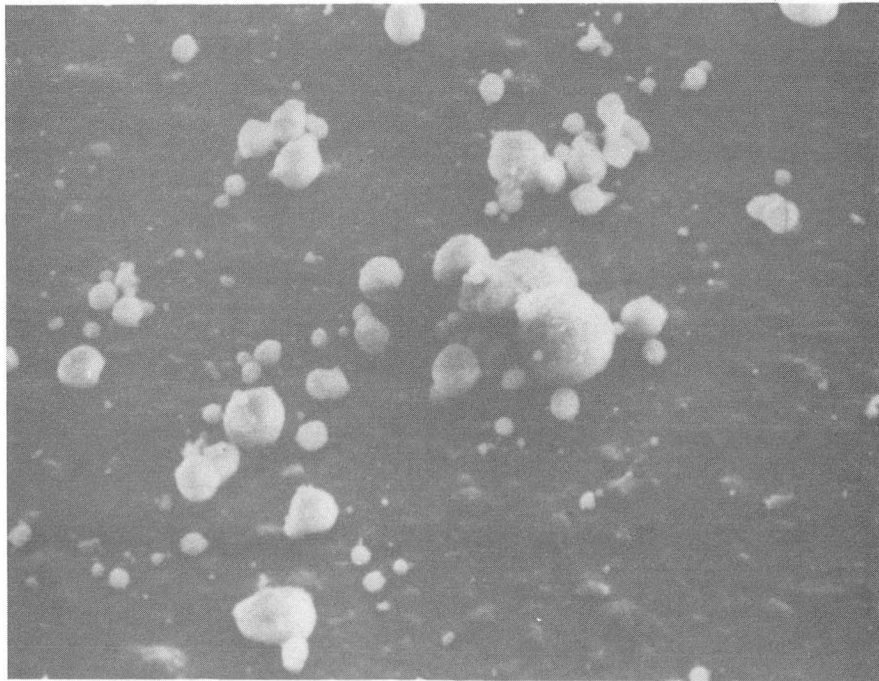


XBL 825-565

FIG 13



(a)



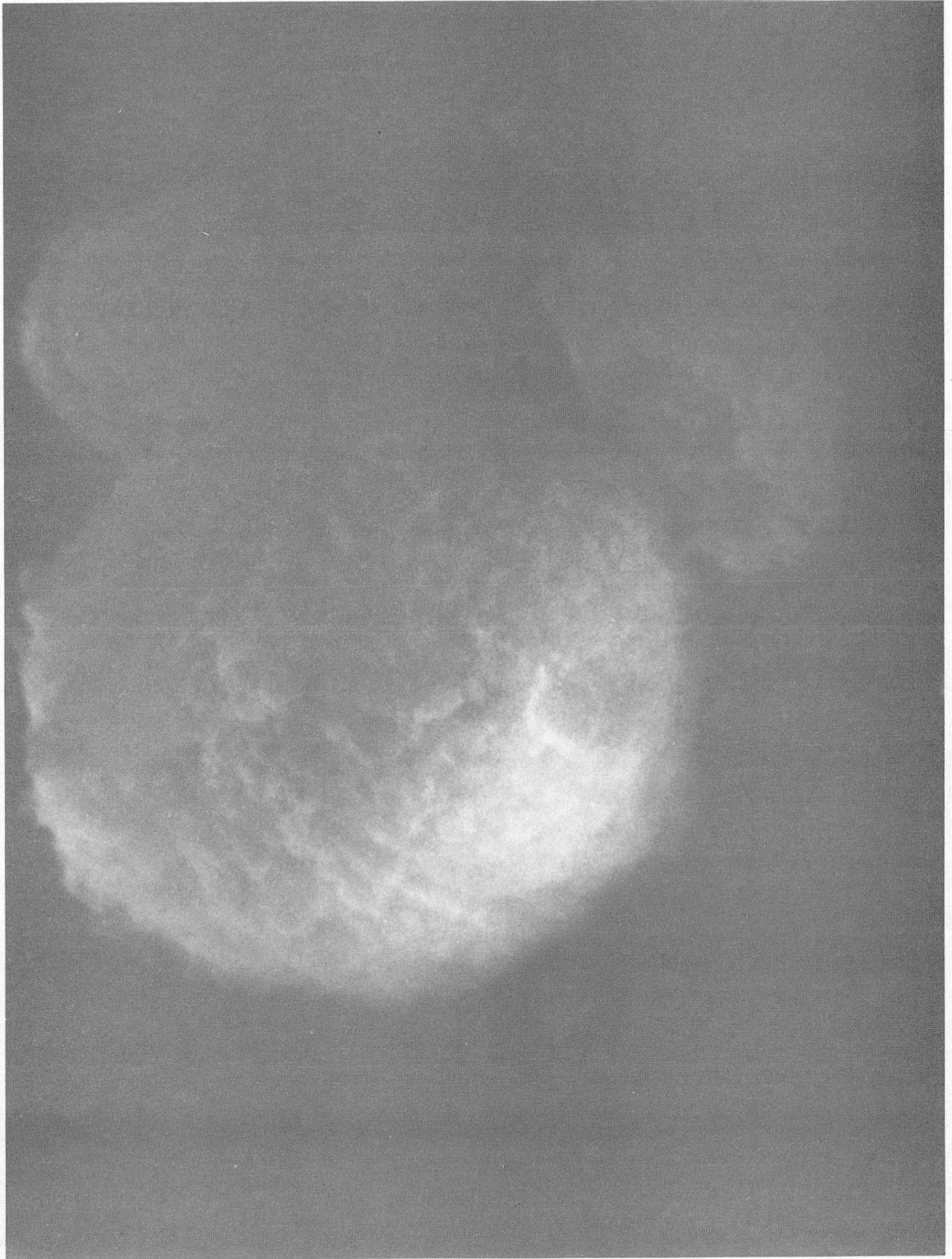
500 X

(b)

40 μm

XBB 823-1679B

FIG 14

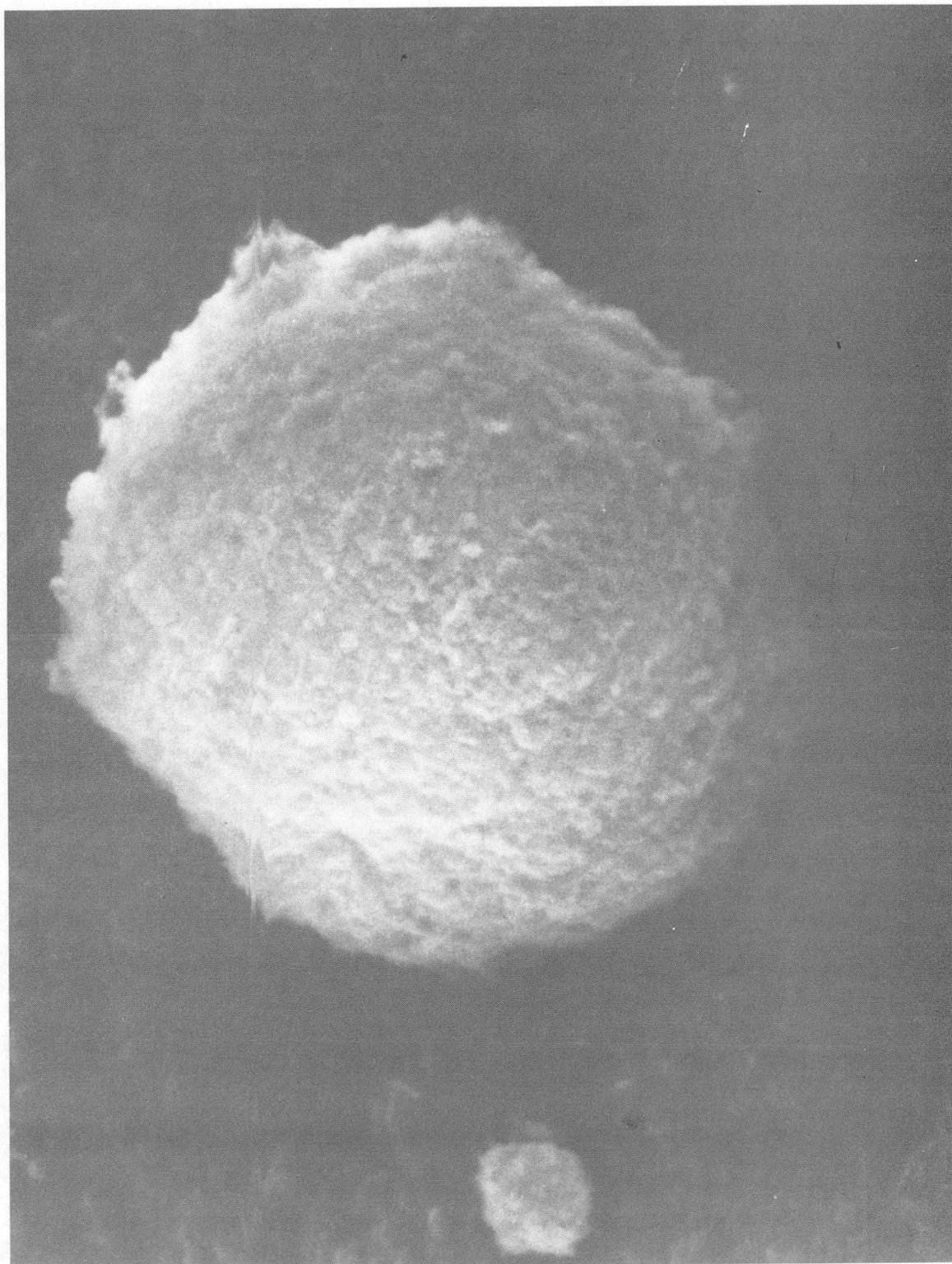


5000 X

4 μ m

XBB 823-2581

FIG 15



5000 X

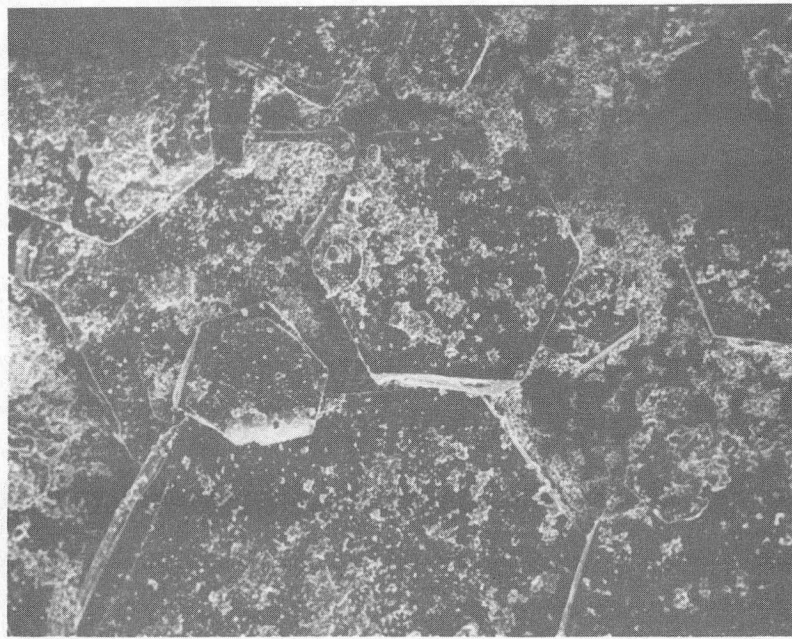
4 μm

FIG 16

XBB 823-2580



(a)



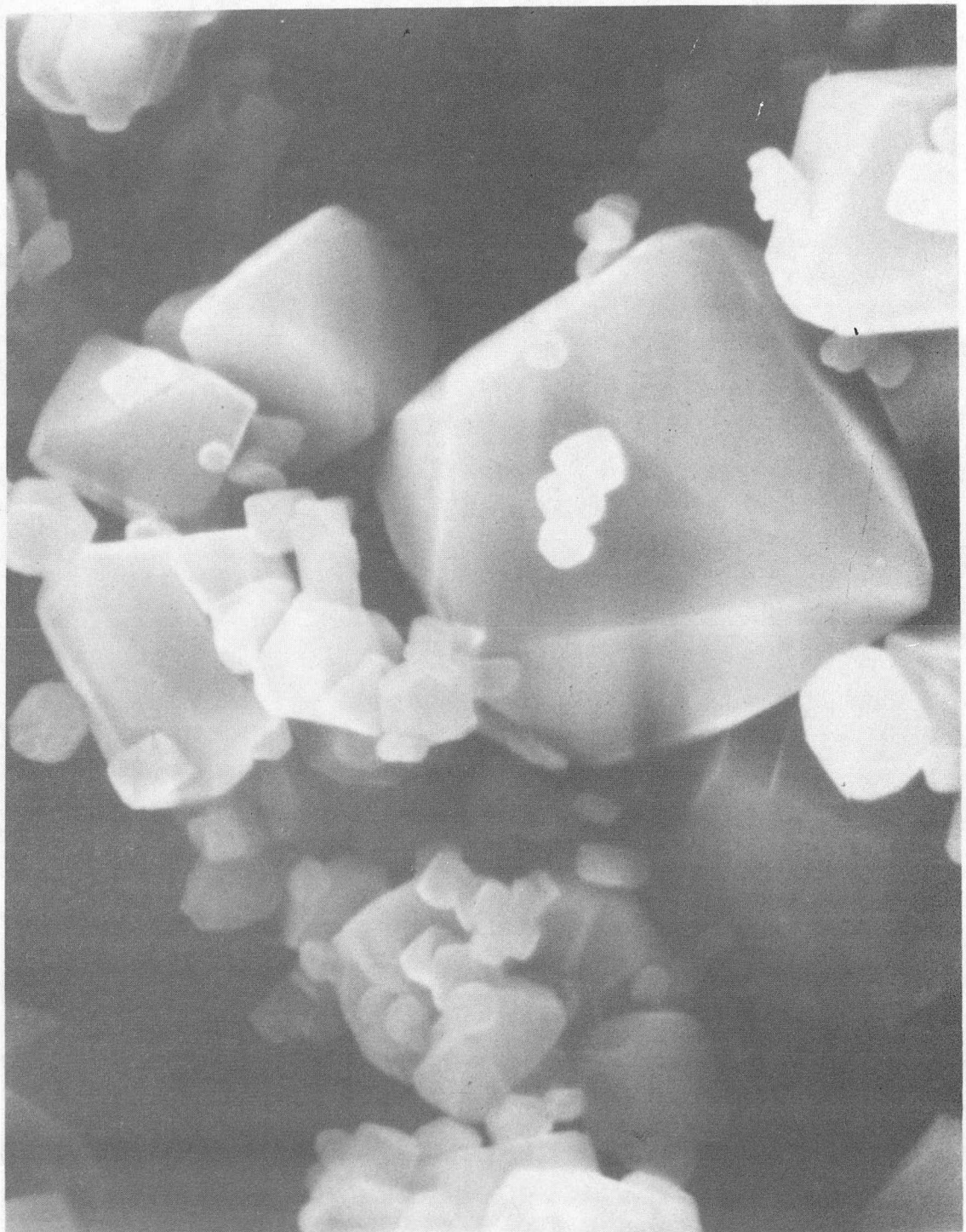
100 X

(b)

200 μm

XBB 822-1680A

FIG 17



5000 X

4 μ m

XBB 822-1678

FIG 18

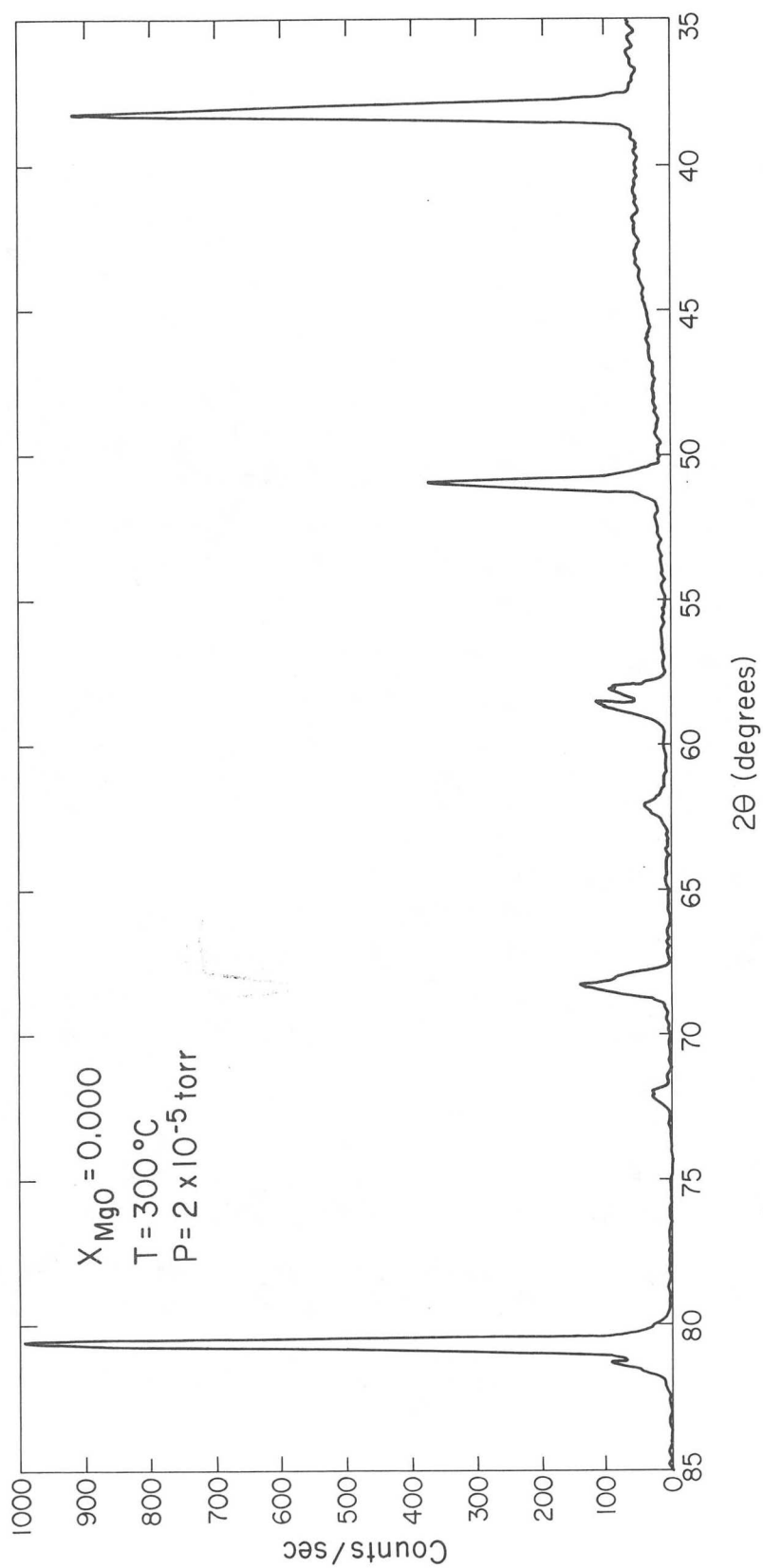


5000 X

4 μm

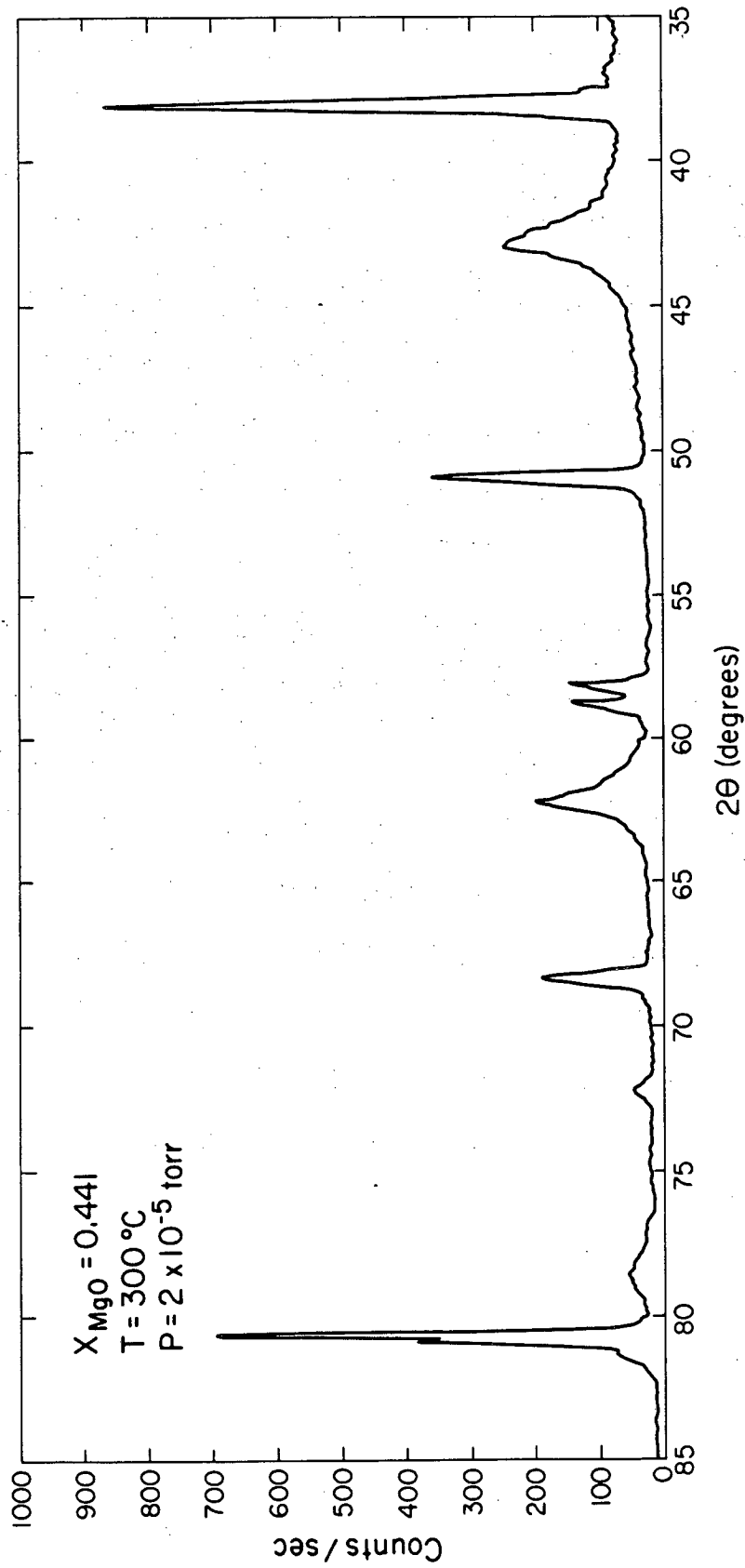
XBB 822-1674

FIG 19



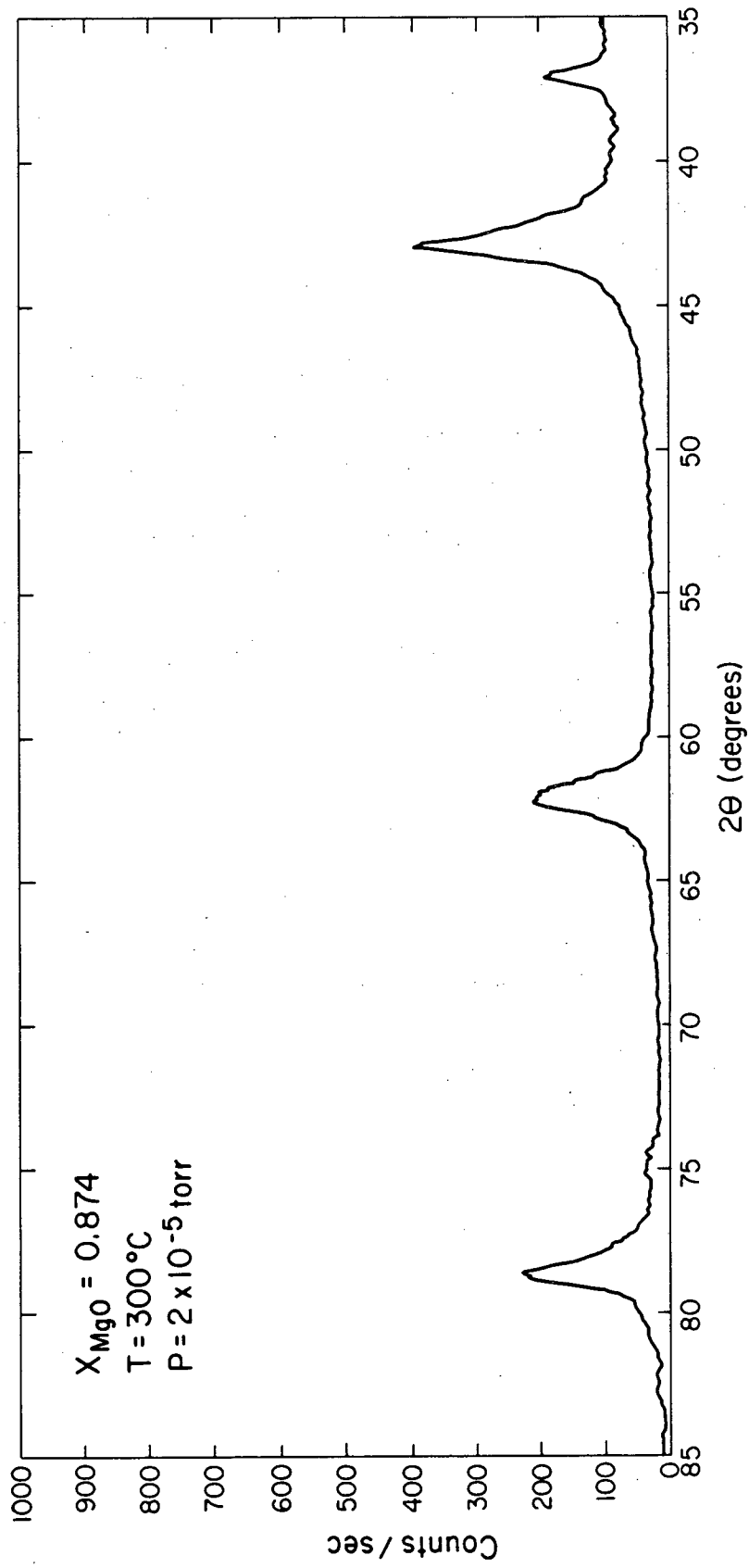
XBL 823-2085

FIG 20



XBL 823-2084

FIG 21



XBL 823-2083

FIG 22

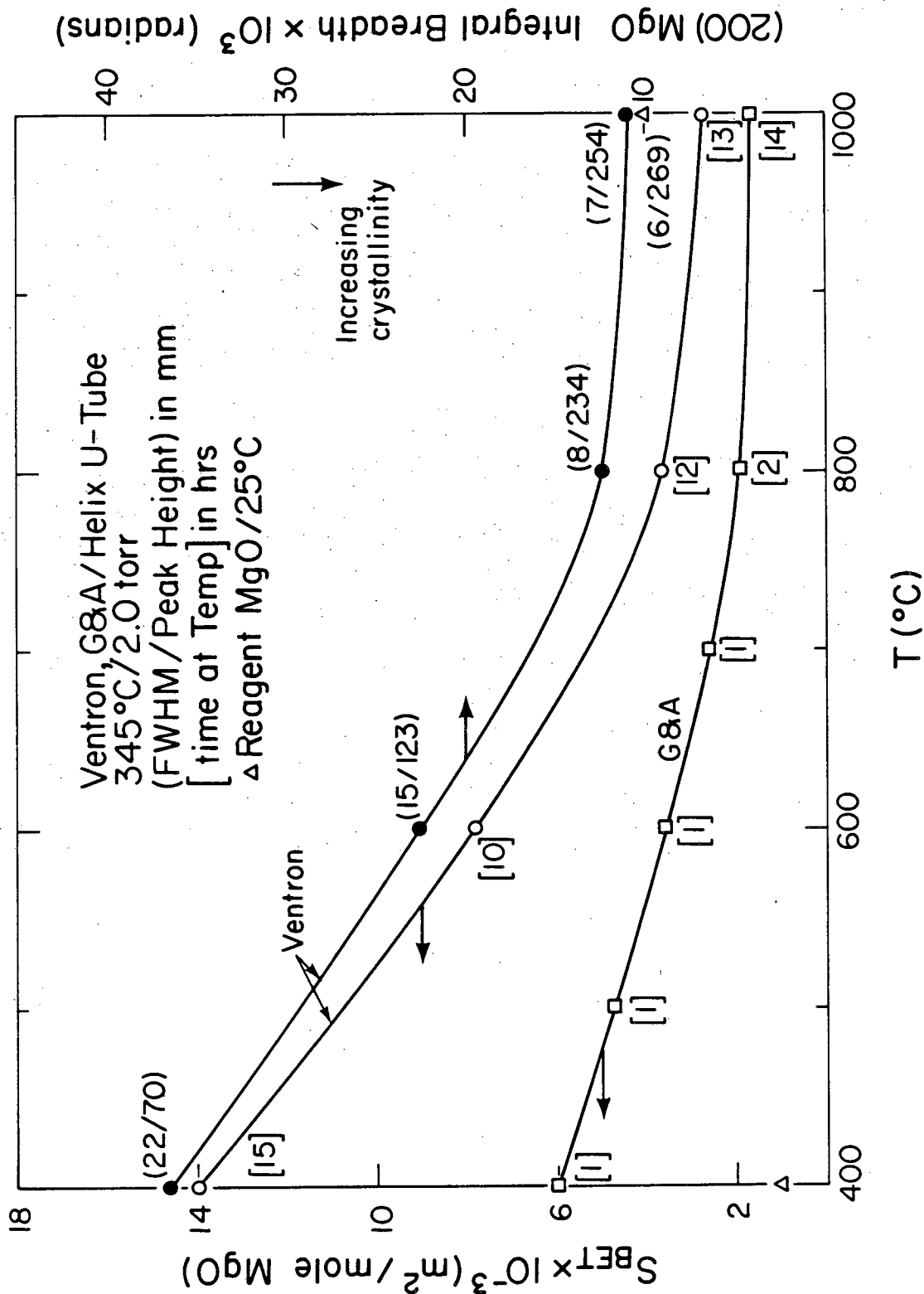
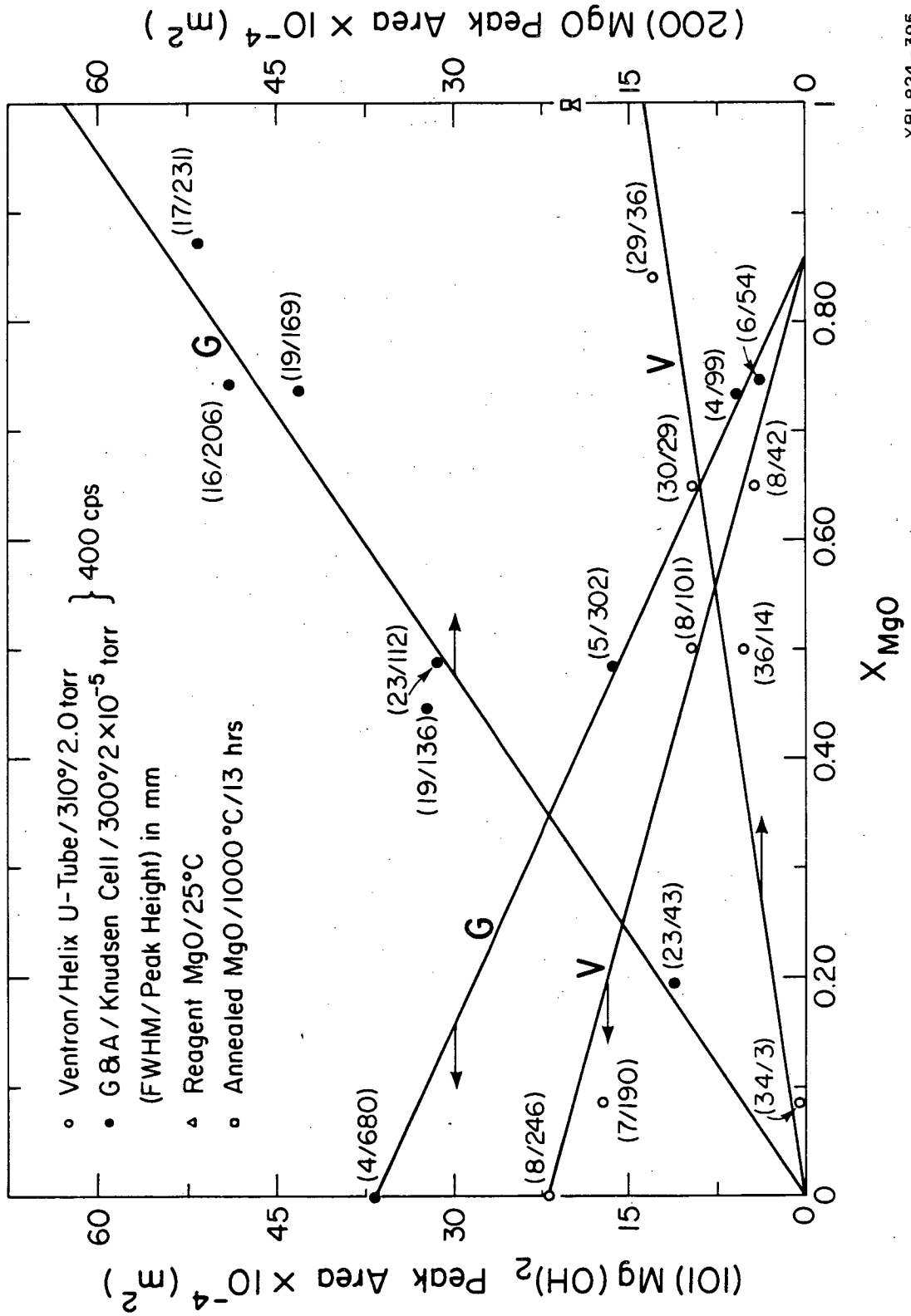
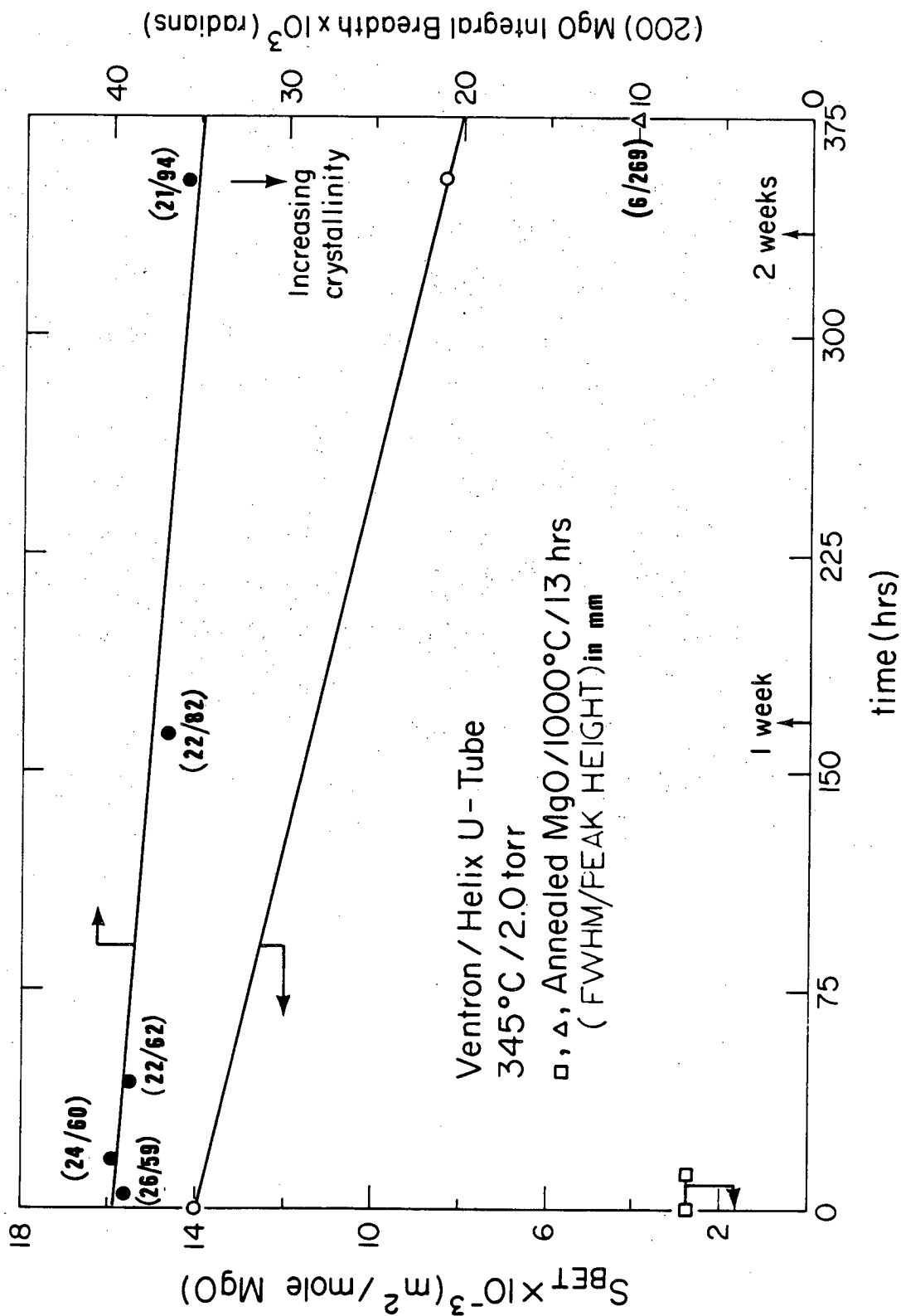


FIG 23



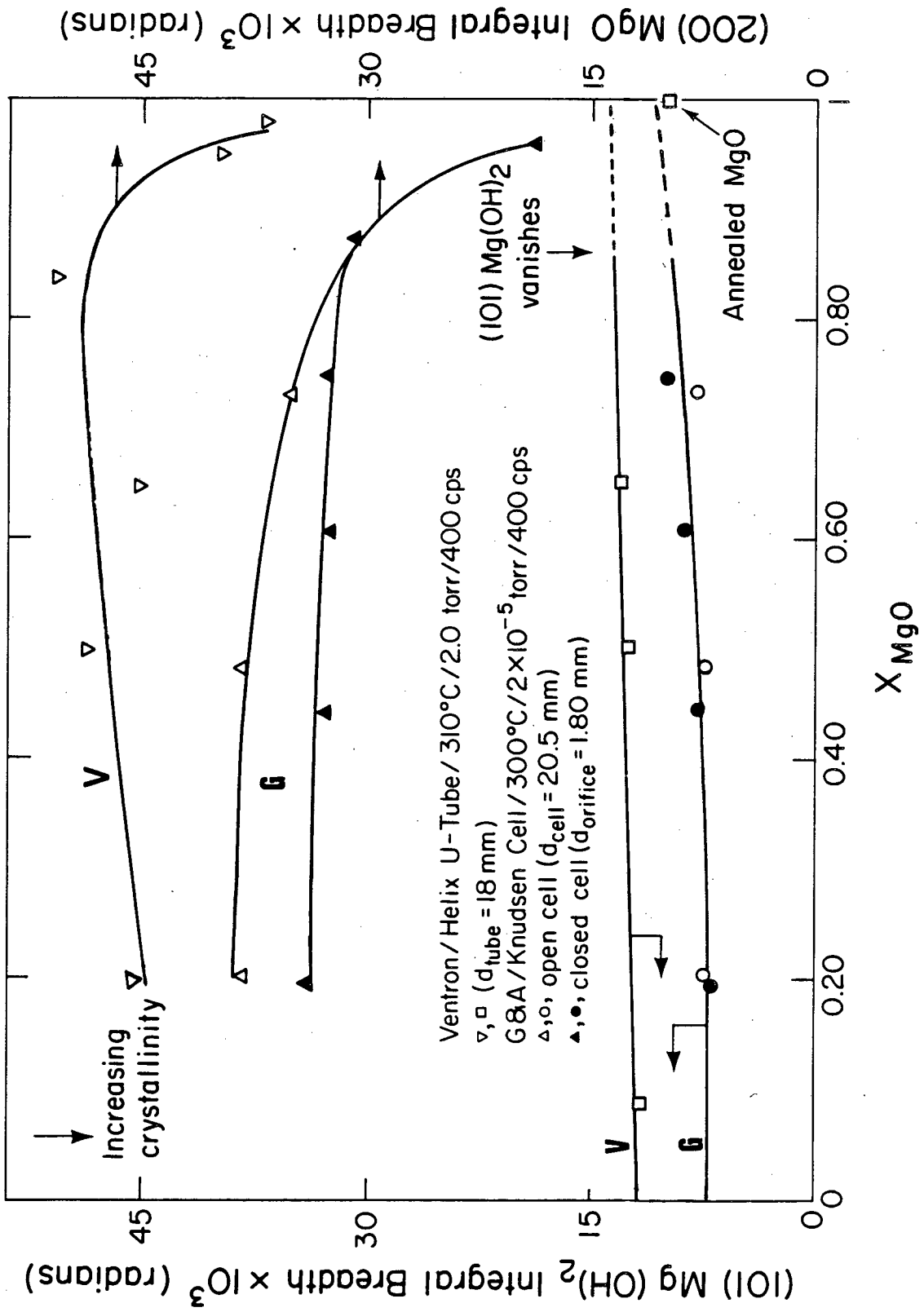
XBL 824-395

FIG 24



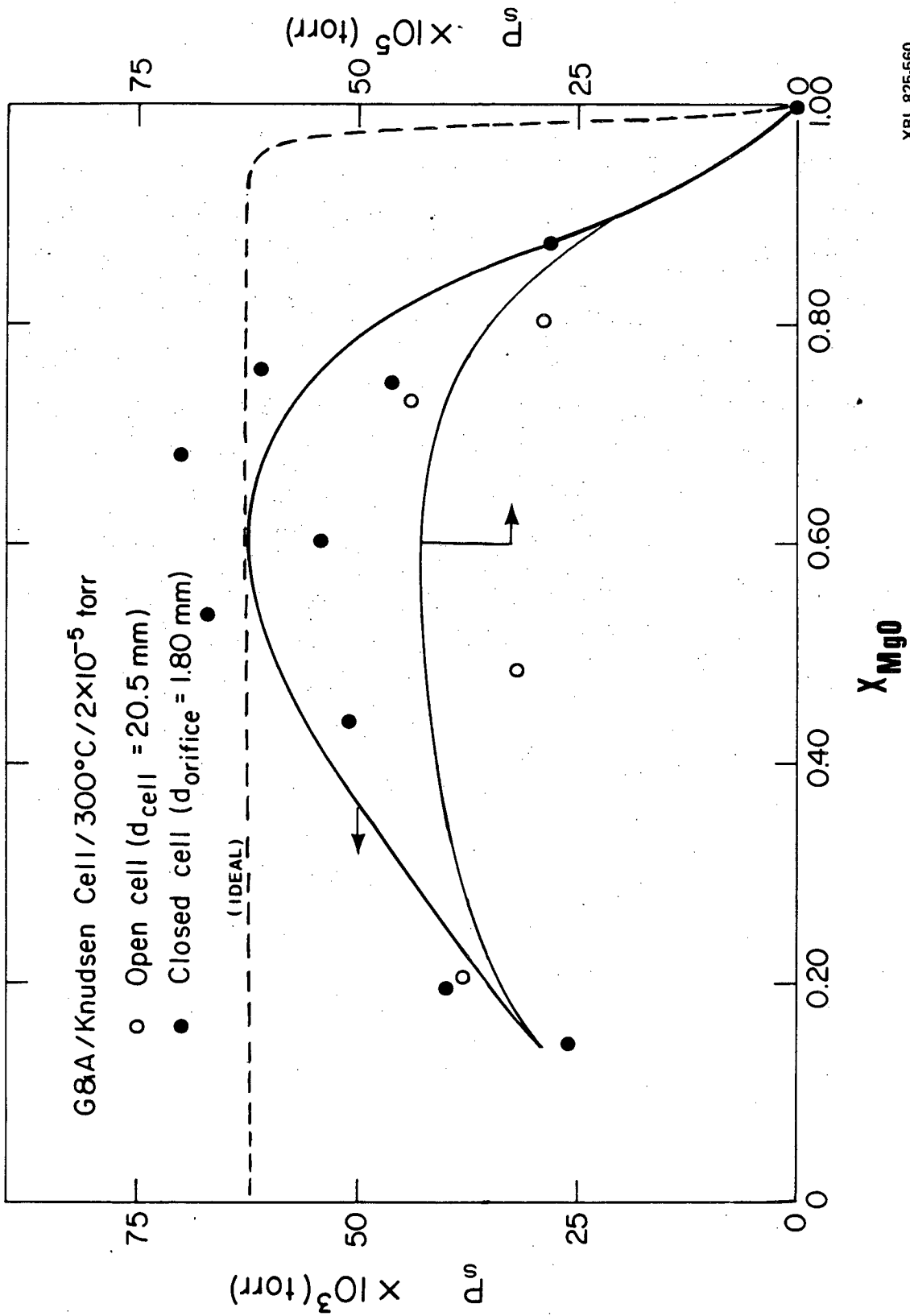
XBL 823 - 2077

FIG 25



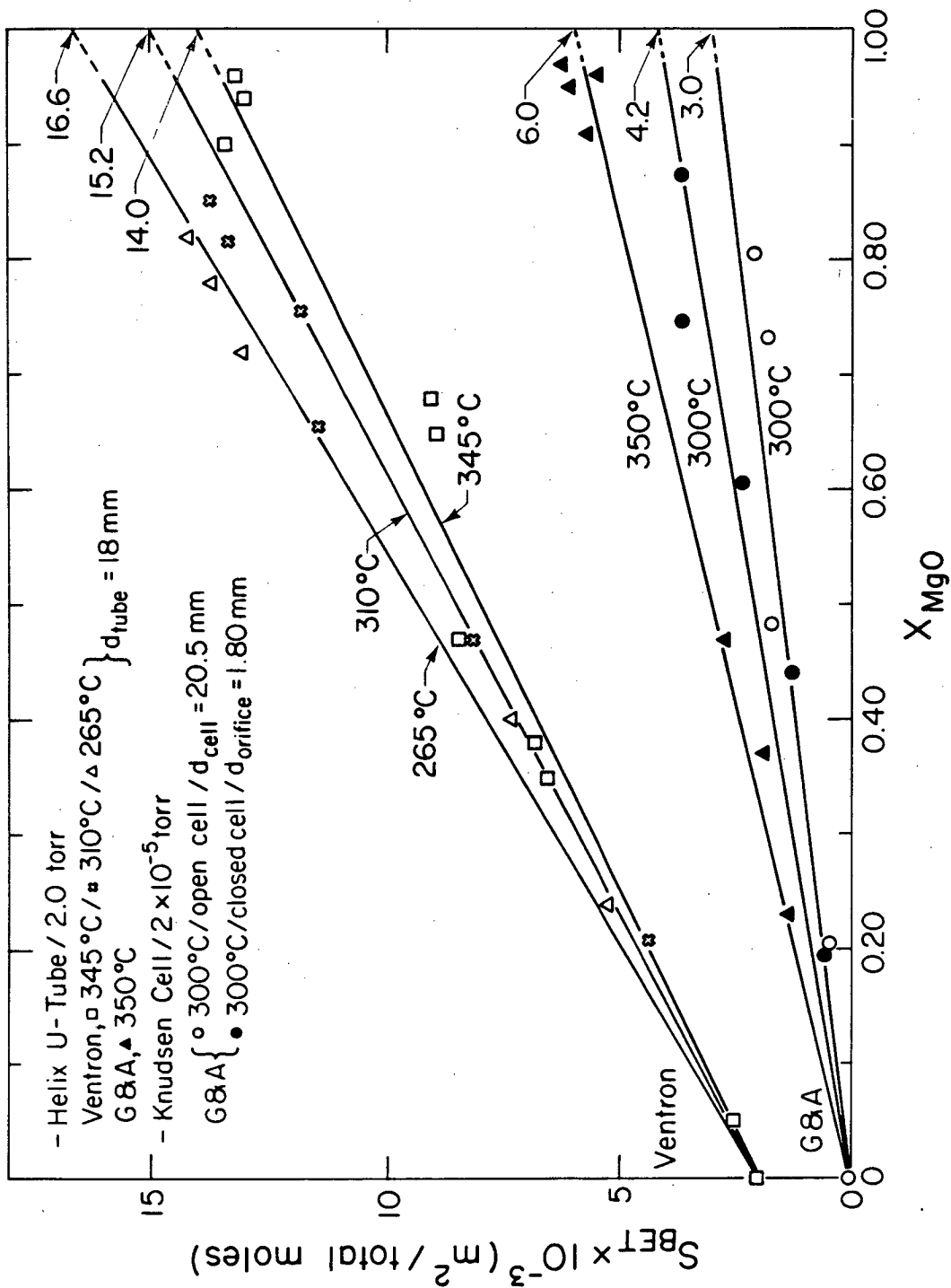
XBL 823-293

FIG 26



XBL 825-560

FIG 27



XBL 823-291

FIG 28

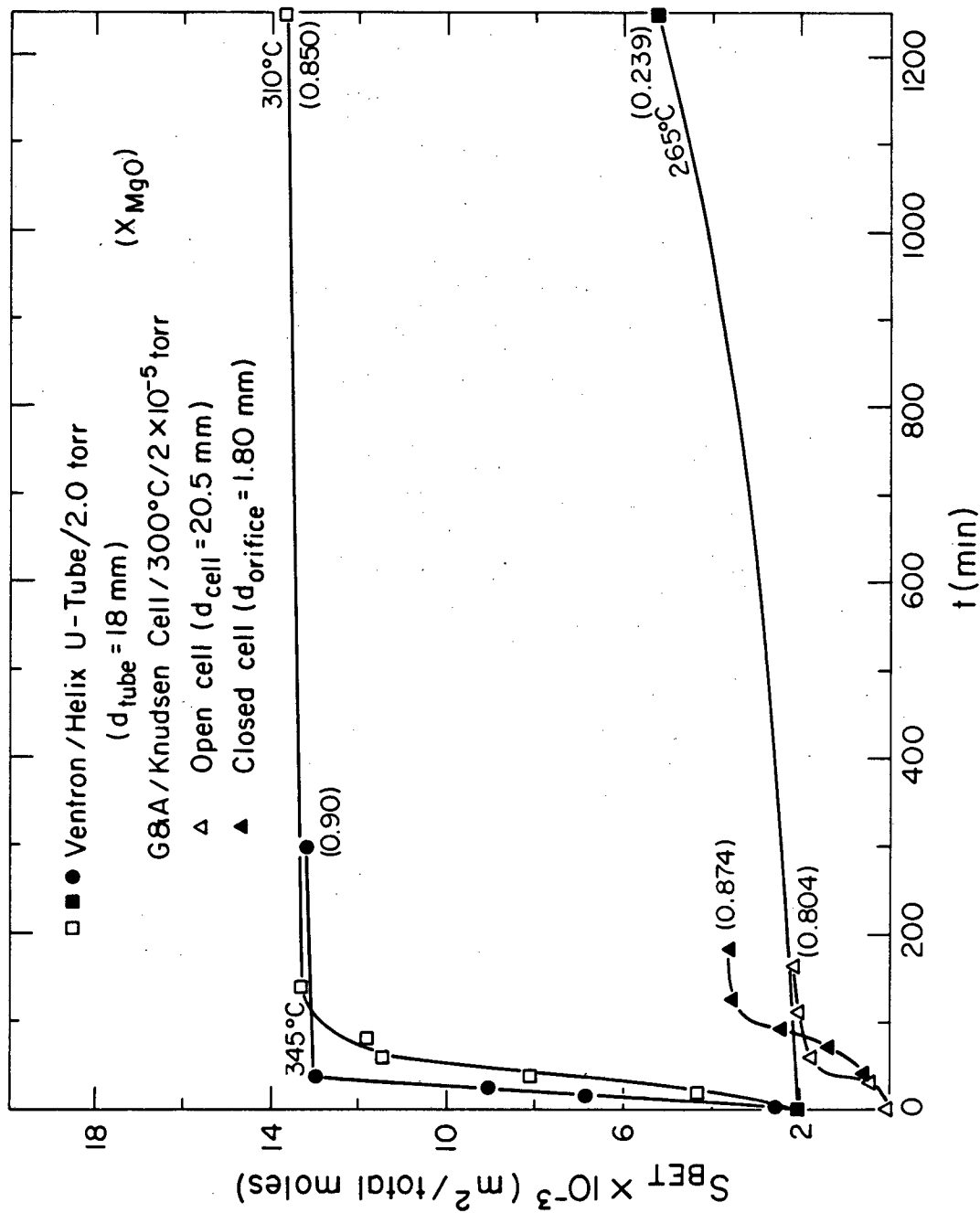
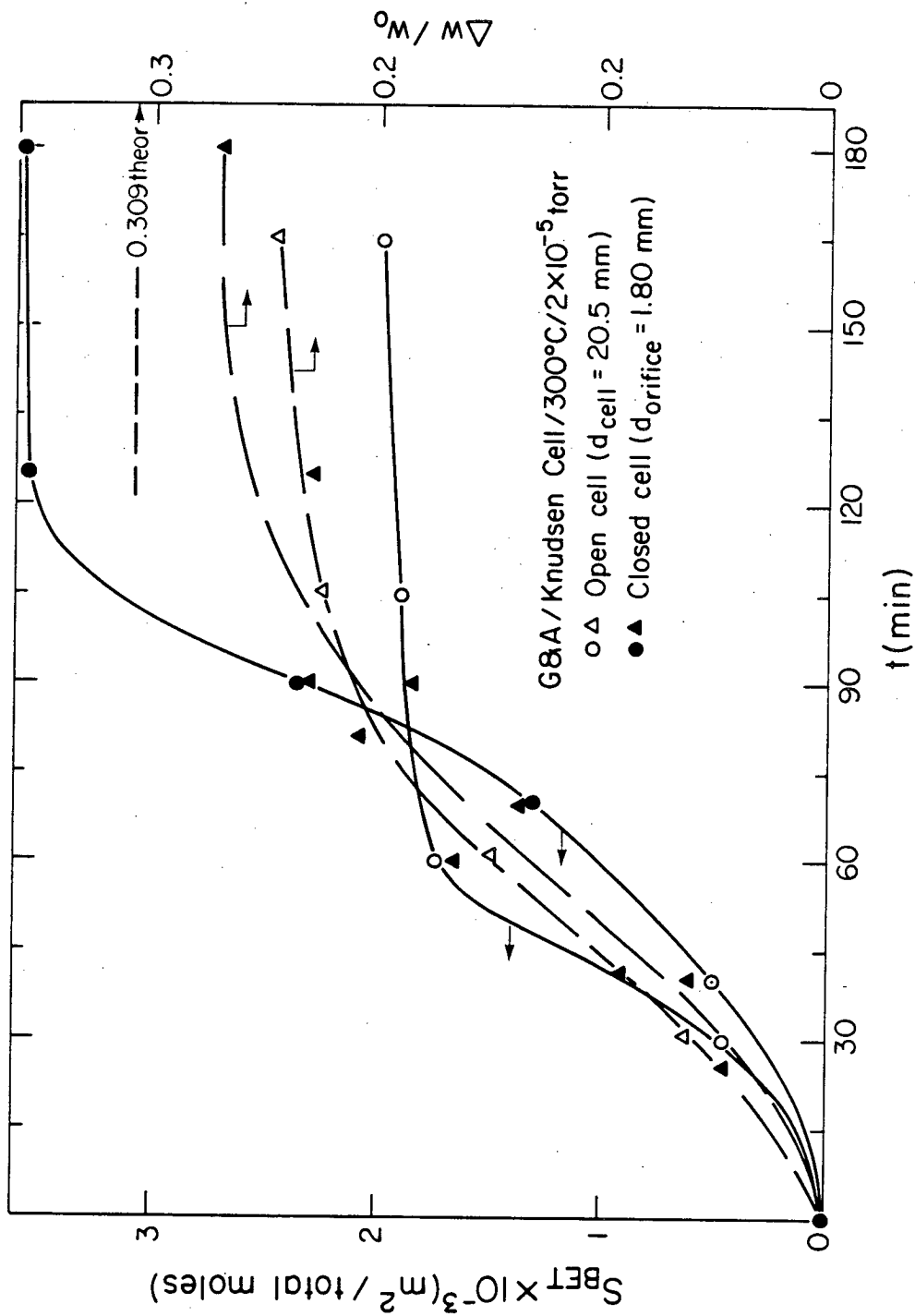
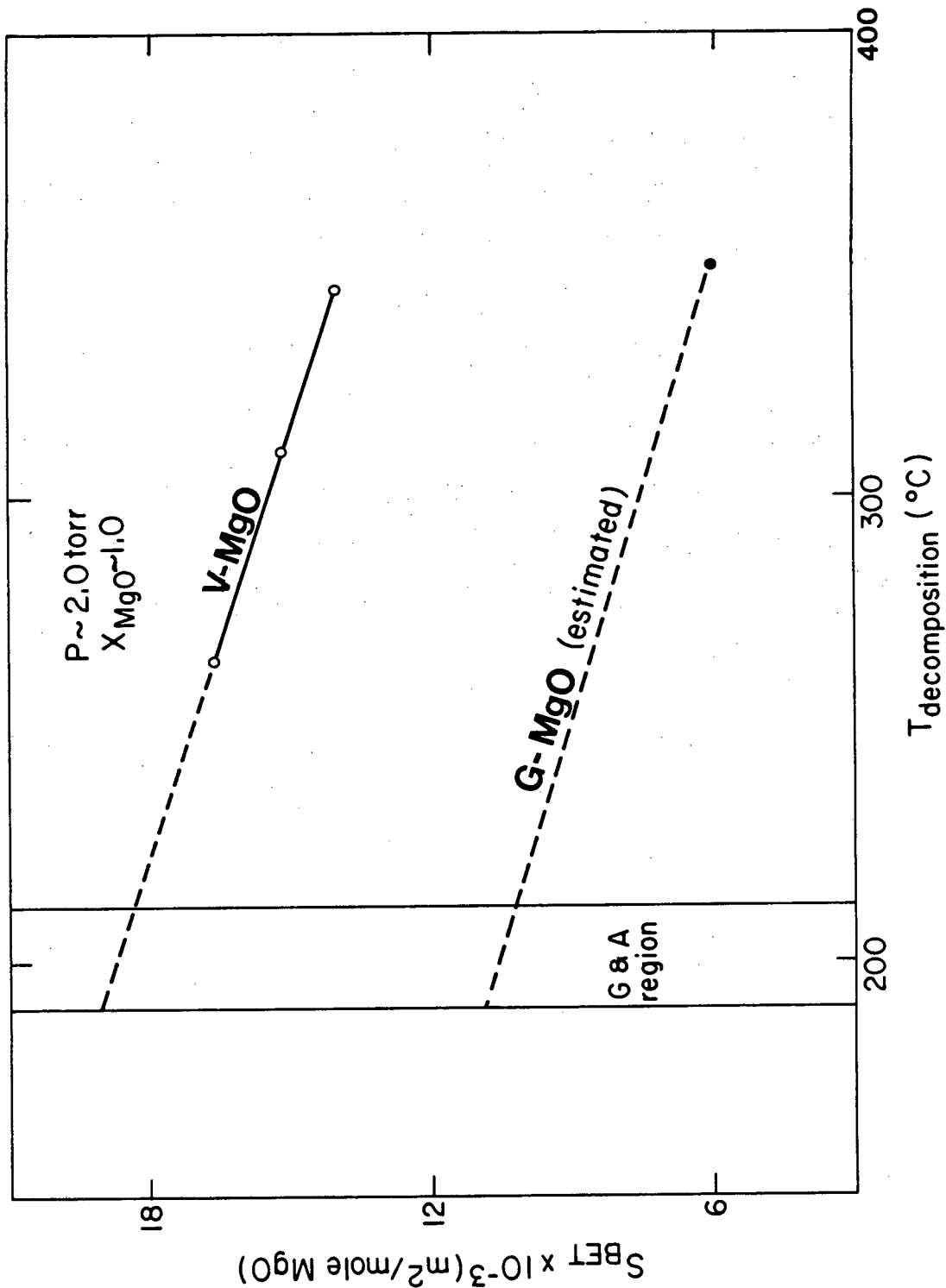


FIG 29



XBL 825-563

FIG 30



XBL 823-2080

FIG 31

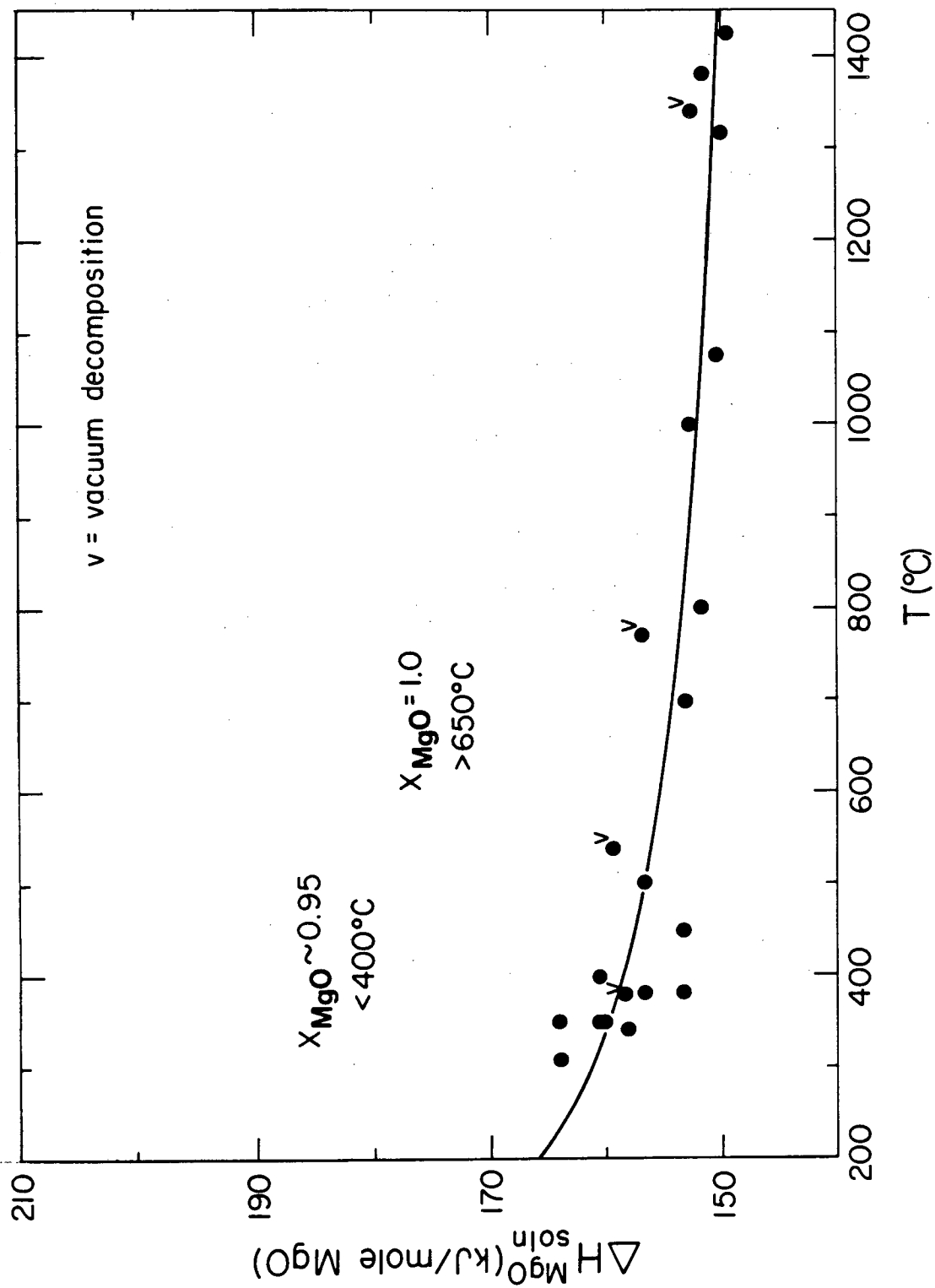
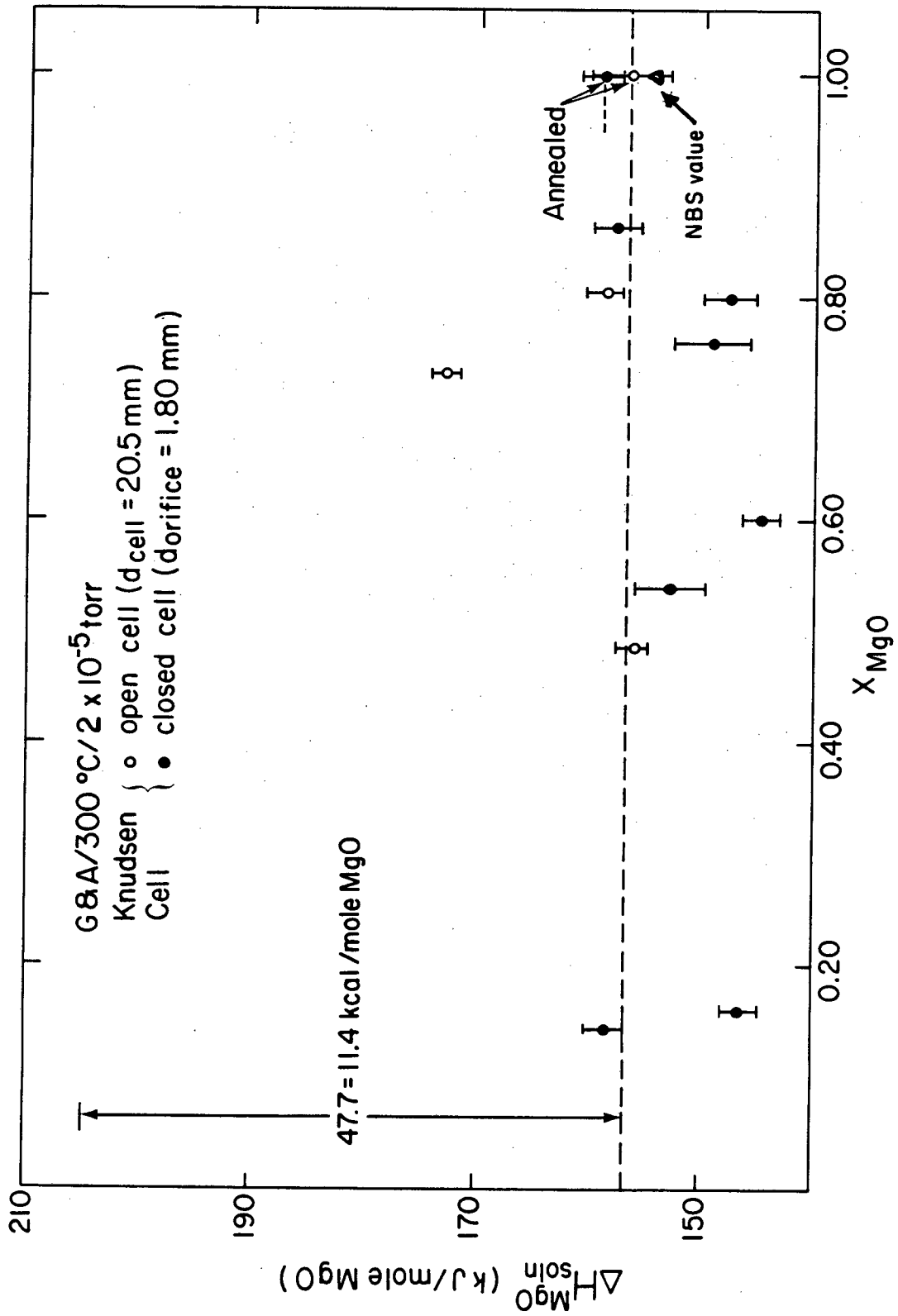
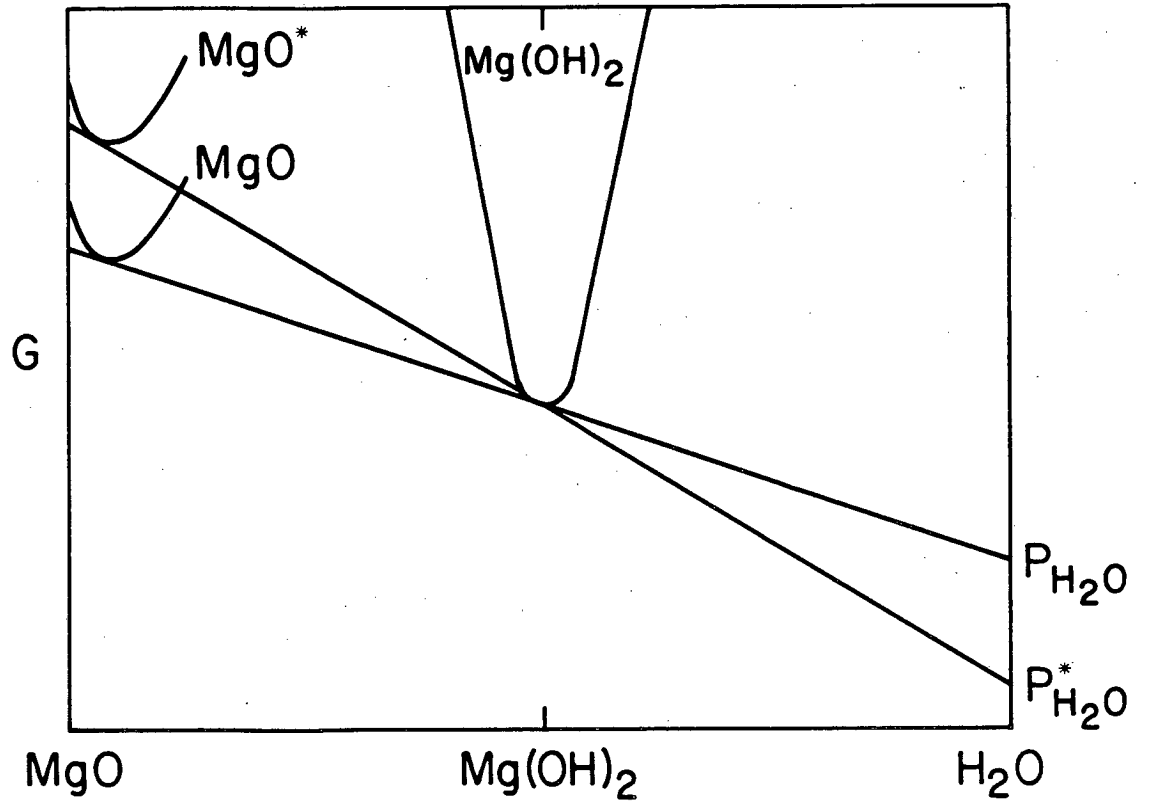


FIG 32



XBL 823-2078

FIG 33



XBL823-2081

FIG 34

This report was done with support from the Department of Energy. Any conclusions or opinions expressed in this report represent solely those of the author(s) and not necessarily those of The Regents of the University of California, the Lawrence Berkeley Laboratory or the Department of Energy.

Reference to a company or product name does not imply approval or recommendation of the product by the University of California or the U.S. Department of Energy to the exclusion of others that may be suitable.

TECHNICAL INFORMATION DEPARTMENT
LAWRENCE BERKELEY LABORATORY
UNIVERSITY OF CALIFORNIA
BERKELEY, CALIFORNIA 94720